Available online at www.sciencedirect.com

ScienceDirect

journal homepage: www.elsevier.com/locate/he

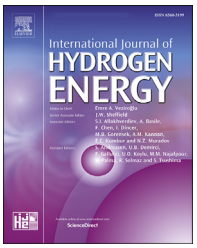

Review Article

A critical review in strategies to improve photocatalytic water splitting towards hydrogen production

Nur Fajrina, Muhammad Tahir *

Chemical Reaction Engineering Group (GREG), Faculty of Chemical and Energy Engineering, Universiti Teknologi Malaysia, 81310, UTM, Johor Bahru, Johor, Malaysia

ARTICLE INFO

Article history:
Received 7 June 2018
Received in revised form
25 October 2018
Accepted 28 October 2018
Available online xxx

Keywords:
Photocatalysis
Hydrogen production
Thermodynamics
TiO_2/g-C_3N_4
Heterojunctions
Photoreactors

ABSTRACT

Water splitting for hydrogen production under light irradiation is an ideal system to provide renewable energy sources and to reduce global warming effects. Even though significant efforts have been devoted to fabricate advanced nanocomposite materials, the main challenge persists, which is lower efficiency and selectivity towards H_2 evolution under solar energy. In this review, recent developments in photo-catalysts, fabrication of novel heterojunction constructions and factors influencing the photocatalytic process for dynamic H_2 production have been discussed. In the mainstream, recent developments in TiO_2 and g-C_3N_4 based photo-catalysts and their potential for H_2 production are extensively studied. The improvements have been classified as strategies to improve different factors of photocatalytic water splitting such as Z-scheme systems and influence of operating parameters such as band gap, morphology, temperature, light intensity, oxygen vacancies, pH, and sacrificial reagents. Moreover, thermodynamics for selective photocatalytic H_2 production are critically discussed. The advances in photo-reactors and their role to provide more light distribution and surface area contact between catalyst and light were systematically described. By applying the optimum operating parameters and new engineering approach on photoreactor, the efficiency of semiconductor photocatalysts for H_2 production can be enhanced. The future research and perspectives for photocatalytic water splitting were also suggested.

Contents

* *Corresponding author.*
E-mail address: mtahir@cheme.utm.my (M. Tahir).

https://doi.org/10.1016/j.ijhydene.2018.10.200
0360-3199/

Please cite this article as: Fajrina N, Tahir M, A critical review in strategies to improve photocatalytic water splitting towards hydrogen production, International Journal of Hydrogen Energy, https://doi.org/10.1016/j.ijhydene.2018.10.200

Introduction

Natural resources such as coal and petroleum products as a source of energy are nearly exhausted [1]. The reduction of fossil fuel reserves has prompted substantial research efforts toward the usage of hydrogen (H_2) as an environmentally friendly energy carrier for the post fossil fuel regime [2]. It is currently generally agreed that H_2 may be the best option for tackling the triple issues of exhaustion, pollution and climate change effects [3]. One of the technologies for H_2 production is photocatalytic water splitting, since it entails photonic energy, which is the most abundant energy resource on the Earth [4]. Previous research states that solar based H_2 generation by photocatalysis provides near zero global warming and air pollutants [5], and can be stored easily [6]. Therefore, H_2 is considered as a possible important energy in future, since it is free from toxic and it can produce high energy content from natural resources such as light (photon) energy and water, which are clean, long lasting sources of energy, and renewable resources [7].

Pioneer work as early as 1972 by Fujishima and Honda [8] reported water splitting for H_2 production over TiO_2 semiconductor. Since then, various types of semiconductors for photocatalytic H_2 productions are under investigation. Among all, titanium dioxide (TiO_2) with band gap 3.2 eV is a recognized photocatalyst and it has been extensively studied because of numerous advantages such as low cost, high photochemical stability and non-toxic [6,9]. On the other hand, wide band gap limits its applications under visible light and faster charges recombination rate lowers its photocatalytic activity [6,10]. Coupling TiO_2 with visible light semiconductors can narrowing the band gap with faster charges separation, thus could enables enhanced photo-catalytic activity. Among the low band gap semiconductors, polymeric graphitic carbon nitride (g-C_3N_4) has attracted more attentions as metal-free polymeric semiconductor in photocatalytic water splitting. It is a visible light responsive with lower band gap and low cost semiconductor. It can be synthesized from cheap precursors such as melamine and urea by simple thermal approach. In addition, g-C_3N_4 has numerous advantages such as high thermal and chemical stability and appropriate band structure (2.7 eV) to absorb visible light irradiation [11]. Among the limitations, g-C_3N_4 has low surface area and small active sites for interfacial (photon) reaction, moderate oxidation reaction of water to H^+ and low charge mobility which disrupt the delocalization of electrons. Hence, the coupling or/and doping g-C_3N_4 with other elements

Please cite this article as: Fajrina N, Tahir M, A critical review in strategies to improve photocatalytic water splitting towards hydrogen production, International Journal of Hydrogen Energy, https://doi.org/10.1016/j.ijhydene.2018.10.200

can overcome its limitations. Among the other alternatives, coupling g-C_3N_4 with TiO_2 to develop type II heterojunction could be promising to get enhanced H_2 production during photocatalytic water splitting under visible light irradiations.

Recently, the formation of Z-scheme photocatalytic system, analogous to artificial photosynthesis, is one of the latest strategies to improve photocatalytic performance as compared to using single semiconductor photocatalyst. Commonly investigated Z-scheme systems have three classifications that are with shuttle redox mediators, without electron mediators, and with solid-state electron mediators [12]. These systems can enhance the efficiency of photocatalyst performance, since it effectively increases the visible-light absorption, accelerates the separation and transportation of charge carriers. In addition, surface modification such as catalyst structure and morphology can improve performance due to increasing surface area and efficient charge carriers separation [13]. The configuration of semiconductors has been designed and investigated in the form of nanoparticles, nanosheets, nanotubes and nanowires [14]. Therefore, semiconductor photocatalyst selection and modification has great potential to narrow the band gap, utilizing visible light and promoting charge separation towards selective H_2 evolution.

In addition, photocatalytic efficiency can be achieved in the presence of sacrificial reagents such as reforming alcohols, which play roles as electron donor and hole scavenger, since the oxidation potential of alcohol is lower than reduction of H^+ to H_2. From the previous research, glycerol is more helping for the generation of H_2 than using methanol and ethanol. Bahruji et al. [15] investigated 20 different sacrificial reagents and proved increasing H_2 production rate in order triols > diols > primary (1°) alcohols > secondary (2°) alcohols > tertiary (3°) alcohols. The production of H_2 also depends on the location of physical properties of alcohols like number of α-H or OH atoms and alcohols polarity [16]. The design and selection of photoreactor is another engineering approach which contributes significantly in evolution of H_2 during photocatalysis. Since, the effectiveness of photocatalytic activity depends on the absorption of photons and reactants on the catalyst surface, the innovations on photoreactors should include selection of light sources and distribution, shape and dimension of reactor, and design of irradiation device such as reflectors. Typically, slurry reactor is used in photo-catalysis process, yet it has limitations such as low light distribution, lower light penetration depth, excessive cost for catalyst separation and cannot maximize H_2 production. Therefore, photo-technology has been developed and recently, monolith reactor has attracted the attention of researchers among the photo-reactors such as slurry, fluidized, fixed bed and optical fiber photoreactor. Monolith, which contains parallel straight channels, have been exploited very efficiently due to higher illuminated surface area, high utilization of photon flux energy and tends to generate more H_2 under flow operation [17].

Herein, an overview and recent developments in semiconductor materials, thermodynamics and engineering approach to maximize photocatalytic water splitting for H_2 production has been discussed. First, the fundamentals and thermodynamics of photocatalysis are briefly explained. Second, the strategies to improve the photocatalytic activity by the design of TiO_2 and g-C_3N_4 structures, morphological impacts, modification with different materials and formations of heterojunctions are summarized. The various factors that affect photocatalytic water splitting such as band gap, morphology, temperature, light intensity, pH, oxygen vacancies, and sacrificial reagents are then critically discussed. Additionally, the technology in photoreactors and the recommendation to improve the H_2 production are also explained.

Fundamentals and thermodynamics of photocatalysis

Fundamentals of photocatalysis

Photocatalytic water splitting is regarded as an artificial photosynthesis, since it is similar to photosynthesis process in green plants under solar energy [18,19]. The production of hydrogen from organic substances within wastewater or from water could be achieved along with principle of photocatalytic processes by exploiting the sun radiation that strikes the earth surface every day [20]. During this process, light energy is converted to chemical energy, while water splitting reaction promotes to build up Gibbs free energy (G^E) [18,21]. Hydrogen can be generated with two methods which can be: (i) photocatalytic water splitting [18] and (ii) photocatalytic reforming of organics [22]. In the first method, water undergoes redox reaction with electron/holes, however, in the second step, organic substances donate electron and oxidize to generate proton ions [18]. The proton ions are finally converted to H_2 by the involvement of electrons over the photocatalyst [22].

In general, photocatalytic system requires reactant, photocatalyst, photoreactor and supply of light to evolve hydrogen. The reactant can be water itself or even mixing with sacrificial reagent. For photocatalyst, it should be working with light, either UV light or visible light, yet photo catalysts absorbing light in the visible range may guarantee to capture significant part of the energy emitted by the sunlight [23]. For efficient hydrogen production, an efficient interaction between light, catalyst and reactants would be required [24,25]. Photocatalysis starts with irradiation of light with energy higher than or equal to its band gap of a semiconductor based photo catalyst, isolating the vacant conduction band (CB) and filled valence band (VB), exciting an electron in VB directly into CB to result in the separation of an electron (e^-)–hole (h^+) pair. The photo-generated electrons are involved for the reduction process while the holes are consumed in oxidation process [26].

The mechanism of photocatalytic water splitting for H_2 production is illustrated as in Fig. 1 [27]. The photo catalysis has four major processes, which are light harvesting (stage 1), charge excitation (stage 2), charge separation and transfer (stage 3 and 4), and surface catalytic reactions (stage 5 and 6) [28]. First, photocatalysis starts with light irradiation with energy greater or equal to the band gap of photocatalyst. Typically, the semiconductor of photo catalyst consists of a VB and a CB, which are separated from one another by a band gap energy (E_{bg}) [6]. The photo-catalyst under appropriate photon

Please cite this article as: Fajrina N, Tahir M, A critical review in strategies to improve photocatalytic water splitting towards hydrogen production, International Journal of Hydrogen Energy, https://doi.org/10.1016/j.ijhydene.2018.10.200

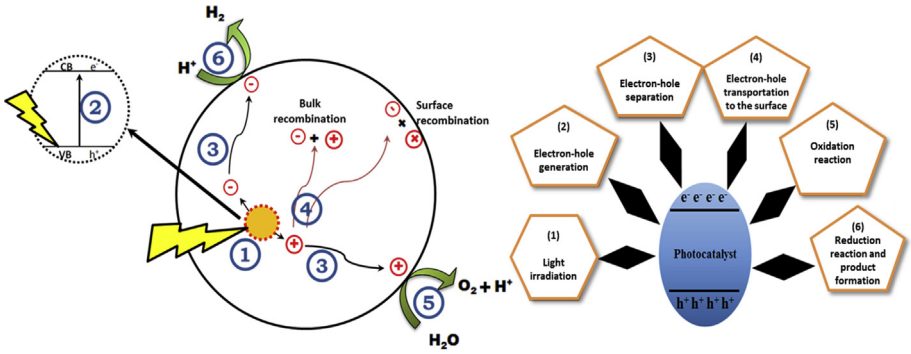

Fig. 1 – Illustration of mechanism of photocatalytic water splitting for H_2 production [27].

excitation causes electronic transitions and generates e^-/h^+ pairs (Eq. (1)). Second, the charges are separated and the electrons are excited from the VB to CB, leaving holes in the VB. Electrons and holes are involved in the reduction (stage 6) and oxidation (stage 5) reaction with water. The oxidation reaction involves decomposition of water into H^+ as shown in Eq. (3), while Eq. (4) shows reduction reaction when H^+ gains electron to produce H_2. Redox reaction on the surface of photocatalyst occurs when the reduction and oxidation potentials are above and below than CB and VB levels, respectively [26,28–30]. Photo-excited holes are powerful oxidants, capable of oxidizing water and organics such as alcohols as shown in Eqs. (3) and (5), respectively. The reaction can be carried out with thermal dissociation of water at temperature more than 2070 K, however, water splitting can be conducted at room temperature using photocatalyst under light irradiation with energy more than the band gap energy [2].

$$Catalyst \rightarrow Catalyst(e^- + h^+) \quad (1)$$

$$Catalyst\ (e^- + h^+) \rightarrow Catalyst \quad (2)$$

$$H_2O + h^+ \rightarrow \frac{1}{2}O_2 + 2H^+ \quad (3)$$

$$2e^- + 2H^+ \rightarrow H_2 \quad (4)$$

$$RCH_2OH + 2h^+ \rightarrow RCHO + 2H^+ \quad (5)$$

However, the major challenge regarding photocatalytic water splitting is the charges (e^-/h^+) recombination. The electron–hole pairs could recombine (stage 4) as illustrated in Eq. (2) with the release of unproductive heat. Therefore, it reduces the effectiveness for the H_2 generation. Particularly in pure water, it is difficult in order to achieve water splitting for H_2 production using photo-catalysts due to fast recombination of photo-generated charge carriers. Consequently, photocatalytic water splitting is usually studied in the presence of sacrificial reagent (methanol, ethanol and glycerol) and electrolytes (Na_2S and KI). The electrolytes are not undergoing reduction or oxidation by CB electrons and VB holes. Electrolytes act as transport of ions and transfer of electrons to adjacent semiconductor. Therefore, they will give improvement on the photocatalytic water splitting reactions. The sacrificial reagent or electron donors are reacting with VB holes to enhance charges separation [26]. Since, the formation of H_2 from pure water has its limitation, the understanding of thermodynamic analysis in terms of energy, band gap and redox potential can enhance the maximum performance for photocatalytic activity.

Thermodynamics for water splitting

The water splitting reaction is a multi-electron process and endothermic reaction [31]. The reaction of water into H_2 and O_2 requires a source of energy to fulfill the Gibbs free energy change ($\Delta H^0 = 238\ kJ\ mol^{-1}$) [32], while the Gibbs energy will be needed to rearrange valence electrons of water regarding formation of H_2 and O_2 [26]. The overall water dissociation and full water splitting reaction are explained in Eqs. (6) and (7). In order to generate one molecule of H_2 as shown in Eq. (6), the energy required simply by water to produced H_2 is 2.458 eV, which shows a work under 1.229 V potential difference for the displacement of two electrons [33]. Since, full water splitting needs four electrons to produce two molecules of H_2 as shown in Eq. (7), the energy input required is 4.915 eV and can be utilized by UV light with wavelength shorter than 252.3 nm or by two photons within the visible spectrum along with wavelength shorter than 504.5 nm [34]. The water splitting involves two half-reactions: the oxidation of water to form O_2 (Eq. (3)) and the reduction of protons to form H_2 (Eq. (4)) [2].

Overall water dissociation reaction:

$$H_2O \xrightarrow{TiO_2/h\upsilon} \frac{1}{2}O_2 + 2H^+;\ 2H^+ + 2e^- \rightarrow H_2 + \frac{1}{2}O_2 \quad (6)$$

Full water splitting reaction:

$$2H_2O \xrightarrow{TiO_2/h\upsilon} O_2 + 4H^+;\ 4H^+ + 4e^- \rightarrow 2H_2 + O_2 \quad (7)$$

When a semiconductor is exposed to light with energy higher than E_g, it stimulates the electrons into CB and leaving holes in VB. The photo-induced electrons and holes are freely moving, capable of being delocalized within the semiconductor. This could cause electrons quickly attaining internal equilibrium within energy level instead of across the band gap, since the relaxation time with in conduction band is shorter as compared to across the band gap as displayed in Fig. 2. States of electrons along with internal equilibrium are referred to as quasi equilibrium states and potential of electrons and holes in quasi-Fermi levels are given in Eqs. (8) and

Please cite this article as: Fajrina N, Tahir M, A critical review in strategies to improve photocatalytic water splitting towards hydrogen production, International Journal of Hydrogen Energy, https://doi.org/10.1016/j.ijhydene.2018.10.200

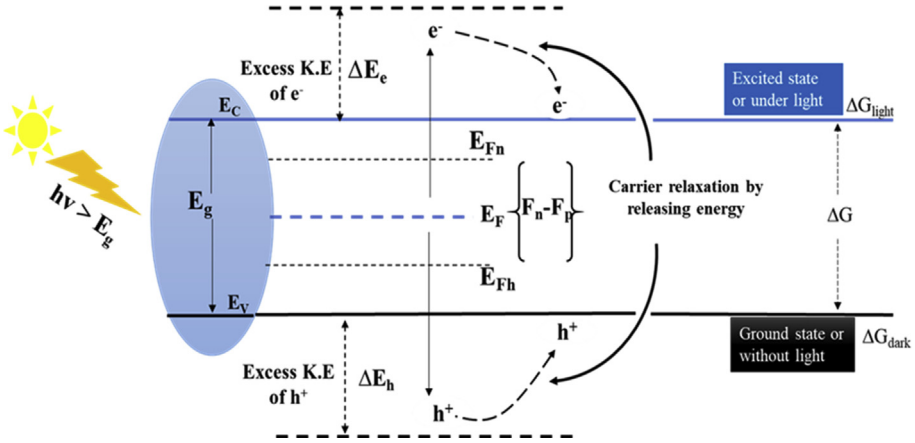

Fig. 2 – Thermodynamics and Gibbs free energy (G) of photocatalyst with light and without light [36].

(9) [35,36]. Under light irradiation with energy greater than Eg, the maximum thermodynamic driving force for electrons and holes to induce photocatalytic reactions are explained in Eq. (10). However, when semiconductor is at thermal equilibrium ($\Delta H = 0$), ΔG becomes zero resulting in zero net force to derive photocatalytic reaction. This indicates that heat is not driving force for the generation of electrons–holes pairs. Thus, for photo-catalysis, energy of reaction is Gibbs free energy (ΔG) supplied by light irradiations to derive photoreaction.

$$F_n = E_c + k_B T \ln \frac{n}{N_c} \quad (8)$$

$$F_p = E_v + k_B T \ln \frac{n}{N_v} \quad (9)$$

$$\Delta G = -|F_n - F_p| = -E_g - k_B T \ln \frac{np}{N_v N_c} \quad (10)$$

where E_c and E_v are CB minimum and VB maximum energy level positions, k_B = Boltzmann constant, T is absolutely temperature, N_c and N_v are effective densities of states in CB and VB, n and p are carriers concentration of electrons and holes, respectively.

The efficiency of semiconductors is greatly affected by its band gap and the type of light irradiation. Fig. 3(a) illustrated the narrowing and expansion of bandgap of semiconductors. There are two types of light irradiations i.e., UV-light which have wavelength between 200 and 400 nm, while visible light has wavelength between 400 and 800 nm. When the band gap is wider, the wavelength of light absorption is decreased. Therefore, the semiconductor with higher band than 3.15 eV is only activated under UV light irradiation, whereas visible light could activate the semiconductor with band gap lower than 3.15 eV. Therefore, sensitivity of semiconductor towards the light irradiation depends on its band gap energy for water splitting process.

Besides the width of band gap, the performance of photo-catalyst is affected by level of CB and VB. There are two important requirements to attain maximum photocatalytic activity. First, the band gap must be 1.23 eV < Eg < 3.26 eV and can be compared with the band gap structures of several typical photo-catalysts as presented in Fig. 3(b) [28,37–40]. TiO_2 has most positive VB level (2.7 eV vs NHE at pH 7) and a wide band gap (3.2 eV). Thus, to utilize more visible light, the band gap should be further narrowed by modifying the photocatalyst. Whereas, g-C_3N_4 has narrow band gap with 2.7 eV and response to visible light irradiation. Second, the reduction and oxidation potential must be within the band gap of photocatalyst to produced desired products [18,26]. The oxidation and reduction potentials of several typical species have been listed in Table 1. The band positions should be located as follows: the bottom of the CB should be more negative than the redox potential of H^+/H_2 (−0.41 eV vs NHE at pH 7) and the top of the VB should be more positive than the redox potential of O_2/H_2O (+0.82 eV vs NHE at pH 7) [31]. Using single semiconductor with less negative CB, it will have lower ability for reduction reaction and thus its combination with other semiconductors having more negative CB would enable transfer of electrons for the reduction of H^+ to H_2 on the adjacent semiconductor. When, TiO_2 is utilized as a catalyst for water splitting at pH 7, the water oxidizes into H^+ and O_2 through Eq. (15). Then, the H^+ and O_2 produce H_2 and $HO_2^{\bullet}$, since CB of TiO_2 is much closer to reactions in Eqs. (11) and (13), respectively. The intermediate $HO_2^{\bullet}$ reduces to H_2O_2 and finally producing H_2O through multiple reduction processes as shown in Table 1. Then, H_2O is reused in the oxidation reaction. Hence, the efficiency of H_2 production depends on the types of semiconductors, pH of the reaction system, and thermodynamic reduction potentials of the reactions.

Advancements in photocatalysts for water splitting

Titanium dioxide (TiO_2) based photo-catalysts

The significant properties of the semiconductor of photocatalytic system are desired band gap, suitable morphology, high surface area and stability. Titanium dioxide (TiO_2) is the first semiconductor employed for photocatalytic activity by Fujishima and Honda [8]. Recently, TiO_2 has attracted much attention and is the most investigated photocatalyst credited to long-term stability, great absorption and photo-produced charge separation properties [42]. Anatase TiO_2 is more

Please cite this article as: Fajrina N, Tahir M, A critical review in strategies to improve photocatalytic water splitting towards hydrogen production, International Journal of Hydrogen Energy, https://doi.org/10.1016/j.ijhydene.2018.10.200

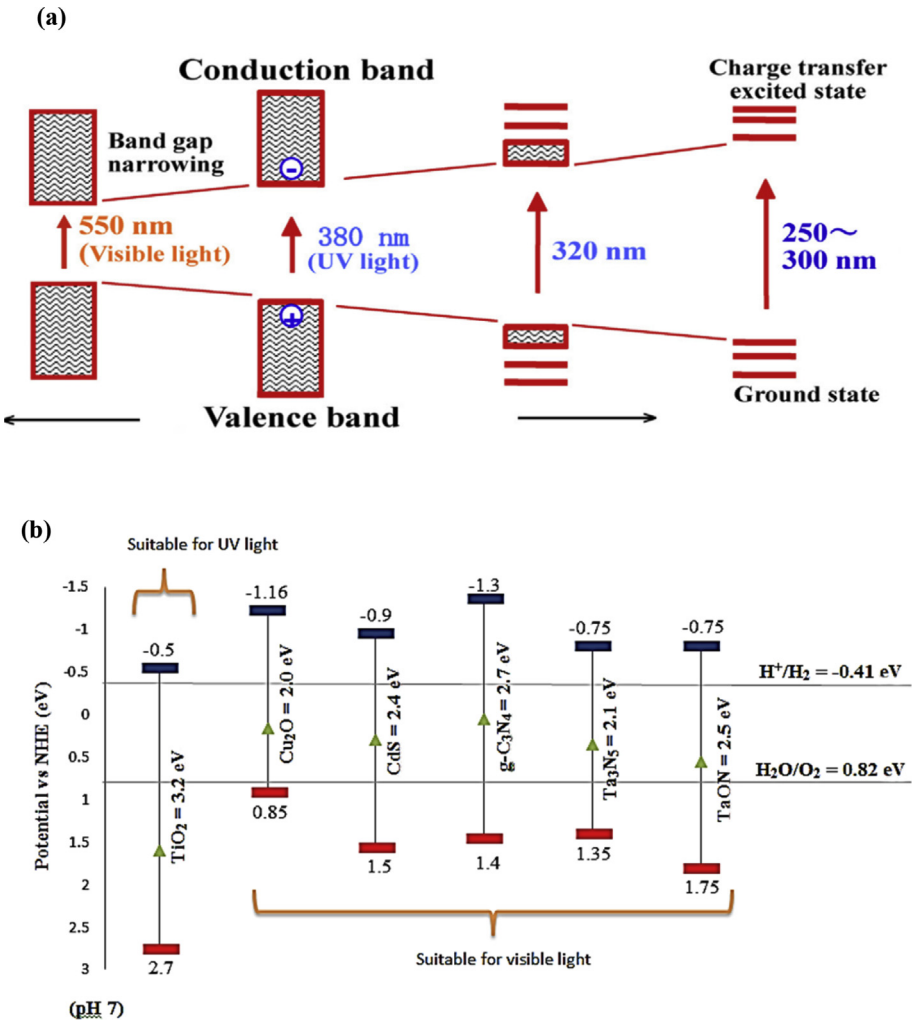

Fig. 3 – (a) Narrowing and expansion of bandgap of semiconductors; and (b) Band gap structures of several typical photocatalysts [28,37–40].

Table 1 – Standard oxidation and reduction potential for some species [28,41].

Reaction	E°(V) vs NHE at pH 7	
$2H^+ + 2e^- \rightarrow H_2(g)$	−0.41	(11)
$O_2(g) + e^- \rightarrow O_2^-(aq)$	−0.74	(12)
$O_2(g) + H^+ + e^- \rightarrow HO_2^{\bullet}(aq)$	−0.456	(13)
$O_2(g) + 2H^+ + 2e^- \rightarrow H_2O_2(aq)$	0.285	(14)
$2H_2O(aq) + 4h^+ \rightarrow O_2(g) + 4H^+$	0.819	(15)
$OH^- + h^+ \rightarrow {}^{\bullet}OH$	2.28	(16)
$O_3(g) + 2H^+ + 2e^- \rightarrow O_2(g) + H_2O$	1.665	(17)
$H_2O_2(aq) + H^+ + e^- \rightarrow H_2O + OH^-$	0.73	(18)
$HO_2^{\bullet} + H^+ + e^- \rightarrow H_2O_2(aq)$	1.03	(19)
$H_2O_2(aq) + 2H^+ + 2e^- \rightarrow 2H_2O$	1.353	(20)

favorable than rutile and brookite as it has better performance for photocatalytic H_2 production [43]. TiO_2 with anatase has appropriate band gap (3.2 eV) than brookite (3.4 eV), in addition of higher kinetic stability than rutile under ambient conditions [30]. It is also one of the most guaranteeing photocatalyst as a result of its excellent photocatalytic performance, easy accessibility, non-toxicity, and low price [3,44].

However, TiO_2 catalyst has limitation to maximize the photocatalytic activity due to faster charge recombination rate. Also, it can be mainly activated by UV light, which makes up only 4–5% of solar spectrum [45]. For water splitting under visible light, photo-catalysts must have narrow band gap, stable under photo irradiation and possess suitable CB and VB for H_2 generation using single photocatalyst [18]. The catalyst can exhibit stability when the photoelectron ready for the reduction reaction over the surface and the photo-generated transient electrons highly energetic with high reduction capability [46]. In order to enhance the performance of photocatalytic activities particularly for visible light irradiation, several methods on TiO_2 have recently been proposed and investigated. Recent developments on TiO_2 modifications include metal modified TiO_2, non-metal modified TiO_2, semiconductors coupling to TiO_2 and ternary TiO_2 photocatalysts.

Metal modified TiO_2

Regarding metal doping, the efficiency of photocatalyst is related to the metals work function value (ϕ), energy required to transfer electron from Fermi level into vacuum (the higher ϕ, the lower Fermi level energy) [47]. The greater the difference

Please cite this article as: Fajrina N, Tahir M, A critical review in strategies to improve photocatalytic water splitting towards hydrogen production, International Journal of Hydrogen Energy, https://doi.org/10.1016/j.ijhydene.2018.10.200

of metals work function with semiconductor, the higher the Schottky barrier, leading to increase H_2 production rate. Schottky barrier is the electronic potential barrier developed simply by the band alignment at the metal–semiconductor heterojunction, which consequently increased efficiency regarding photo-generated electrons to be transferred and trapped with the metal. Therefore, the Fermi level must be lower in energy than the CB of the semiconductor, while migrated electrons can be captured by the metals, whereas holes remained in the TiO_2 valence band [29]. Hence, modification of semiconductor with metals can enhanced the performance of water splitting to be effective and functional under visible light irradiation.

Several metals such as Pt, Au, Ag, Ni and Pd have been investigated in recent years. Metal loading onto TiO_2 has become the most widely applied surface modification method for suppressing the recombination of photo-generated electron–hole pairs. Metal as a co-catalyst to trap electrons provides additional site reactions on the catalyst surface. The schematic of charge transfers for metal/TiO_2 under UV light irradiation due to the existence of the Schottky junction has been illustrated in Fig. 4(a). Basically, when loading metal nanoparticles (NPs) on the TiO_2, Schottky barrier can be formed and the Fermi levels of the metal NPs is lower than the CB of the TiO_2. The photo-generated electrons will transfer from CB of TiO_2 to metal NPs through Schottky barrier right up until their Fermi levels are equal and holes will certainly remain on the VB of TiO_2. Thus, the spatial separation of photogenerated electron–hole pairs can be attained. Furthermore, the work function of metals also takes an important part in limiting the electron–hole pairs separation over the semiconductor surface. In particular, the electron–hole pairs separation can be enhanced by increasing work function of metals, which improves the electron accepting ability of the metal [48].

The photocatalysis process can also be improved using noble metal nanoparticle doped TiO_2 through surface plasmon resonance (SPR) effect. In this perspective, noble metals such Pt, Au, and Ag have strong surface plasmon band in the visible range. The schematic of photogenerated charge transfer for metal/TiO_2 under visible light irradiation due to the surface plasmon resonance (SPR) effects was illustrated in Fig. 4(b). The hot photogenerated electrons contained in localized surface plasmon resonance (LSPR) of metal can efficiently be transferred to the CB of TiO_2 by direct electron transfer (DET) under visible light irradiations, when they are directly in contact with the semiconductor and undergoes reduction reactions at the semiconductor surface [23].

Recently, Rather et al. [49] reported that the SPR effect of Ag, which doped on TiO_2, was found to be decisive for the high photocatalytic activity to produce H_2 from water as shown in Fig. 4(c). The experimental recorded Ag/TNR has highest rate for H_2 production with 90 and 105 μmol after 8 h at 457 nm and under sunlight, respectively. As shown in Fig. 4(d), when the nanostructure is irradiated with the matching SPR wavelength (457 nm or sunlight) the Ag NPs are activated, which shift their local electric field effect towards the TNR interface resulting in the transfer of electrons towards the CB of TNR due to the formation of Schottky barrier. Zhu et al. [50] reported that Pt/TiO_2(hollow sphere) is a promising photocatalyst to efficiently generate H_2 at room temperature and proposed mechanism for H_2 evolution over Pt/TiO_2 as illustrated in Fig. 4(e). As shown in Fig. 4(f), the average H_2 produced for 1.0 wt%Pt/TiO_2 reached 1023.71 μmol h^{-1} g^{-1} after 5 h of irradiation, and did not show significant deactivation after 30 h irradiation. Table 2 shows recent progress on metal loading on TiO_2 for photocatalytic water splitting. Metals such as Ag, Pt and Au were attracted among the researchers due to the SPR effect under visible light irradiation. It can be concluded that metal loading is an efficient approach to improve TiO_2 performance for photocatalytic H_2 production by transfer of electron to metal or semiconductor and followed by reducing the electron–hole recombination rate.

Non-metal modified TiO_2

For non-metal doping, anion will boost the visible-light photocatalytic performance in a semiconductor and is a relatively new method compared to other techniques. When the semiconductor is doped with non-metal, the band gap became narrow and caused the hybrid 2p band produced by non-metal in between the CB and VB of a semiconductor. Under visible light irradiation, the electrons were transferred to the intermediate 2p band from VB of semiconductor and then, excited to the CB from the intermediate band to produce H_2. This electron excitation process requires lower energy and also hindered charges recombination [77]. Improved visible-light absorption has been observed using variety of anions (N, F, C, S, etc.) doped TiO_2 [142]. Non-metal dopants were found to be more efficient compared to most of the metal ions due to the less formation of charge recombination centers and narrowing the band gap energy, thus highly responsive to visible light irradiations [78]. Wang et al. [79] recorded the use of N-doped TiO_2 with 4.91% nitrogen contents which leads to narrow optical band gap to 2.65 from 3.20 eV. As shown in Fig. 5(a), the H_2 production rate of the N-TiO_2 film is about 601 μmol g^{-1} h^{-1} higher than the un-doped TiO_2 film. Wang et al. [80] observed an enhanced TiO_2 efficiency by the use of non-metal ions with (211) orientation is an effective route to enhance the activity of TiO_2-based catalyst in water splitting as shown in Fig. 5(b). This is because (211) facets can destabilize O_2p states on the TiO_2 surface, thus water can be easily absorbed and be dissociated. When water molecules are dissociated, the electron transfer would be more effective to reduce H^+ to H_2. It was detected that the H_2 rates of N-doped TiO_2 was increased from 760 μmol m^{-2} h^{-1} to 4500 μmol m^{-2} h^{-1}. Similarly, Li et al. [81] found that the H_2 production improved from 0.73 mmol h^{-1} g^{-1} to 2.98 mmol h^{-1} g^{-1} using N-doped titania with optimal ethylenediamine to sol volume ratio 1:1 as shown in Fig. 5(c). Xing et al. [82] recorded the synthesis of in-situ S-doped porous anatase TiO_2 nanopillars and produced 163.9 μmol h^{-1} g^{-1} of H_2 evolution under optimum temperature. By implying the S-doped TiO_2, the band gap of TiO_2 can be reduced and is favorable for visible-light adsorption towards improvement of photon utilization, thus increase the photocatalytic performance as shown in Fig. 5(d). Hence, previous research proved that non-metal doping is another important strategy to narrow the band gap of a semiconductor for visible light absorption with enhanced H_2 production.

Please cite this article as: Fajrina N, Tahir M, A critical review in strategies to improve photocatalytic water splitting towards hydrogen production, International Journal of Hydrogen Energy, https://doi.org/10.1016/j.ijhydene.2018.10.200

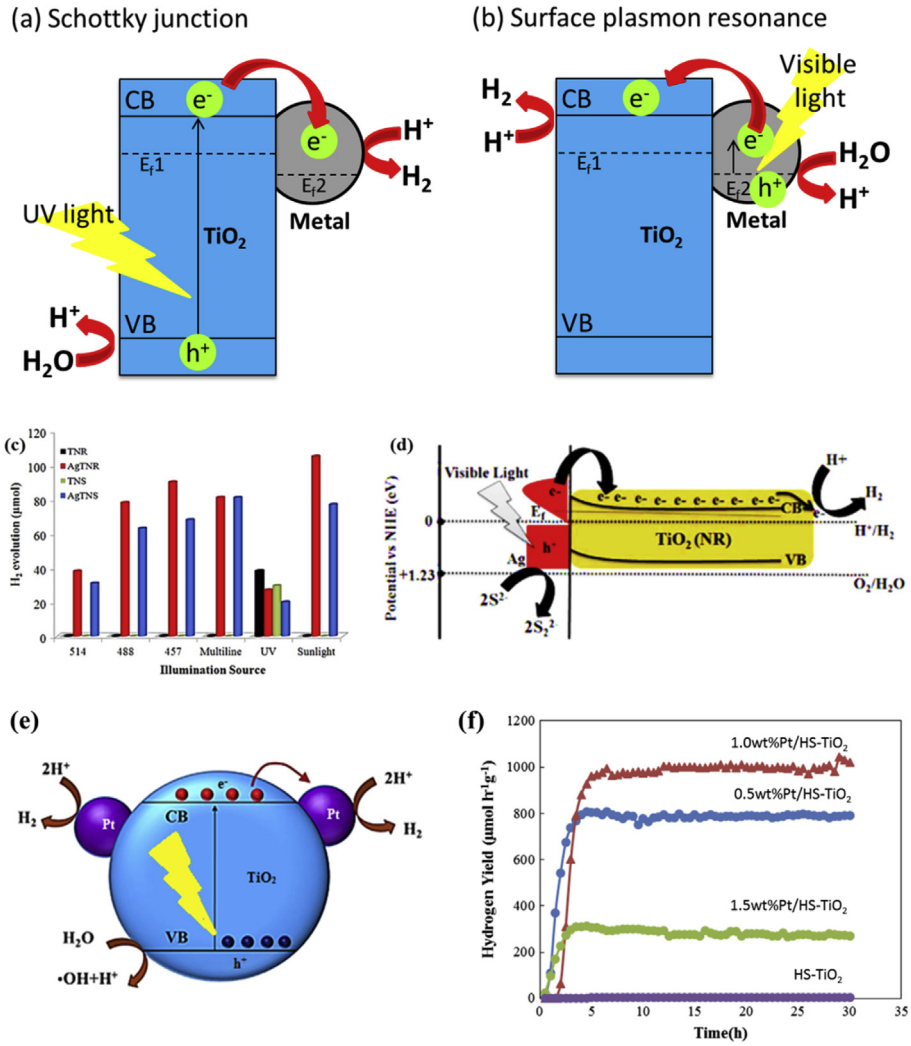

Fig. 4 – (a) Schematic of charge transfer for metal/TiO_2 under UV light irradiation due to the existence of the Schottky junction; (b) Schematic of charge transfer for metal/TiO_2 under visible light irradiation due to the surface plasmon resonance (SPR) effects; (c) Hydrogen evolution under different monochromatic and UV wavelengths by different photocatalysts; (d) Scheme of Water Splitting using AgTNR; (e) Mechanism of H_2 evolution by water splitting over an Pt/HS-TiO_2 photocatalyst; and (f) Photo catalytic H_2 evolution over Pt/TiO_2 [49,50,318].

Semiconductors coupling TiO_2

The photocatalytic water splitting for hydrogen production using pure TiO_2 is low even under UV–visible light irradiation due to fast charge recombination. However, coupling TiO_2 with binary composites (e.g., WO_3, SiO_2, Al_2O_3, SnO_2 CdS, PbS, Bi_2S_3) and also transition metal oxide (e.g., Cu_2O, Fe_2O_3, Zno, NiO) can produce better results due to their surface area, lowering band gap, ability to utilize visible light, absorption ability and stability [83]. The heterojunction can improve performance by coupling wide band gap with narrow band gap semiconductors to make functional under visible light with faster charges separation. In Fig. 6(a), Lakshmana et al. [84] reported the use of Bi_2O_3 clusters immobilized on anatase TiO_2 nanostructures to enhance H_2 evolution and BT-2 photocatalyst, 10 and 6 folds higher H_2 production rate than using TNP and TNS. This is because photo-excited electrons migrated to TNS surface was effectively captured by Bi_2O_3 clusters where reduction of H^+ ions to H_2 gas took place as shown in Fig. 6(b). Bi_2O_3 in BT-2 acts as a co-catalyst that facilitated the high rate of H_2 production. Fujita et al. [85] reported that as semiconductor loading increased, the band gap (E_g) value was decreased and thus the rate of H_2 production tends to increase with a decrease in Eg value as shown in Fig. 6(c) and (d). Table 3 summarized the literature of semiconductors coupling TiO_2 based photo-catalysts with their heterojunctions. It reveals that to create coupled colloidal structures in which illumination of one semiconductor produces a response in the second semiconductor at the interface makes it possible to be active under visible light irradiations. Coupling semiconductor photocatalysts exhibits very high photocatalytic activity by inhibiting charge recombination and extending the energy range of photo-excitation.

Ternary TiO_2

Ternary photocatalyst consists of three different elements or semiconductors with different functions by three steps

Please cite this article as: Fajrina N, Tahir M, A critical review in strategies to improve photocatalytic water splitting towards hydrogen production, International Journal of Hydrogen Energy, https://doi.org/10.1016/j.ijhydene.2018.10.200

Table 2 – Metal modified TiO_2 based photo-catalysts for H_2 production.

Year	Catalyst	Reactor/Parameter	Products	Ref.
2019	Au/TiO_2	300 W Xe lamp	3550 μmol g^{-1} h^{-1}	[51]
2018	Ni/TiO_2	Pyrex reactor 100 W SB-100P/F lamp ($\lambda = 365$ nm)	26,000 μmol g^{-1} h^{-1}	[52]
2018	Fe/TiO_2	Pyrex glass 300 W Xe arc lamp	174.3 μmol g^{-1} h^{-1}	[53]
2018	Ag/TiO_2	Hg vapor lamp ($\lambda = 365$ nm)	910 μmol g^{-1} h^{-1}	[54]
2018	Cu/TiO_2	300 W Xenon lamp ($\lambda = 420$ nm)	28,700 μmol g^{-1} h^{-1}	[55]
2018	K/TiO_2	300 W Xe lamp	740 μmol g^{-1} h^{-1}	[56]
2018	Au/TiO_2	300 W Xe lamp	4900 μmol g^{-1} h^{-1}	[57]
2018	Au/TiO_2	Quartz reactor 300 W Xe lamp– UV light	11595.6 μmol g^{-1} h^{-1}	[58]
2018	Pd/TiO_2	Pyrex glass 400 W Xe arc lamp	38 mL g^{-1} h^{-1}	[59]
2018	Au/TiO_2	Pyrex reactor SB-100P/F lamp (100 W, 365 nm)	30,300 μmol g^{-1} h^{-1}	[52]
2017	Au/TiO_2	Visible light, $\lambda = 420$ nm	924 μmol h^{-1} g^{-1}	[60]
2017	3 wt%Ag-TiO_2	400 W Hg vapor lamp – UV light	7030 mmol h^{-1} g^{-1}	[61]
2017	Au/TiO_2	Quartz reactor 150 W CERAMIC-Metal-Halide Lamp (solar light simulation)	500 μmol h^{-1} g^{-1}	[62]
2017	Au/TiO_2	Quartz reactor UV light – HeCd laser ($\lambda = 325$ nm)	125 μL h^{-1} cm^{-2}	[63]
2017	AgTNR	Monochromatic wavelengths (457 nm, 487 nm, 514 nm), and sunlight irradiation for 8 h	90 μmol (457 nm) 105 μmol (sunlight)	[49]
2017	0.5 wt% Pt/TiO_2	125 W Hg lamp	ca. 5.5 s^{-1}	[64]
2017	1 wt% Pt/TiO_2	125-W high-pressure mercury lamp	9.92 mmol	[65]
2016	Ag/TiO_2	250 W Xenon arc lamp	200 μmol g^{-1} h^{-1}	[66]
2016	Pt/TiO_2	Pyrex reactor 400 W mercury lamp ($\lambda < 420$ nm)	1023.71 μmol g^{-1} h^{-1}	[50]
2016	Ag/TiO_2	Pyrex reactor 300 W Xenon lamp ($\lambda > 420$ nm)	40 μmol g^{-1} h^{-1}	[67]
2015	Au/TiO_2	Borosil reactor 300 W power UV–vis (AIM 1.5 filter) and visible ($\lambda > 400$ nm)	307 μmol g^{-1} h^{-1} (UV) 66 μmol g^{-1} h^{-1} (vis)	[68]
2015	1 wt% Pd/TiO_2	UV, $\lambda = 365$ nm	47.5 mmol g^{-1} h^{-1}	[69]
2015	2 wt% Au/TiO_2	100 W F lamp, $\lambda = 365$ nm – UV light	32.4 mmol g^{-1} h^{-1}	[70]
2015	TiO_2Ag-F; 4.5%Ag	Quartz reactor 250 W UV-filtered mercury lamp	180 mmolH_2 $gcat^{-1}$	[71]
2015	1.5 wt% Au/TiO_2 (P25)	Spectroline model SB-100P/F lamp – UV light	27.9 mmol g^{-1} h^{-1}	[72]
2015	2.1 wt%Pt/TiO_2	3 Philips Solarium lamps (4 × 15 W each) fluorescent tubes	1134 μmol h^{-1}	[73]
2014	1.0 wt%Pt/TiO_2	300 W Xe arc lamp, $350 < \lambda < 400$ nm	10.5 mmol h^{-1} $gcat^{-1}$	[42]
2014	0.8 wt% Au/TiO_2	Solarium Philips HB175 lamps 4 × 15 W Philips CLEO florescent tubes	1542.9 μmol h^{-1}	[74]
2014	1 wt%Pt-TiO_2	Osram Ultramed 400 W – UV light	7.2 mmol h^{-1} g^{-1}	[75]
2014	Cu-doped TiO_2 film	300 W Xe lamp	810 μmol g^{-1} h^{-1}	[76]

method. Based on the literature, it could be expected that ternary semiconductor composites provide an opportunity for multi (two)-photon excitation of photoactive materials with lower energy photons and utilization of heterojunction to drive electronic processes in the desired direction. Consequently, the selective photo-excitation of localized electronic states to gain better selectivity can be achieved [104]. Previously, Xie et al. [105] reported Pt/TiO_2–ZnO (Ti/Zn = 10) as an effective catalyst for water splitting for H_2 production with maximum hydrogen rate 2150 μmol h^{-1} g^{-1} and improved stability as shown in Fig. 7(a). The ternary photocatalyst mechanism for H_2 production is shown in Fig. 7(b). When Pt/TiO_2–ZnO is irradiated, electrons may be excited from the VB to the CB on the TiO_2–ZnO and Pt nanoparticles act as electrons traps to produce H_2. In 2016, Zhao et al. [106] concluded that CdS and AuNPs not only makes up for the UV light responsive weakness of TiO_2 but also enhances the separation of photo-generated charges. The AuNPs existing between TiO_2 and CdS is to accelerate the transfer of photo-generated electrons and produce more active sites for H_2 production under visible light, the photogenerated electrons of CdS transferred to the CB of TiO_2 via AuNPs while under UV light, the photogenerated electrons of TiO_2 are transferred to the VB of CdS and recombine with holes as shown in Fig. 7(c). Table 4 summarizes the ternary TiO_2 based photo-catalysts used for H_2 production. From the above discussion, mostly ternary composite contains heterojunction of two semiconductors and deposited with metal. It is obvious that doping metal to TiO_2 can enhance H_2 production rate significantly by trapping and accelerating the electron transfer. The coupling of TiO_2 with other narrow band gap semiconductors could also enhance its visible light activity because photo-generated electrons could be migrated into TiO_2, resulting in more charge separation.

Please cite this article as: Fajrina N, Tahir M, A critical review in strategies to improve photocatalytic water splitting towards hydrogen production, International Journal of Hydrogen Energy, https://doi.org/10.1016/j.ijhydene.2018.10.200

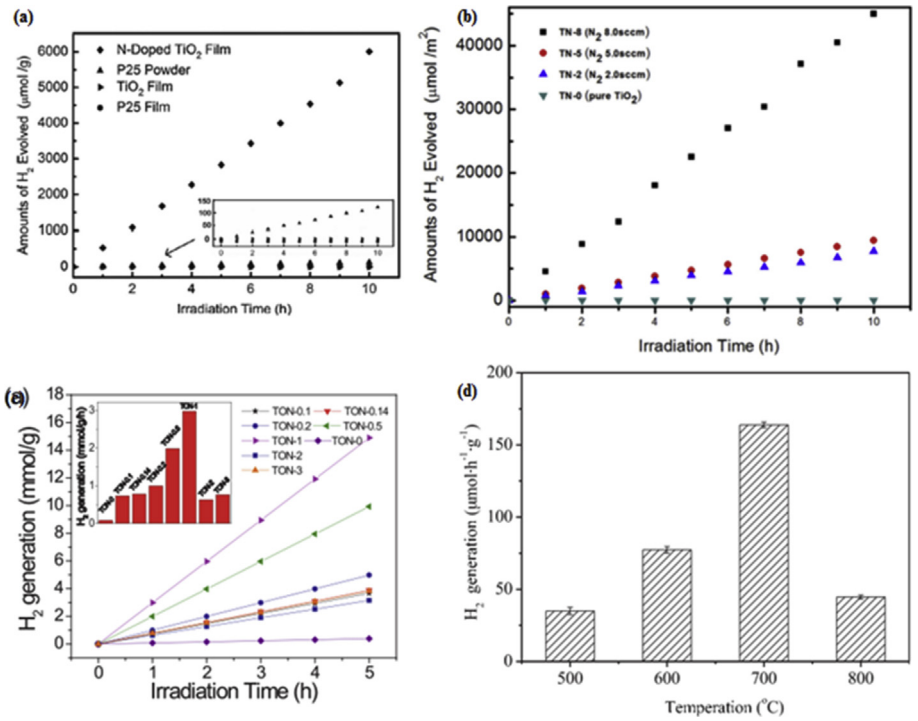

Fig. 5 – (a) Hydrogen evolution profiles of N-doped TiO_2 film; (b) Hydrogen evolution profiles of N-doped TiO_2; (c) H_2 generation on different samples sintered at 500 °C; and (d) Visible-light photocatalytic hydrogen evolution of S-TiO_2 samples prepared [79–82].

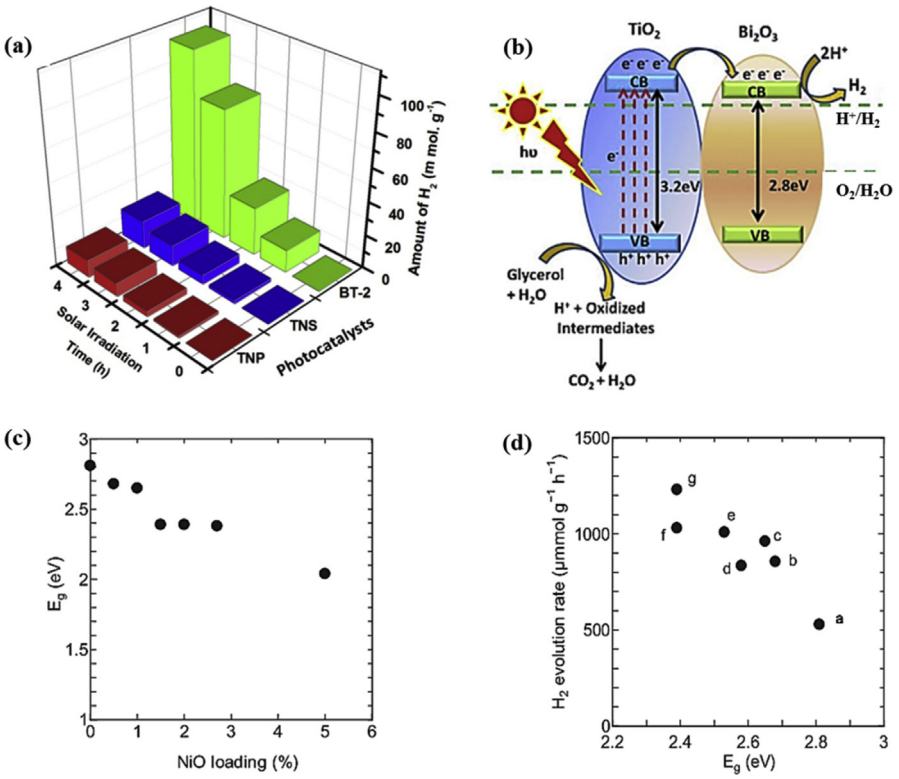

Fig. 6 – (a) Solar photocatalytic activity of Bi_2O_3-TNS Photocatalysts; (b) Reaction mechanism of Bi_2O_3@TiO_2 photo catalyst under solar irradiation; (c) Influence of NiO loading on the band gap energy, E_g, of NiO/TiO_2 samples; and (d) Plot of the rate of H_2 evolution against the band gap energy [84,85].

Please cite this article as: Fajrina N, Tahir M, A critical review in strategies to improve photocatalytic water splitting towards hydrogen production, International Journal of Hydrogen Energy, https://doi.org/10.1016/j.ijhydene.2018.10.200

Table 3 – Semiconductor coupled TiO_2 based photocatalysts for H_2 production.

Year	Catalyst	Reactor/Parameter	Product	Ref
2019	MoS_2/TiO_2	Pyrex reactor 300 W Xe arc lamp	2160 μmol h^{-1} g^{-1}	[86]
2019	MoS_2/TiO_2	300 W Xe arc lamp	8.43 μmol cm^{-2} h^{-1}	[87]
2019	TiO_2/g-C_3N_4	Pyrex reactor 300 W Xe arc lamp	808 μmol h^{-1} g^{-1}	[88]
2018	CdS/TiO_2	Sun irradiation	68,000 μmol h^{-1} g^{-1}	[89]
2018	CdS/TiO_2	Pyrex reactor 300 W Xe lamp, $\lambda > 400$ nm	128.3 mmol g^{-1} h^{-1}	[90]
2018	Co_3O_4/TiO_2	300 W Xe lamp	41.8 μmol g^{-1} h^{-1}	[91]
2018	Cu_2O/TNAs	Quartz reactor 300 W Xe lamp, $\lambda > 400$ nm	2142 μmol m^2 h^{-1}	[92]
2018	g-C_3N_4/TiO_2	300 W Xe lamp, $\lambda > 420$ nm	513 μmol g^{-1} h^{-1}	[93]
2018	g-C_3N_4/TiO_2	300 W Xe lamp	13.8 mmol h^{-1} m^{-2}	[94]
2017	rGO/TiO_2	Pyrex reactor 300 W Xe lamp, $\lambda > 300$ nm	720 μmol h^{-1} g^{-1}	[95]
2017	CdS/TiO_2	Quartz reactor 300 W Xe lamp, $\lambda = 420$ nm	678.61 μmol h^{-1} g^{-1}	[96]
2017	Bi_2O_3@TNS	Light intensity 1.15 ± 0.10 × 10^5 lx	26.02 mmol h^{-1} g^{-1}	[84]
2016	10 wt% ZnO-TiO_2	Hg lamp l ¼ 254 nm – UV illumination	1048 μmol h^{-1}	[97]
2016	2 wt% NiO-loaded TiO_2	500 W Hg lamp	1230 μmol h^{-1} g^{-1}	[85]
2015	2.5-Cu_2O/TiO_2	500 W Xe arc lamp, $\lambda = 365$ nm	2048.25 μmol h^{-1} g^{-1}	[98]
2015	0.25 wt% NiO/TiO_2	Pyrex reactor 300 W Xenon lamp	337 μmol h^{-1} g^{-1}	[99]
2014	rGO/TiO_2	150 W Hg-Xe lamp	127.5 μmol cm^{-2} h^{-1}	[3]
2014	$NiFe_2O_4$@TiO_2	UV-lamps, $\lambda = 365$ nm	18.5 mL of H_2	[100]
2014	RGO/TiO_2	Quartz flask 3 W, $\lambda = 365$ nm – UV-light	203 μmol h^{-1}	[101]
2013	TiO_2/CuO	Pyrex reactor 500 W Xe lamp	8.23 mmol h^{-1} g^{-1}	[102]
2012	10 wt% ZnO-TiO_2	Pyrex reactor Hg lamp, $\lambda = 254$ nm	12,970 μmol h^{-1} g^{-1}	[103]

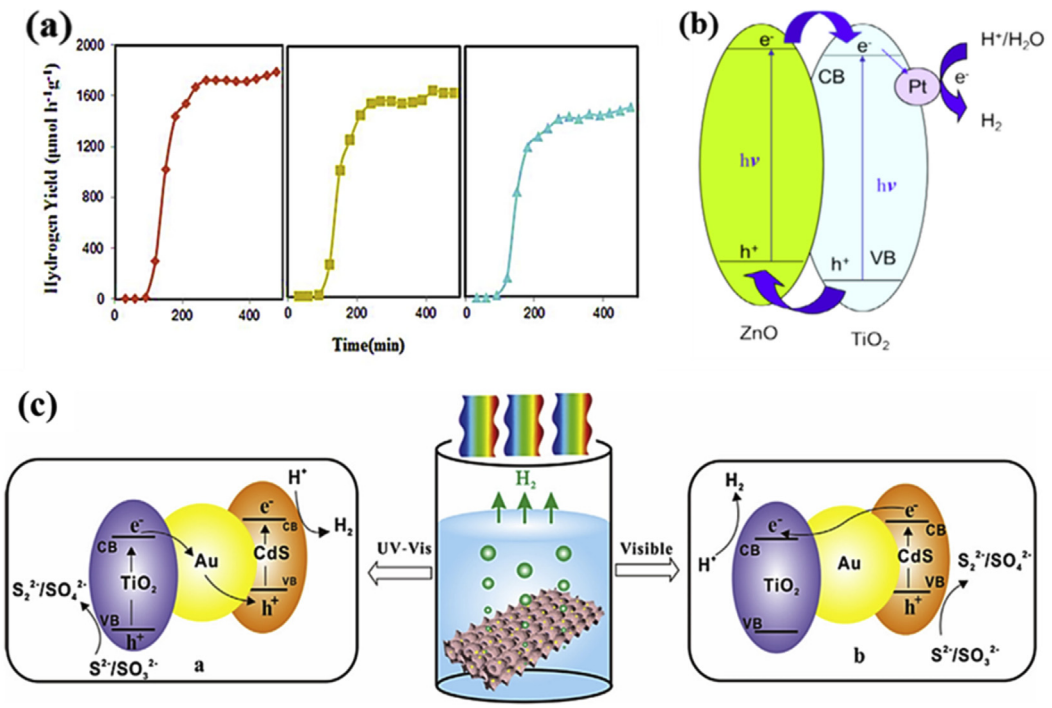

Fig. 7 – (a) Re-use of photocatalysts of 0.1 wt% Pt/TiO_2–ZnO; (b) Illustration of hydrogen production of water splitting on Pt/TiO_2–ZnO; and (c) Illustrates the two different internal electron-transfer processes under UV–visible light and visible light irradiation, respectively [105,106].

Table 4 – Ternary TiO_2 based photo-catalysts for H_2 production.

Year	Catalyst	Reactor/Parameter	Product	Ref.
2019	$Ti_3C_2(TiO_2)$@CdS/MoS_2	Pyrex reactor 300 W Xe lamp, $\lambda \geq 420$ nm	344.74 μmol h^{-1} g^{-1}	[107]
2019	N/Au/TiO_2	300 W Xe lamp	4880 μmol h^{-1} g^{-1}	[51]
2019	Cu-TiO_2/porphyrin	300 W Xe lamp	1300 μmol h^{-1} g^{-1}	[108]
2019	MWCNTs/TiO_2/MMT	Pyrex reactor 35 W HID Xenon lamp	1888 μmol g^{-1} h^{-1}	[16]
2018	F-Pt-TiO_2	Pyrex Reactor UV light	58.9 μmol g^{-1} h^{-1}	[109]
2018	Pt-WO_3-TiO_2	UV light (LED Opsytec, $\lambda = 365$ nm)	5.2 μL h^{-1} cm^{-2}	[110]
2018	Cu/TiO_2/Ti_3C_2	300 W Xe lamp	860 μmol h^{-1} g^{-1}	[111]
2018	MoS_2/CdS/TiO_2	Pyrex reactor 300 W Xe lamp, $\lambda < 400$ nm	4146 μmol h^{-1} g^{-1}	[112]
2018	TiO_2/WO_3@MoS_2	Quartz reactor 300 W Xe arc lamp	273.69 μmol h^{-1} g^{-1}	[113]
2018	g-C_3N_4-TiO_2/rGO	Borosilicate reactor 250 W Xenon lamp, 200 nm $< \lambda <$ 800 nm	23,143 μmol g^{-1} h^{-1}	[114]
2018	TiO_2/rGO/Pt	4 Philips PL-S (9 W) lamp, 315 $< \lambda <$ 400 nm	259.12 μmol g^{-1} h^{-1}	[115]
2017	1.0 mol% Bi_2O_3-QDS-TiO_2	3 W UV-LEDs, $\lambda = 365$ nm	920 μmol h^{-1} g^{-1}	[116]
2017	Pt-TiC@C-TiO_2	300 W Xe lamp – Visible light	558.46 μmol g^{-1}	[117]
2017	10 mg of COP	300 W Xe-lamp (Microsolar300)	15.02 mmol h^{-1} g^{-1}	[118]
2017	0.5 wt% Pt/TiO_2–ZnO (Ti/Zn = 10)	400 W mercury arc lamp, $\lambda > 400$ nm	2150 μmol h^{-1} g^{-1}	[105]
2017	Ir-C-N-TiO_2	250 W Xe lamp	6 mmol h^{-1} g^{-1}	[119]
2016	Pt-RuO_2-TiO_2	3 W LED lamp, $\lambda = 365$ nm (UV light)	4200 μmol g^{-1} h^{-1}	[120]
2016	3DOM TiO_2-Au-CdS	PLS-SXE-300C lamp Visible light, $\lambda = 420$–780 nm	1.81 mmol h^{-1} g^{-1}	[106]
2016	Cu/N/TiO_2	500 W halogen lamp, $\lambda_{max} = 630$ nm – visible 400 W halide lamp, $\lambda_{max} = 360$ nm – UV light	283 μmol g^{-1} h^{-1} (vis), 27.4 mmol g^{-1} h^{-1} (UV)	[121]
2014	PdO/Pt/N-TiO_2	400 W mercury lamp, $\lambda > 400$ nm	2460 μmol g^{-1} h^{-1}	[44]
2014	Au-Cu_2O/TiO_2	UV–PC mercury lamp, $\lambda = 254$ nm	2064 μmol g^{-1} h^{-1}	[122]
2014	Eosin Y/TiO_2/0.5 wt%Au	300 W Xenon lamp, $\lambda = 420$ nm	110.48 μmol h^{-1}	[123]

Graphitic carbon nitride (g-C_3N_4) based photo-catalysts

Graphitic carbon nitride (g-C_3N_4) has attracted much attention and intensively studied as a sustainable photocatalyst as a result of its advantages such as non-toxic and metal-free semiconductor together and responsiveness to visible light, which has narrow band gap (2.7 eV) [124]. Besides, it is low cost, simply consists of earth-abundant carbon and nitrogen and has exceptional photo corrosion resistance due to the strong covalent bonds between carbon and nitride atoms [125]. The g-C_3N_4 also has unique photoluminescence (PL) properties and can be used like a good co-catalyst for the semiconductor catalysts [126]. Unfortunately, the application of g-C_3N_4 in photocatalysis is restricted due to low specific surface area and high recombination rate of photo induced electron–hole pairs [127].

However, the loading of g-C_3N_4 with other semiconductors can boost the photocatalytic performance which promotes electron–hole separation, improving the specific surface area, and exploiting the light utilization ability [28]. The promising and efficient strategy is the coupling with other photo catalysts which can significantly improve the separation of electron–hole pairs as a result of well-matched band structures [128]. Therefore, many modification have been investigated in order to enhance the photocatalytic efficiency of g-C_3N_4 include coupling with other semiconductors [129] and innovation in configuration of g-C_3N_4 by template synthesis [130], thermal oxidation etching [131], liquid phase exfoliation [132], acidity treatment of precursor [133], and acid treatment of bulk g-C_3N_4 [134]. The recent development of g-C_3N_4 loading with metals, non-metals and coupling with semiconductor has been systematically discussed.

Metal doping

Doping is one of the effective strategies to tune electronic structures of g-C_3N_4 and accelerate the reaction surface in order to increase photocatalytic activity due to the work function and SPR effect as explained in previous section [135]. The deposition of metals onto semiconductor can provide active sites for better photocatalytic H_2 production. In addition, the fine control of spatial distribution and particles size of metal can provide sufficient active size and thus, maximize the light transmittance [136]. Modification of g-C_3N_4 induced more electron–hole pairs by extending the optical absorption range, thus producing more electrons for H_2 production [137]. As a Lewis base and filled with abundant nitrogen lone-pair electrons, g-C_3N_4 can coordinate with transitional metals to construct metal–N active sites in the covalent polymeric framework [138]. Improved visible-light absorption was observed for a variety of metals such as Ni and Cu, and noble metals such as Ag, Au and Pt. Bi et al. [139] studied the change of surface band on the performance of photo-catalyst, which was confirmed by the work function (WF) to enhance the photo-generated charges separation. As shown in Fig. 8(a), the

Please cite this article as: Fajrina N, Tahir M, A critical review in strategies to improve photocatalytic water splitting towards hydrogen production, International Journal of Hydrogen Energy, https://doi.org/10.1016/j.ijhydene.2018.10.200

WF of g-C_3N_4 and Ni was detected using a Kelvin Probe that offers the contact potential difference (CPD) between the samples and Au (5.1 eV). In Fig. 8(b), the energy level diagram shows the WF of g-C_3N_4 is 4.34 eV, which is lower than the Ni (4.86 eV). Then, the free electrons of g-C_3N_4 can be transferred to Ni until the Fermi levels of two semiconductors are aligned since the g-C_3N_4 is brought in contact with Ni, and leaded to an interface electric field orienting from g-C_3N_4 to Ni as shown in Fig. 8(c). For a typical n-type semiconductor, g-C_3N_4 has upward band bending and the degree of bending becomes deeper after being loaded with Ni. In addition, the data of WF measurements also suggest that the interfacial electric field is about 0.5 V and this interfacial electric field may partly be a driving force for the efficient hole-capturing effect of Ni, leading to better separation efficiency. It was concluded that photogenerated charge carriers recombination can be lower by Ni loading deepens on g-C_3N_4 surface band bending which be the factor to improve the photocatalytic H_2 production [139].

In 2017, Chen et al. [138] synthesized Co-g-C_3N_4 by one-step thermal poly-condensation using cobalt phthalocyanine (CoPc) and melamine as precursors. A good interaction between melamine and CoPc was observed and the results are shown in Fig. 8(d). Thus as shown in Fig. 8(e), it increased light response and maximized H_2 production rate with yield of 28.0 μmol h^{-1}, 3 times higher than using pure g-C_3N_4. Table 5 summarized the use of metals doping to g-C_3N_4 based photocatalysts for H_2 production. The noble metals such as Pt and Au are commonly deposited onto g-C_3N_4 in order to extent the visible light absorption ability and SPR effect. It is evident that metals loading to be very effective to enhance photo-catalysis process due to the Fermi levels of metal loading, which is lower than that of pure semiconductor. Therefore, photo-excited electrons can be transferred from the CB of semiconductor to the metal for H_2 evolution.

Heterojunction semiconductor

The g-C_3N_4-based semiconductors can enhance photocatalytic activity through formation of semiconductor heterojunctions. It could reduce the band gap and the formation of internal electrical field. Hence, it can significantly improves spatial charges separation and maximize the redox potential and ability of reactions [159]. The heterojunction semiconductors could also help to promote the water oxidation activity [160]. The commonly used semiconductors with g-C_3N_4 are TiO_2, NiS, and CdS. Under visible-light irradiation, Yin et al. [161] concluded that the photocatalytic activity of g-C_3N_4 for H_2 evolution was significantly enhanced by NiS_2 nanoparticles grown on the g-C_3N_4 surface. In Fig. 9(a), the research recorded the optimal loading of 2 wt% NiS_2 produces 4.06 mmol h^{-1} of H_2. The proposed principle of NiS_2/g-C_3N_4 for photocatalytic H_2 generation is shown in Fig. 9(b). The photo-generated electrons transferred from g-C_3N_4 to NiS_2, whereas NiS_2 co-catalyst can effectively suppress the recombination of charge photo-generated and acts as active sites for H_2 production. Wu et al. [162] demonstrated that the Ag_2O/g-C_3N_4 could achieve H_2 production, 274 times higher than that of pure g-C_3N_4. It is believed that Ag_2O/g-C_3N_4 could achieve the positive synergic effect for accelerating the separation of charge carriers, thus

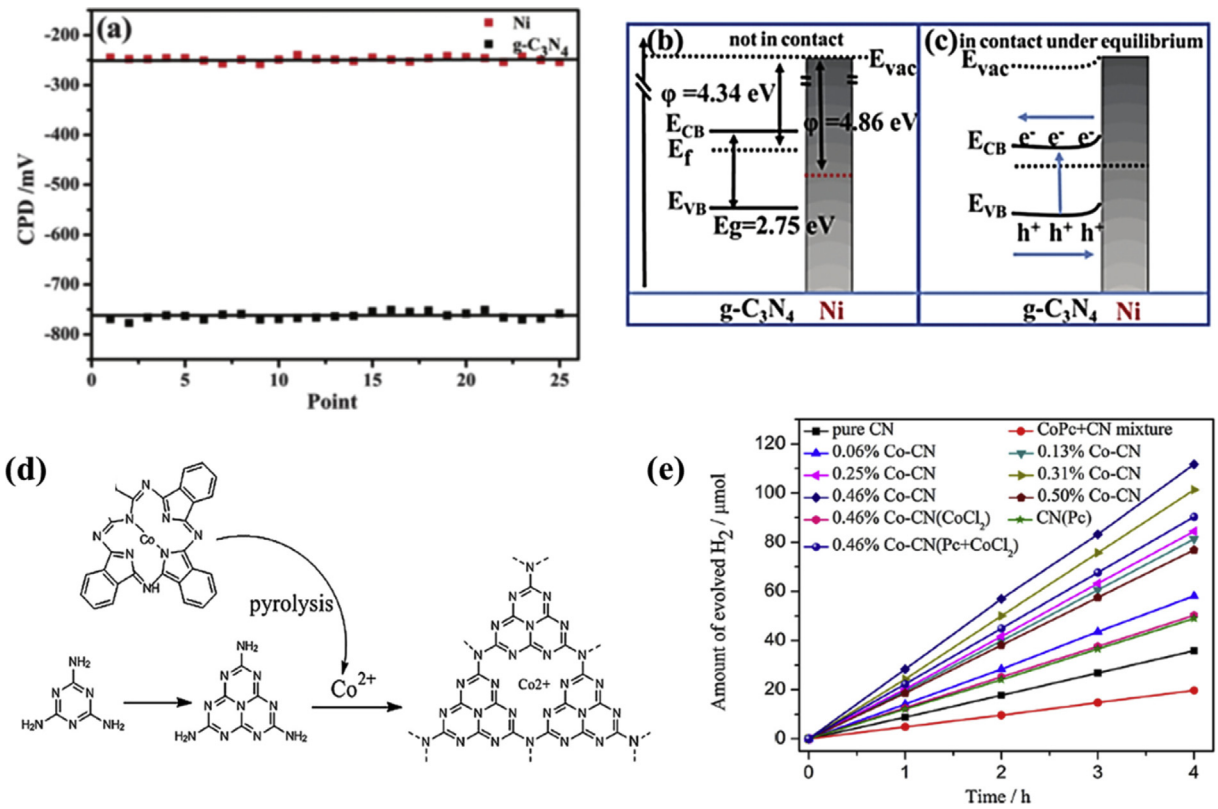

Fig. 8 – (a) The working function of g-C_3N_4 and Ni; (b) The energy level diagram of g-C_3N_4 and Ni; (c) The interfacial electron transfer between g-C_3N_4 and Ni under irradiation; (d) Schematic illustration of preparation of cobalt-doped g-C_3N_4; and (e) Photocatalytic H_2 evolution under visible light irradiation overpure CN and Co-CN catalysts [138,139].

Please cite this article as: Fajrina N, Tahir M, A critical review in strategies to improve photocatalytic water splitting towards hydrogen production, International Journal of Hydrogen Energy, https://doi.org/10.1016/j.ijhydene.2018.10.200

Table 5 – Summary of metal doping g-C_3N_4 based photo-catalysts for H_2 production.

Year	Catalyst	Feed	Reactor	Parameter	Product, (μmol h^{-1} g^{-1})	Ref.
2019	Mo/g-C_3N_4	5 vol% TEOA	Pyrex reactor	300 W Xe lamp	79	[140]
2018	Au/g-C_3N_4	20 vol% CH_3OH	Quartz reactor	300 W Xe lamp	265	[141]
2018	Cu/g-C_3N_4	10 vol% TEOA	Pyrex reactor	300 W Xe lamp, $\lambda > 420$ nm	3020	[142]
2018	Ni/g-C_3N_4	Na_2SO_4		300 W Xe lamp, $\lambda > 420$ nm	529.1	[143]
2018	Ni-P/g-C_3N_4	12.5 vol% TEOA	Pyrex reactor	350 W Xe lamp	937	[144]
2018	Pt/g-C_3N_4	10 vol% TEOA	Pyrex reactor	350 W Xe lamp	4210.8	[145]
2018	K/g-C_3N_4	10 vol% TEOA	Pyrex reactor	300 W Xe lamp, $\lambda = 400$ nm	1337.2	[146]
2018	Au/g-C_3N_4	10 vol% TEOA	Pyrex reactor	300 W Xe lamp, $\lambda > 420$ nm	74	[147]
2018	Co/g-C_3N_4	20 vol% TEOA		300 W Xe lamp	2296	[148]
2017	Pt/g-C_3N_4	10 vol% TEOA		UV–vis lamp, $\lambda > 380$ nm	3900	[149]
2017	Cu/g-C_3N_4	10 vol% TEOA	Pyrex reactor	300 W Xe lamp, $\lambda > 420$ nm	3643	[150]
2017	Pt/g-C_3N_4	10 vol% TEOA	Pyrex reactor	300 W Xe lamp, $\lambda = 400$ nm	1218.75	[151]
2017	Co/g-C_3N_4	10 vol% TEOA		300 W Xe lamp, $\lambda > 420$ nm	28	[138]
2016	Pt/g-C_3N_4	10 vol% TEOA	Pyrex reactor	300 W Xe lamp, $\lambda > 420$ nm	28.55	[152]
2016	Cu/g-C_3N_4	25 vol% CH_3OH		Xe lamp, $\lambda > 400$ nm	1.025	[153]
2015	AuPd/g-C_3N_4	10 vol% TEOA	Quartz reactor	300 W Xe arc lamp, $\lambda \geq 400$ nm	16.3	[154]
2015	Pt/g-C_3N_4	10 vol% TEOA	Pyrex reactor	300 W Xe lamp, $\lambda > 420$ nm	34	[133]
2015	Pt/g-C_3N_4	10 vol% TEOA	Quartz reactor	300 W Xe lamp, $\lambda > 420$ nm	261.8	[155]
2015	Pt/2D g-C_3N_4	10 vol% TEOA		300 W Xe lamp, $\lambda > 420$ nm	89.28	[156]
2014	Au/g-C_3N_4	10 vol% TEOA		125 W Hg lamp, $\lambda > 400$ nm	177.4	[157]
2014	Pt/g-C_3N_4	10 vol% TEOA		300 W Xe lamp, $\lambda > 420$ nm	41.7	[158]

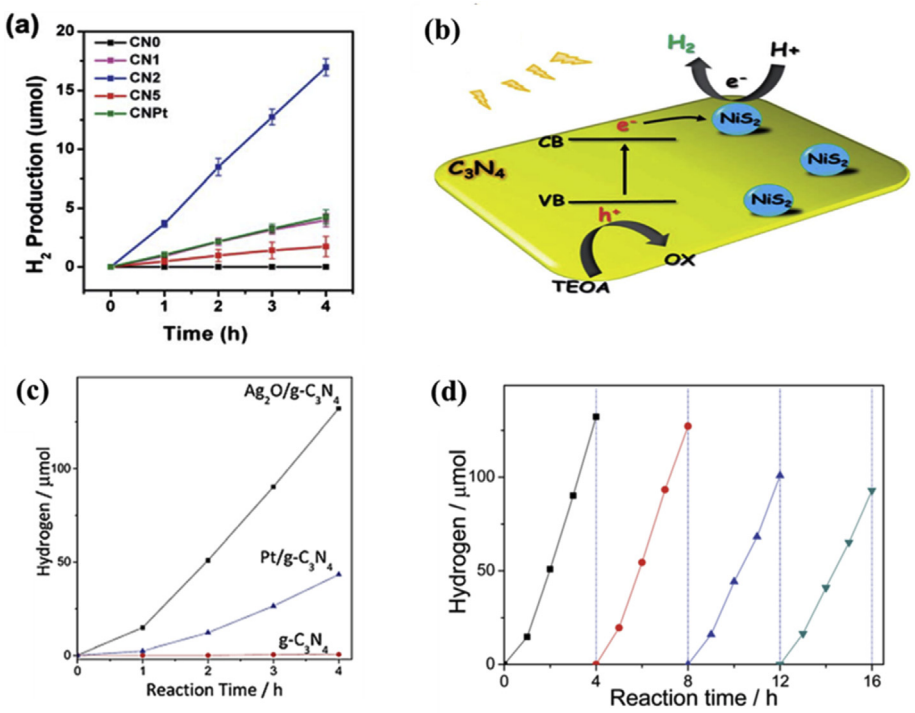

Fig. 9 – (a) Time-resolved H_2 generation amount; (b) Schematic illustration of the proposed mechanism for photocatalytic H_2 generation over NiS_2-loaded g-C_3N_4; (c) Time course of hydrogen evolution over pure g-C_3N_4, Ag_2O/g-C_3N_4; and (d) Stability tests for hydrogen evolution with Ag_2O/g-C_3N_4 under visible light irradiation [161,162].

greatly enhancing the photocatalytic activity and photo-stability as shown in Fig. 9(c) and (d). Table 6 shows the over-view of semiconductor coupled g-C_3N_4 based photocatalysts to form heterojunction in the present of sacrificial electron donor for H_2 production. It can be concluded that the constructing of g-C_3N_4-based semiconductor heterojunctions can improve photocatalytic activity since it induces the band bending along with the internal electrical field formation and cause an effective spatial charge separation.

Non-metal loading

In addition of metal doping, the non-metals doping could effectively improve the photo-activity of semiconductors. When, g-C_3N_4 polymers were modified with non-metal

Table 6 – Summary of semiconductor doping g-C_3N_4 based photo catalysts for H_2 production.

Year	Catalyst	Feed	Reactor	Parameter	Product ($\mu mol\ h^{-1}\ g^{-1}$)	Ref
2019	$AgNbO_3$/g-C_3N_4			Visible light	88	[163]
2018	Ni_2P and g-C_3N_4	TEOA		$\lambda > 420$	474.7	[164]
2018	$Ni_2P_2O_7$/g-C_3N_4	10 vol% TEOA	Pyrex reactor	300 W Xe arc lamp, $\lambda > 420$ nm	207	[165]
2018	NiO/g-C_3N_4	10 vol% TEOA	Pyrex reactor	300 W Xe arc lamp, $\lambda > 420$ nm	68.8	[166]
2018	Ni_2P/g-C_3N_4	20 vol% TEOA	Quartz reactor	300 W Xe arc lamp, $\lambda = 420$ nm	1503	[167]
2018	MoS_2/g-C_3N_4	25 vol% CH_3OH		300 W Xe lamp, $\lambda > 420$ nm	867.6	[168]
2018	Cu_2O/g-C_3N_4	20 vol% TEOA	Quartz reactor	300 W Xe arc lamp, $\lambda = 400$ nm	33.2	[169]
2018	CoO/g-C_3N_4	DI water		White LED, $\lambda > 400$ nm	50.2	[170]
2018	ZnO/ZnS/g-C_3N_4	0.25 M Na_2S and 0.25 M Na_2SO_3		300 W Xe lamp, $\lambda = 420$ nm	301.25	[171]
2018	ZnS/g-C_3N_4	Na_2S and Na_2SO_3	Pyrex reactor	300 W Xe lamp, $\lambda = 420$ nm	713.68	[172]
2018	MoS_2/g-C_3N_4	0.5 M Na_2SO_4		350 W xenon lamp, $\lambda = 400$ nm	191.2	[173]
2017	CoP/go-C_3N_4	10 vol% TEOA	Pyrex reactor	300 W Xe arc lamp, $\lambda > 420$ nm	474.4	[174]
2017	g-C_3N_4/Ni_2P	10 vol% TEOA		300 W Xe arc lamp, $\lambda > 420$ nm	567	[175]
2017	Ni_2P/g-C_3N_4	20 vol% TEOA	Pyrex reactor	300 W Xe arc lamp, $\lambda = 420$ nm	180	[176]
2017	Ni_2P-$Cd_{0.9}Zn_{0.1}S$/g-C_3N_4	Na_2S and Na_2SO_3	Pyrex reactor	300 W Xe arc lamp, $\lambda = 420$ nm	2.1	[177]
2016	TiO_2/g-C_3N_4	25 vol% CH_3OH	Pyrex reactor	4 × UV-LEDs 3 W, $\lambda = 420$ nm	5.6	[178]
2016	g-C_3N_4/MoS_2/TiO_2	25 vol% CH_3OH	Pyrex reactor	300 W Xe arc lamp, $\lambda > 400$ nm	125	[179]
2015	NiS/g-C_3N_4	10 vol% TEOA	Quartz reactor	150 W Xe lamp, $\lambda > 400$ nm	4.2	[180]
2015	Ag_2O/g-C_3N_4	10 vol% TEOA	Pyrex reactor	300 W Xe lamp, $\lambda > 420$ nm	33.04	[162]
2015	g-C_3N_4/CdS/NiS	0.35 M Na_2S and 0.25 M Na_2SO_3	Pyrex reactor	350 W Xe arc lamp, $\lambda \geq 420$ nm	207.6	[181]
2014	NiS/g-C_3N_4	10 vol% TEOA		300 W Xe lamp, $\lambda > 420$ nm	44.77	[182]
2014	Ag_2S/g-C_3N_4	20 vol% CH_3OH	Pyrex reactor	4 × UV-LEDs 3 W, $\lambda = 420$ nm	10	[183]
2014	ZnS/g-C_3N_4	25 vol% CH_3OH	Pyrex reactor	4 × UV-LEDs 3 W, $\lambda = 420$ nm	9.7	[184]
2014	NiS_2/g-C_3N_4	TEOA		300 W Xe lamp, $\lambda \geq 420$ nm	406	[161]
2013	1.25 wt% NiS/g-C_3N_4	15 vol% TEOA	Pyrex reactor	300 W Xe lamp, $\lambda > 420$ nm	46	[185]

elements, such as N, B, O, S, and P, the electronic and optical properties were efficiently optimized to promote photocatalytic performance due to the enhanced optical absorption and accelerated charges mobility. The H_2 production can be increased since non-metal loading tune the structure of catalyst by lowering the band gap, hindered charge recombination rate and providing stability to catalyst [186].

In 2016, Zhou et al. [186] reported the H_2 generation over optimized N-doped g-C_3N_4 photo-catalyst (CN-20) and maximum H_2 of 64 $\mu mol\ h^{-1}$ obtained, which is almost 3.3 times higher than using pristine g-C_3N_4 (Fig. 10(a)). The catalyst of CN-20 also provides stability since there is no significant decrease in the H_2 rate by repeating the experiment under the same condition for four cycles (24 h) as shown in Fig. 10(b). Chen et al. [187] reported the sulfur doping has increased the photocatalytic activity, which is 12 times higher than pure g-C_3N_4 and stable for water splitting process for long-term as shown in Fig. 10(c). It was concluded that sulfur doping can effectively increase the specific surface area, induce the formation of nitrogen vacancies, prevent photogenerated charge recombination rate and improved the visible response on the catalyst. Lan et al. [188] also reported non-metal, which is Br doped g-C_3N_4, have long-term stability for 20 h under visible irradiation with highest H_2 production rate of about 48 $\mu mol\ h^{-1}$ as shown in Fig. 10(d) and proposed reaction mechanism for photocatalytic water splitting for CN-Br as illustrated in Fig. 10(e). Table 7 shows the examples of non-metal loading on g-C_3N_4 for photocatalytic water splitting. In general, non-metal doping on g-C_3N_4 has long term stability and can lower band gap for enhanced light absorbance, redox potential and charge carrier mobility. An additional advantage of reconstruction of structural photocatalyst is to enhance optical absorption and hindered charge recombination on g-C_3N_4, causing the increased photocatalytic activity [137].

Heterojunction construction

Designing efficient photo-catalysts for the production of H_2 through water splitting has become one of the challenges in developing solar hydrogen economy. The main factors influencing the efficiency of photocatalytic systems include: (1) light absorption, (2) separation and transportation of charge carrier (e^-/h^+), and (3) the chemical reaction of adsorbed species with e^-/h^+. Over the past 40 years, numerous efforts have been implemented to fabricate novel materials for enhancing the photocatalytic performance [204,205]. For TiO_2, many different kinds of strategies in order to enrich evolvement of H_2 have been reported such as ternary nanocatalyst of TiO_2 [206], coupling TiO_2 with boron carbon nitride (BCN) compound [207] and noble metal-loaded TiO_2 [208]. The hetero-structured photo-catalyst depends on the difference in photo induced e^-/h^+ transfer mechanism, which can be divided into two categories as follows: (1) Heterojunctions type II transfer mechanism and (2) Z scheme charge transfer mechanism.

Please cite this article as: Fajrina N, Tahir M, A critical review in strategies to improve photocatalytic water splitting towards hydrogen production, International Journal of Hydrogen Energy, https://doi.org/10.1016/j.ijhydene.2018.10.200

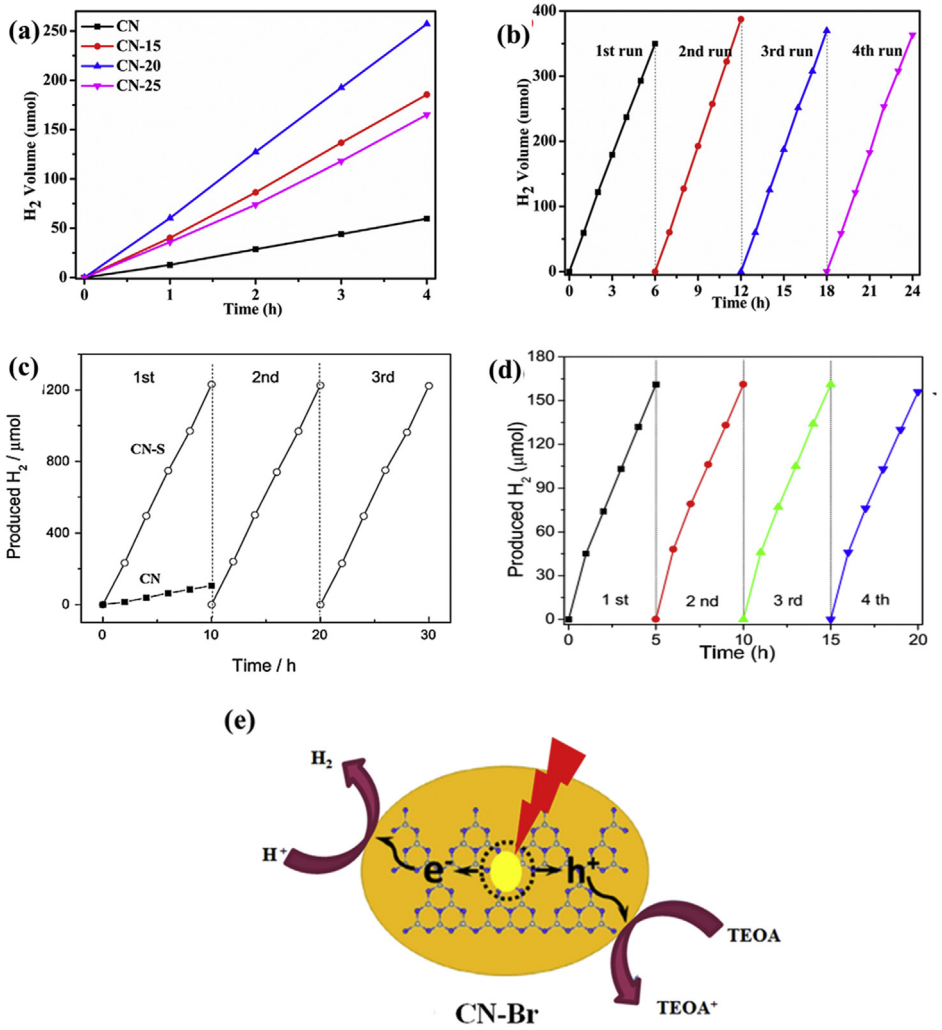

Fig. 10 – (a) Photocatalytic H_2 evolution performances on CN and CN-x, (x = 15, 20, 25); (b) Recycling behavior of H_2 evolution on CN-20; (c) Photocatalytic H_2 evolution over CN and CN-S under visible light irradiation and; (d) Long-term H_2 evolution by CNU-Br0.1 under visible light irradiation ($\lambda \geq 420$ nm); and (e) Illustration of mechanism for photocatalytic H_2 evolution on CN-Br.

Type II heterojunction

Combining TiO_2 with other semiconductors to form heterojunction can provide benefits to hinder fast charge recombination and improve redox reaction which results in improved H_2 production. Typically, the TiO_2-based materials form conventional heterojunction by the combination of higher CB of photosystem I (PS I) with lower CB of photosystem II (PS II). Under light irradiation, the photo-generated electrons of PS I will be transferred to PS II, leaving the photo-generated holes on the VB of PS I as shown in Fig. 11(a). By this way, recombination of photo-generated charge carrier can be avoided, enriching the photocatalytic performance. Meanwhile, the reduction and oxidation reaction occurs at different semiconductors. However, redox reaction occurs at lower redox potential and sacrificed its ability to be maximized [48].

Z-scheme heterojunction

The study of Z-scheme photocatalytic system that biomimetic the natural photosynthesis system has been extensively fabricated for efficient mechanism in water splitting [209]. Z-scheme has been designed to overcome the problems that arise in the classic photocatalytic system by providing stronger redox ability and excellent spatial separation of charge carrier. The Z-scheme photocatalytic system can be divided into three types which are Z-scheme system with shuttle redox mediator, solid state electron linkers and direct systems.

Z-scheme system with shuttle redox mediators

Z-scheme photocatalytic system consisting of two independent semiconductors with the presence of redox coupled ions (Fe^{3+}/Fe^{2+}, IO_3^-/I^-, NO_3^-/NO_2^-) are usually acted as electron

Please cite this article as: Fajrina N, Tahir M, A critical review in strategies to improve photocatalytic water splitting towards hydrogen production, International Journal of Hydrogen Energy, https://doi.org/10.1016/j.ijhydene.2018.10.200

Table 7 – Summary of non-metal doping g-C_3N_4 based photo-catalysts for H_2 production.

Year	Catalyst	Feed	Reactor	Parameter	Product (μmol h^{-1} g^{-1})	Ref.
2019	S/g-C_3N_4	25 vol% TEOA	Pyrex reactor	300 W Xe lamp, $\lambda \geq 420$ nm	1511.2	[189]
2019	P/g-C_3N_4	10 vol% TEOA	Pyrex reactor	300 W Xe lamp, $\lambda > 420$ nm	2020	[190]
2019	P/g-C_3N_4	5 vol% TEOA	Pyrex reactor	300 W Xe lamp	63	[140]
2018	P/g-C_3N_4	20 vol% CH_3OH	Quartz reactor	300 W Xe lamp	120	[141]
2018	O/g-C_3N_4	15 vol% TEOA	Pyrex reactor	300 W Xe lamp, $\lambda = 420$ nm	29.6	[191]
2018	O/g-C_3N_4	10 vol% TEOA	Pyrex reactor	300 W Xe lamp, $\lambda = 420$ nm	1968	[192]
2018	S/g-C_3N_4	Na_2SO_4		300 W Xe lamp, $\lambda > 420$ nm	24.2	[143]
2018	B/F/g-C_3N_4	10 vol% TEOA		$\lambda > 400$ nm	6870	[193]
2018	O/g-C_3N_4	10 vol% TEOA	Pyrex reactor	300 W Xe lamp, $\lambda = 420$ nm	1968	[192]
2018	C/g-C_3N_4	Methanol		300 W Xe lamp, $\lambda = 420$ nm	807.4	[194]
2018	C/g-C_3N_4	CH_3OH		300 W Xe lamp, $\lambda = 420$ nm	807.4	[194]
2017	P/g-C_3N_4	20 vol% CH_3OH		300 W Xe lamp, $\lambda = 420$ nm	570	[195]
2017	C/g-C_3N_4	15 vol% TEOA		350 Xe arc lamp, $\lambda > 420$ nm	212.8	[196]
2016	Br/g-C_3N_4	10 vol% TEOA		300 W Xe lamp, $\lambda \geq 420$ nm	48	[188]
2016	N/g-C_3N_4	10 vol% TEOA	Pyrex reactor	300 W Xe lamp, $\lambda \geq 420$ nm	64	[186]
2016	O/g-C_3N_4	10 vol% TEOA		300 W Xe lamp, $\lambda > 400$ nm	189.3	[197]
2016	O/g-C_3N_4	20 vol% TEOA		300 W Xe arc lamp, $\lambda = 420$ nm	202.56	[198]
2015	P/g-C_3N_4	10 vol% TEOA	Pyrex reactor	300 W Xe arc lamp, $\lambda > 400$ nm	104.1	[199]
2015	P/g-C_3N_4	10 vol% TEOA	Pyrex reactor	300 W Xe lamp, $\lambda > 420$ nm	50.6	[200]
2015	C/g-C_3N_4	10 vol% TEOA	Pyrex reactor	350 W Xe arc lamp, $\lambda > 420$ nm	54	[201]
2015	S/g-C_3N_4	10 vol% TEOA		$\lambda = 420$ nm	121	[187]
2014	C/g-C_3N_4	25 vol% CH_3OH	Quartz reactor	Visible light, $\lambda > 420$ nm	69.8	[202]
2013	S/g-C_3N_4	25 vol% CH_3OH	Quartz reactor	300 W Xe arc lamp, $\lambda > 400$ nm	12.16	[203]

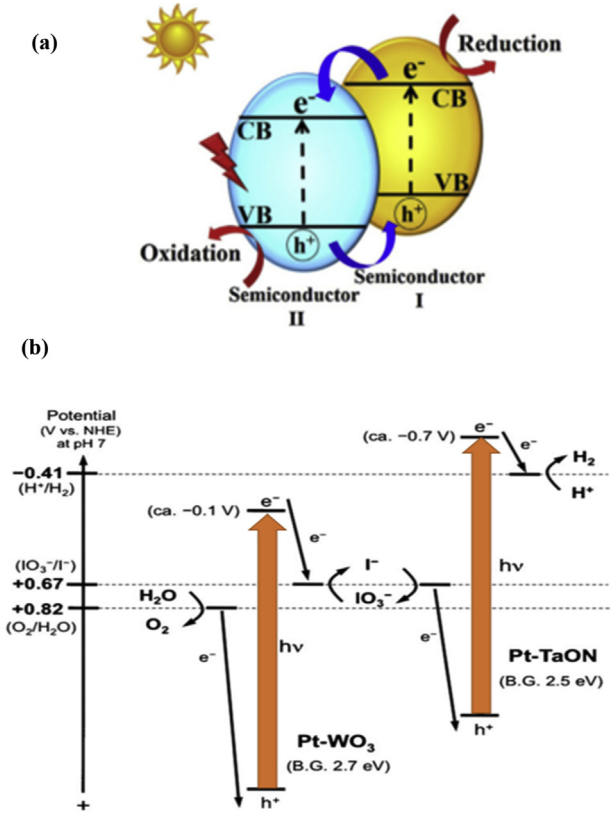

Fig. 11 – (a) Schematic of the type-II heterojunction [129]; (b) Schematic diagram on overall water splitting reaction mechanism over Pt/TaON and Pt/WO_3 with an IO_3^-/I^- shuttle redox mediator [210].

transport chain in Z-scheme water splitting. During illumination with visible light, photo induced holes in the VB of one semiconductor and photo induced electrons in the CB of another semiconductor will react with the redox coupled ions. As shown in Fig. 11(b), Abe et al. [210] successfully reported on the forward reactions for H_2 evolution in the Z-scheme system over nanohybrid composite of Pt-doped TaON and Pt–WO_3. The quantum efficiency for the reaction was determined to be estimated 0.5% at 420 nm with 25 μmol $gcat^{-1}$ of hydrogen production. The photoinduced hole from the VB of the Pt/WO_3 photocatalyst and the photoinduced electron from the CB of the Pt/TaON photocatalyst react with the electron acceptor/donor pairs. However, the introduction of IO_3^-/I^- complicates the photocatalytic reaction, limiting the photocatalytic efficiency. In addition, the backward reactions occur as well as lower diffusion rate of the redox couple ions limit the production of H_2.

In 2015, Chen et al. [211] been successful in water splitting by using a Z-scheme system in the presence of I^-/IO_3^- redox mediator using Pt loaded $MgTa_2O_{6-y}N_x$/TaON and PtO_x-WO_3 as nanocomposite photo-catalysts. Interestingly, the backward reactions, for example oxidation of I^- ions on the Pt-loaded $MgTa_2O_{6-y}N_x$/TaON and the reduction of IO_3^- on the PtO_x-WO_3, were significantly reduced, resulting in enhanced apparent quantum efficiency (AQE) of 6.3% at 420 nm. All primary semiconductor based Z-scheme photo-catalysis systems in the presence of shuttle redox mediators are summarized in Table 8 using I^-/IO_3^- and Fe^{3+}/Fe^{2+} as redox mediator and new redox mediator such as VO_2^+/VO^{2+} and $[Fe(CN)_6]^{3-}/[Fe(CN)_6]^{4-}$.

Z-scheme with solid state electron mediator

For Z-scheme systems consisting of two different semiconductors and a solid state electron linker, the electron transfer is driven by ohmic contact due to solid interface

Table 8 – Summary of Z-scheme photocatalytic system using redox couple ion as electron mediator.

Year	PSI	PSII	Redox Mediator	Hydrogen (μmol g^{-1} h^{-1})	Ref.
2019	g-C_3N_4	MnO_2	Mn^{3+}/Mn^{4+}	60.6	[212]
2018	$SrTiO_3$(La,Cr)/Pt	Pt/WO_3	I^-/IO_3^-	91	[213]
2018	Ir-MgO/Ta_3N_5	Pt/Cr_2O_3-ZrO_2/TaON	I^-/IO_3^-	70.6	[214]
2018	PtO_x/WO_3	Ru/$SrTiO_3$:Rh	$[SiW_{11}Mo^{VI}O_{40}]^{4-}/[SiW_{11}Mo^{V}O_{40}]^{5-}$	44	[215]
2018	$BiVO_4$	g-C_3N_4/Zn	Fe^{3+}/Fe^{2+}	1333.3	[216]
2018	$BiVO_4$	ZrO_2/TaON	$[Fe(CN)_6]^{3-}/[Fe(CN)_6]^{4-}$	1300	[217]
2017	Fe-H-Cs-WO_3	Ru/$SrTiO_3$	VO_2^+/VO^{2+}	200	[218]
2015	Pt/$MgTa_2O_{6-y}N_x$/TaON	PtO_x-WO_3	I^-/IO_3^-	108.3	[211]
2015	Pt/carbon	WO_3	I^-/IO_3^-	1330	[219]
2011	Pt/TaON	Pt/WO_3	I^-/IO_3^-	790	[210]
2011	Pt/ZrO_2/TaON	RuO_2/TaON	I^-/IO_3^-	8.0	[220]
2010	Pt/ZrO_2/TaON	Ir/R-iO_2/Ta_3N_5	I^-/IO_3^-	7.0	[221]
2008	Ru/$SrTiO_3$:Rh	$BiVO_4$	Fe^{3+}/Fe^{2+}	18.9	[222]

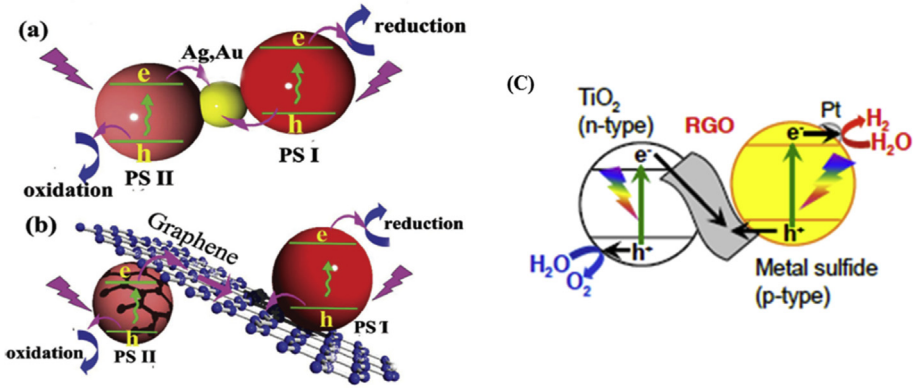

Fig. 12 – (a) Schematic illustrations of a Z-scheme in the presence of Au with Ag as the solid electron linker; (b) Schematic illustrations of a Z-scheme in the presence of rGO as the solid electron linker; and (c) Schematic illustrations of Z-schematic water splitting system using $CuGaS_2$/rGO/TiO_2 photocatalyst [227].

formed. The properties formed within the solid–solid interface are equal to the property of metals (low-resistance). As shown in Fig. 12(a) and (b), the ohmic contact is beneficial for the rapid recombination between photo-induced electrons from the lower potential CB of photosystem II (PS II) and photo-induced holes from the higher potential VB of photosystem I (PS I). Thus, more electrons and holes would leave at different active sites, resulting in stronger redox ability [223,224].

To date, noble-metal particles and reduced graphene oxide (rGO) were demonstrated as electron linker for the Z-scheme photo-catalysis system, and provide excellent efficiency of the charge-carrier separation [225]. Table 9 shows the application of Z-scheme in hydrogen evolution applications. For the first time, all solid state Z-scheme systems were reported by Tada et al. [226] using CdS/Au/TiO_2 fabricated by simple photo-chemical deposition method. Under UV illumination, electrons in the CB of TiO_2 transferred to the VB of CdS through Au, then recombined with the holes in CdS. Concurrently, the photo-induced electrons and holes of different sites exhibited a strong reduction and oxidation ability, respectively, leading to a higher photocatalytic H_2 evolution.

Apart of noble metals, low cost metal oxides with significant conductivity such as rGO have been employed as electron linker to accelerate electron movement between the photo-catalysts in Z-scheme system. Iwashina et al. [227] reported a solid state Z-scheme system $CuGaS_2$/rGO/TiO_2 for water splitting. Under visible light illumination, the rGO provides routes for the photo-generated electrons within TiO_2 and the holes in $CuGaS_2$ to recombine, leaving holes in TiO_2 and electrons in $CuGaS_2$ to split water, thus resulting in H_2 and O_2 production simultaneously.

For TiO_2-based Z-scheme, photocatalytic H_2 evolution has been reported using Ag as the electron mediator [206]. The resulting TiO_2/Ag/Cu_2O photo-catalyst gives highest H_2 production activity due to the synergetic effect of Ag and Cu_2O on electro spun of TiO_2 nanotubes. The addition of Cu_2O and Ag leads to stronger visible light absorption ability and moreover, the SPR-induced local electric field results in dual Z-scheme charge transfer routes in the composite, which increases separation efficiency and high redox ability of photo-induced charge carriers.

Direct Z-scheme hydrogen production

In direct Z-scheme systems, what is important is the properties of the solid-solid interface which allows the electron transfer within two photocatalysts. Hence, the selection of photo-

Table 9 – Z-Scheme photo-catalyst system with solid redox mediators.

Year	PSI	PSII	Redox Mediator	Hydrogen (μmol g^{-1} h^{-1})	Ref.
2019	AgBr	TiO_2	rGO	10,125	[225]
2019	NiO	$BiVO_4$	Carbon dots	1.21	[228]
2019	Mo_2C	g-C_3N_4	Mo	219.7	[229]
2018	TiO_2 (Rutile)	TiO_2 (Anatase)	Ag	40.4	[230]
2018	CdS	ZnO	Au	102.9	[231]
2018	$ZnIn_2S_4$	TiO_2	Au	186.3	[232]
2018	$CaTiO_3$	AgCl	Ag	220	[233]
2018	Bi_2WO_6	g-C_3N_4	rGO	21	[234]
2018	CdS	TiO_2	Ag	1910	[235]
2017	CdS	$BiVO_4$	Carbon dots	1.24	[236]
2017	g-C_3N_4	$Cd_xZn_{1-x}S$	Au	123	[237]
2017	Pt/$ZnIn_2S_4$	CoO_x/Bi_2MoO_6	rGo	740.4	[238]
2017	g-C_3N_4	CdS	rGO	676.5	[239]
2017	Cu_2O	Fe_2O_3	rGO	5	[240]
2017	$ZnIn_2S_4$	$BiVO_4$	rGO	4.1	[241]
2016	$ZnRh_2O_4$	$Ag_{1-x}SbO_{3-y}$	Ag	0.0168	[242]
2014	Ru/$SrTiO_3$:La/Rh	Ir/CoO_x/Ta_3N_5	Ir	280	[243]
2013	CdS	TiO_2	Au	64	[244]
2012	CdS	ZnO	Cd	1920	[245]
2006	Pt/CdS	TiO_2	Au	10	[226]
2004	$CuGaS_2$	TiO_2	rGO	19.8	[227]

catalysts is vital in designing direct Z-scheme systems. Table 10 shows the application of direct Z-scheme systems for hydrogen evolution applications. Guo et al. [246] has conducted study on hydrogen evolution over ZnO and $Zn_{0.2}Cd_{0.8}S$ nanocomposite from water using SO_3^{2-} and S^{2-} ions as sacrificial agents. The ultimate production rate of H_2 by the direct Z-scheme ZnO/$Zn_{0.2}Cd_{0.8}S$ heterojunction was 25,180 μmol h^{-1} g^{-1}. The excellent photocatalytic activity of H_2 evolution rate due to the development of direct Z-scheme $ZnO_{1-x}/Zn_{0.2}Cd_{0.8}S$ system and oxygen-vacancy rich ZnO_{1-x} in the heterojunction and the results showed the similarity in properties to the conductor as presented in Fig. 13(a). These characteristics enable the excellent spatial separation of charge carriers. Wang et al. [247] conducted study on photocatalytic Z-scheme ZnO/CdS system that revealed H_2 production rate of 1805 μmol h^{-1} g^{-1}. The H_2 production rate was significantly higher than produced using pure ZnO or CdS photo-catalysts. They concluded that during separation of photo-induced electron and holes of two semiconductors, electrons travel from the CB of ZnO to the VB of CdS, contributing to enhance performance.

Fig. 13(b) shows artificial photosynthetic Z-scheme WO_{3-x} nanorods supported $Zn_{0.3}Cd_{0.7}S$ heterostructures system, in

Table 10 – Summary on direct Z-scheme photocatalytic system for H_2 evolution.

Year	SI	SII	Hydrogen (μmol g^{-1} h^{-1})	Ref.
2019	g-C_3N_4	ZnO	152.7	[249]
2019	CdS	ZnO	4143	[250]
2019	Cu_3P	g-C_3N_4	808	[251]
2018	CdS	$CoWO_4$	15,910	[252]
2018	g-C_3N_4	Ti^{3+}-TiO_2	1938	[253]
2018	CdS	Bi_2WO_6	1223	[254]
2018	$Cd_{0.5}Zn_{0.5}S$	Bi_2O_3	2540	[255]
2018	CdS	WO_3	15,522	[256]
2018	MoS_2	g-C_3N_4	577	[257]
2018	CdS	Polybenzothiadiazole (BE)	1229.7	[258]
2018	Ta_3N_5	ZnO	500	[259]
2017	g-C_3N_4	Fe_2O_3	776	[260]
2017	$Zn_{0.4}Cd_{0.6}S$	Fe_2O_3	5368	[261]
2017	TiO_2/Au	WO_3	3476.2	[262]
2017	BCN	TiO_2	19.7	[207]
2017	ZnO_{1-x}	$Zn_{0.2}Cd_{0.8}S$	25,180	[246]
2017	WO_{3-x}	$Zn_{0.3}Cd_{0.7}S$	352.1	[248]
2017	Pt/CdS	$BiVO_4$	1150	[263]
2016	CdS	$CdWO_4$	9.17	[264]
2014	g-C_3N_4	WO_3	110	[265]
2014	anatase TiO_2	rutile TiO_2	324	[266]
2013	Si	TiO_2	875	[267]
2013	Ru/$SrTiO_3$:Rh	Ir/$CoO_xTa_3N_5$	23	[268]
2009	CdS	ZnO	1805	[247]

Please cite this article as: Fajrina N, Tahir M, A critical review in strategies to improve photocatalytic water splitting towards hydrogen production, International Journal of Hydrogen Energy, https://doi.org/10.1016/j.ijhydene.2018.10.200

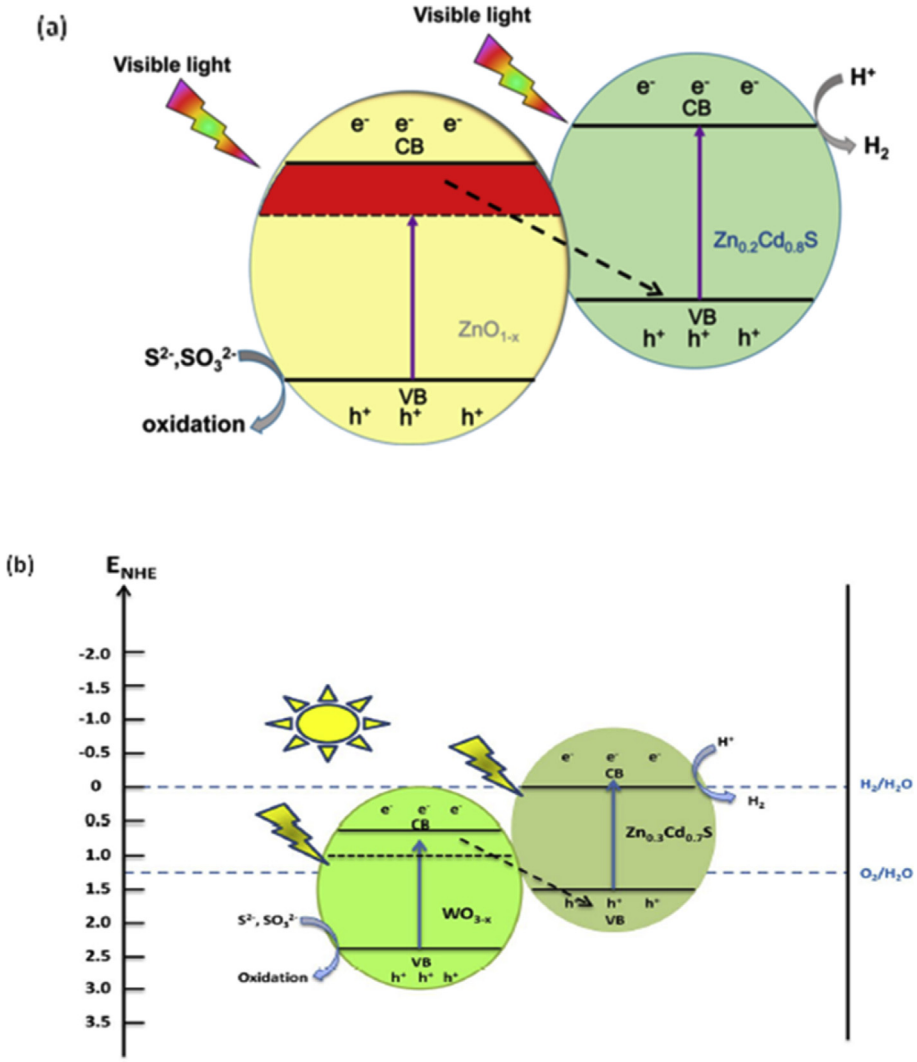

Fig. 13 – (a) Schematic illustration of photocatalytic H_2 production over Z-scheme $ZnO_{1-x}/Zn_{0.2}Cd_{0.8}S$ [246]; and (b) Scheme process of charge transfer for $WO_{3-x}/Zn_{0.3}Cd_{0.7}S$ heterostructure [248].

presence of Na_2SO_3 and Na_2S as sacrificial reagents. The rate of H_2 evolution reached 352.1 μmol h^{-1} g^{-1} with an apparent quantum efficiency (AQY) of 7.3% at wavelength 420 nm [248]. The defect rich $WO_{3-x}/Zn_{0.3}Cd_{0.7}S$ heterostructure enables both high spatial separation efficiency of photo generated electrons and holes. However, direct Z-scheme has limitation as the electron transport process is poor due to surface relaxation and recombination charge carrier within each semiconductor.

TiO_2 has been reported tightly coupled to construct Z-scheme heterostructures with boron carbon nitride (BCN) compound [207]. The TiO_2/BCN nanostructure evolves the excellent enrichment of photocatalytic H_2 production activity and higher stability than pure TiO_2. The loading BCN have significant influence on the photocatalytic performance. The ultimate photocatalytic activity was achieved for 4% BCN/TiO_2 nanocomposite at H_2 evolution rate of 19.7 μmol g^{-1} h^{-1}, two folds higher than using pure TiO_2. In this type of mechanism charge transfer, formation of middle sub-band single electron oxygen vacancies in the forbidden gap of novel TiO_2 has resulted to be beneficial for absorption of visible light. Moreover, the oxygen vacancies provide advantages to the Z-scheme charge transfer due to the construction of ohmic contact at the interface between BCN and novel TiO_2. Hence, the BCN/TiO_2 nanocomposites by Z-scheme charge transfer can provide excellent oxidation ability of TiO_2 and high reduction ability of BCN.

Factors that influence photocatalyst activity

Band gap energy

The electronic structure of the semiconductor electrodes is usually represented in terms of energy bands or band gap and can be regarded as a continuum of energy levels due to difference in energy between VB and CB. In general, the relative potential level of the acceptor is thermodynamically required to be less than the CB of the semiconductor [23]. Thermodynamically, the H_2 is produced by the initial hydrogenation of

Please cite this article as: Fajrina N, Tahir M, A critical review in strategies to improve photocatalytic water splitting towards hydrogen production, International Journal of Hydrogen Energy, https://doi.org/10.1016/j.ijhydene.2018.10.200

intermediates, H^+ is absorbed at the active site and reduced to H_2 by use of photoelectrons [269]. As presented in Fig. 14(a), the band gap of TiO_2 is appropriate for water splitting, since the top of the VB (+2.7 V vs NHE at pH 7) is more positive compare to O_2/H_2O redox couple (+1.23 V vs. NHE), and the bottom part of the CB (−0.5 V vs NHE at pH7) is more negative than the H_2O/H_2 redox couple (−0.41 V vs. NHE at pH 7) [72]. However, TiO_2 is not suitable for visible light irradiation since it has band gap 3.2 eV. In order to be able to absorb visible light irradiation, TiO_2 must be doped with metals, non-metals, coupling semiconductors and by employing feasible strategies to further reduce a band gap. As in contrast to $BiVO_4$ and WO_3, band gap of g-C_3N_4 is medium with 2.7 eV with most negative CB level (−1.3 V vs NHE at pH 7), facilitating its wide application in visible light photocatalysis [28]. Therefore, g-C_3N_4 usually recommended as the co-doping with additional photo-catalysts to increase visible light absorption response of semiconductors. Besides, co-catalysts can play the extra roles in improving the photostability and charge separation of semiconductors, a prospective way to enhanced hydrogen production rate. As shown in Fig. 14(b), Fe metal doped g-C_3N_4 narrow the band gap by 2.5 eV and non-metal doping can also decrease the band gap of g-C_3N_4 less than 2.7 eV [28,37–40,270–275]. However, coupling TiO_2 with g-C_3N_4 and modifying with metals and or non-metals would be prospective strategy to maximize the photocatalytic activity for hydrogen production.

Structure/surface area

Alteration of surface texture is one of the surface modifications strategies to narrow the band gap of catalyst [276]. The crystal structure of catalyst significantly affects the photocatalytic activity for H_2 production. The large size nanoparticles can be attributed to a weaker metal support interaction in the case regarding metal modified TiO_2 [69]. The larger surface area will provide even more reactive sites, resulting in increased photocatalytic activity [277]. The crystalline photocatalysts with smaller particle size have the shorter distance for the photo generated electrons and holes to quickly move to the active reaction sites on the catalyst surface, thus lowering the recombination probability [4]. Mostly, the structure of photocatalyst is dependent on the synthesis technique applied for catalyst preparation. The treated g-C_3N_4 with HNO_3 performance better photocatalytic activity compared to untreated g-C_3N_4 with the same operating conditions [278]. The protonation of g-C_3N_4 leads to exfoliation on the structures and forms ultra-small pores. This aids in the higher separation and transfer efficiency of the photo-generated electrons and holes. The most common synthesis methods employed are solvothermal, hydrothermal, sol–gel, mechanical mixing, chemical vapor deposition, and impregnation [279,280]. The different temperature applied for catalyst preparation also helps to produce different sizing, shape and structure of nanomaterials. When the temperature increase, the size of crystallites improve from 6 nm at 250 °C, 11 nm at 380 °C, 30–45 nm at 550 °C, above 45 nm at 650 °C and above 100 nm at 800 °C [281]. Besides, the pH used also can give effect upon the size of catalyst. The concentration of H^+ or OH^- greatly influences the morphology and dimensionality of nanomaterials.

The particular surface area of $I_{0.1}$-N-TiO_2/CMAC is 199.3 $m^2\ g^{-1}$ with 2.33 eV band gap was favorable to produce

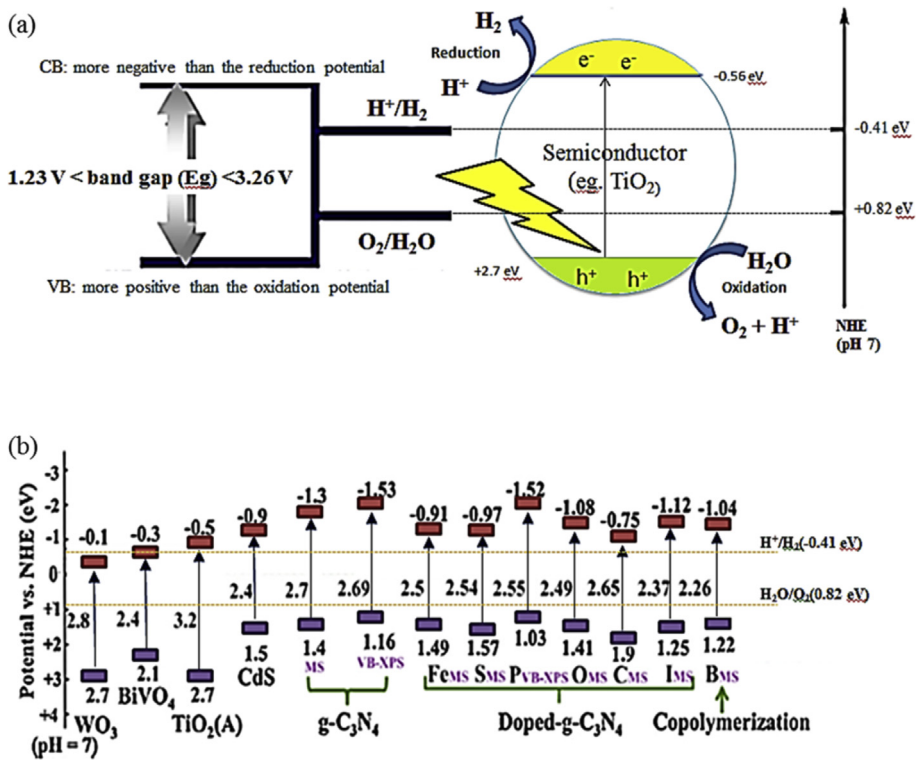

Fig. 14 – (a) The principle of photocatalytic water splitting reaction; and (b) Schematic illustration of the band structures of different types of photo-catalysts [28,37–40,270–275].

Please cite this article as: Fajrina N, Tahir M, A critical review in strategies to improve photocatalytic water splitting towards hydrogen production, International Journal of Hydrogen Energy, https://doi.org/10.1016/j.ijhydene.2018.10.200

maximum photocatalytic activity [282]. Similarly, Au/ZnO-r and Au/ZnO-t catalyst samples with size 6.2 nm were not very efficient with 231 μmol h^{-1} $gcat^{-1}$ H_2 production compared to Au/ZnO-f of 427 μmol h^{-1} $gcat^{-1}$ with size 5.4 nm [283]. The photocatalytic tests by Kumar et al. [284] recorded that the TNT photocatalyst revealed higher rate of H_2 production with 4.6 mmol h^{-1} $gcat^{-1}$ when compared with TNR and TNS due to its large surface area (see Fig. 15). Luo et al. [285] proved the effectiveness of atomic layer deposition (ALD)-growth of TiO_2 with hematite as it suppresses the charge recombination in hematite and improve the electrical conductivity. While, Li et al. [286] stated that nanostructure and short charge collection distance of the hematite nanotubes is systematically exhibited improved in water oxidation activity. Cai et al. [287] proposed the surface-disorder-engineering of TiO_2 photonic crystal for photocatalytic H_2 production to enhance the light harvesting and charge separation.

Light intensity

The efficiency of photocatalytic water splitting can be improved by increasing light intensity with energies more than the activation threshold [288,289]. There are two regimes regarding the photocatalytic reaction with respect to the UV–photon flux. The first order regime is for fluxes from laboratory researches, which usually are 25 mW cm^{-2} and the electron–hole pairs are consumed faster by chemical reactions than by recombination reactions. While the half-order regime is for higher intensities, which the rate of recombination is usually dominant and resulting fewer effect on the rate of reaction. The variation of reaction rate as a function of wavelength comes after the adsorption spectrum of the catalyst with a threshold corresponding to the band energy [1]. In 2013, Baniasadi et al. [290] recorded that the photocatalytic hydrogen production using ZnS showed 20% improved photoactivity by increasing light intensity from 900 to 1000 W m^{-2}. Tambago and Leon [291] reported the performance of $Cd_{0.4}Zn_{0.6}S$ for H_2 production increases as the light intensity was increased.

Temperature

Thermodynamically, temperature cannot induce the photocatalysis activity, since it did not contribute toward the generation of electrons and holes. However, temperature plays a role to enhance desorption of products from the surface of catalyst to increase the photocatalytic activity. The temperature speeds up the reaction rate. The temperature applied differs for different catalyst. Therefore, this factor could quickly be adjusted to increase the photocatalytic activity. Reduce temperature gives negative effect by slowing the H_2 production rate as desorption of the products limits the reaction, since it is slower the adsorption of the reactants. High temperature provides higher electron transfers in valance band to higher energy levels. Thus, it facilitates the electron–hole formation that could be utilized in initiating oxidation and reduction reactions, respectively, and helps the reaction to compete more effectively with charge carries recombination [1]. Boudjemaa et al. [13] revealed that the H_2 evolution increased with temperature with 59, 92 and 370 mol/g.s of H_2 produced at 30, 40 and 50 °C, respectively. Similarly, Pt/TiO_2 photocatalyst revealed after 4 h at 45 °C H_2 production was 4.71 mmol g^{-1}, increasing to 15.18 mmol g^{-1} when temperature was increased to 55 °C [292]. In another work in 2006, the optimum temperature is reported to be between 60 and 80 °C in photocatalytic study [293].

pH

It can be regarded that the production of H_2 from water splitting is dependent upon the proton concentration, which is the pH of the solution, since proton reduction by the photogenerated electron is generated throughout water splitting. This specific aspect is particularly importance in the case of photo reforming as the presence of a sacrificial organic species

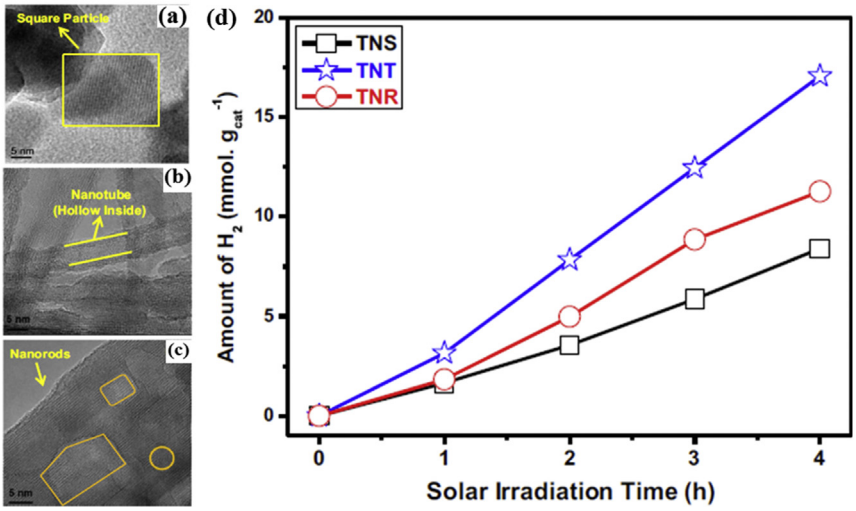

Fig. 15 – TEM images of (a) TNS, (b) TNT, (c) TNR, and (d) Comparison of the photocatalysts for H_2 production under solar light irradiation [284].

is required. The H_2 is more effective to be generated in weak basic pH solution than in acidic or strong basic (>10) as well as the band gap energy shift is dependent on the change in pH [20]. Wu et al. [294] reported the CuO_x/TiO_2 produced maximum H_2 in weak basic medium (pH 10). While, the lowest production of H_2 was obtained with pH 2, since the Cu(I) species has lower stability on the TiO_2 surface in acidic medium. Similarly, the Si/CdS/TiO_2/Pt catalyst has lowest performance under visible light because of reduce stability of TiO_2 in strong acid or base solution [295]. Brahimi et al. [296] estimated the optimal pH of photocatalytic for H_2 production over $CuAlO_2/TiO_2$ was 11. The adjustment in pH can lead to the modification of catalyst band gap. Pt/r-TiO_2 produced highest H_2 around 56.6 μmol at pH 5.5 after 4 h followed by pH 12 and pH 2.0 [297]. The research by Fujita on NiO/TiO_2 recorded the H_2 yield of 1200 μmol g^{-1} h^{-1} with pH value of about 6.6 obtained. Thus, the rate of H_2 evolution depends on the pH of the mixture while the optimum pH is close to the zero-point charge [85]. However, Nada et al. [298] stated that photosensitized TiO_2/RuO_2-MV^{2+} from methanol–water mixture produce more H_2 in acidic condition. At acidic pH, more H^+ ions are adsorbed on the photo catalyst, so the possibility of the reduction of H^+ to H_2 by e^- will be increased. It was reported that in the acidic condition, H_2 evolution rate was more effective than in a basic medium [299]. However, in general conclusion, based on the previous research, the photocatalytic reaction in the basic system gives more advantages to enhance H_2 evolution.

Oxygen vacancies

The metal oxide can be introduced to effect oxygen vacancies by catalyst synthesis, reduction and doping [300]. For TiO_2, the oxygen vacancies are existed along with Ti^{3+}. When the oxygen vacancies concentration is higher, more Ti^{3+} ions are produced, thus causes Ti^{3+} defect state, surface disorder and associate oxygen vacancies. Due to missing oxygen atom, the oxygen vacancies defect can trap and prolong the life of electrons. Whereas, the regular lattice of the oxygen atom was taken by electrons and local state was formed by oxygen vacancies and Ti^{3+}. Then, the VB holes of TiO_2 were generated and the electrons excited to the CB of TiO_2. At CB, the H^+ reduce to H_2 through reduction reaction [77]. It can be concluded that this approach is effective to increase the lifetime of the charges without metals loading, consequently hindered the electron–holes recombination for enhanced H_2 production.

Sacrificial reagent

The performance of photo catalyst activity can be improved with the presence of organic species such as methanol, ethanol, phenol, and glycerol as sacrificial agents which act as a hole scavenger compare to the water alone [74]. The enhancement of highly efficient photocatalysts for H_2 production has drawn increased attention and the effects of the composition and structure of sacrificial agents has been rarely studied. When alcohols are used to improve H_2 rate, the process is called photo-reforming, which make semiconductors to promote the oxidation of organic molecules and the reduction of H^+ to H_2. According to this, H_2 is obtained while sacrificial agents are mineralized. The photo reforming of the alcohols in the overall reaction can be represented as in Eq. (21) [65].

$$C_xH_yO_z + (2x - z)H_2O \rightarrow xCO_2 + \left(2x - z + \frac{y}{2}\right)H_2 \quad (21)$$

Table 11 summarizes the previous researches on water splitting using various sacrificial agents. As shown in Fig. 16(a), the production H_2 using sacrificial reagents is decreased in the order from glycerol > ethylene glycol > methanol > ethanol [72]. Based on the pattern reactivity series, it was concluded that the sacrificial hole scavenger must have an α-H adjacent to the OH groups, with the other main by-products of alcohols photo-reforming is largely predictable based on the alcohol structure. The photo reforming of alcohol liberated the alpha-hydrogen into H^+, finally converted for H_2 production by the use of electrons. Fig. 16(b) shows the structure of sacrificial agents according to the hydrogen production rate. The presence of α-H atom influences the H_2 production rate. Since the glycerol has 5 α-H atoms, it can generate more H_2 than ethylene glycol, methanol and ethanol. Its concentration also affects hydrogen production. In addition, Police et al. [279] reported that the sacrificial reagent concentration is also affecting the H_2 production. As in Fig. 16(c), the highest amount of H_2 is produced by using 5% methanol solution and with the increase in methanol concentration, no further increase in H_2 production was observed. This occurs since the surface of the photocatalyst reaches saturation with no further increase in H_2 production.

Advancements in photoreactors

Design of photoreactor

The photocatalytic performance depends on the configuration of catalyst in photoreactor. The photoreactor is the vessel for the reaction of photocatalyst and reactants with the presence of light (photon) to produce product. The type of reactor for UV and visible light irradiation has been depicted in Fig. 17. The main constructions of photoreactor are the suspended or immobilized catalyst and light irradiation [301]. An ideal photoreactor need to have uniform light distribution for the entire photoreactor in order to get the higher photocatalytic efficiency. The parameters which determine the types of photoreactor are the phase involved and the mode of operation. Table 12 summarized the advantages and limitations of different types of photoreactor.

Slurry photoreactor

A slurry reactor contains catalyst in a powder or granular form. Typically, this reactor is used when the reactants come in both the gas and liquid phase while the catalyst is a solid. The gaseous reactant is bubbled through the liquid and then diffuses onto the catalyst surface where the reaction takes place. The commonly used slurry photoreactor is an annular reactor. Annular design is a tubular reactor with a lamp array located only at the axis as shown in Fig. 18 [305].

Please cite this article as: Fajrina N, Tahir M, A critical review in strategies to improve photocatalytic water splitting towards hydrogen production, International Journal of Hydrogen Energy, https://doi.org/10.1016/j.ijhydene.2018.10.200

Table 11 – Summary of various sacrificial agents used in photocatalytic hydrogen.

Year	Feed	Catalyst	Reactor/Parameter	Product H_2 & Comment	Ref.
2019	5 vol% alcohol–water Water, methanol, ethanol, propanol, ethylene glycol, glycerol	0.05 g MWCNTs/TiO_2/MMT	Quartz glass flask Visible light 35 W Xe lamp	(1888 ppm h^{-1}) Glycerol > ethylene glycol > methanol > ethanol > propanol > water.	[16]
2017	10% v/v alcohol-water Water, glycerol and propan-2-ol	85 mg 0.5 wt% Pt//TiO_2	Pyrex reactor 125 W Hg lamp Medium pressure Light intensity of ca. 1.2×10^{-5} Einstein s^{-1} Time = 1000 min	(ca. 5.5 s^{-1}) Pt > Pd > Au Propan-2-ol > glycerol	[64]
2016	25 vol% alcohol–water Water, *tert*-butyl alcohol (*t*-BuOH), *n*-butanol (*n*-BuOH), *n*-propanol (*n*-PrOH), ethanol (EtOH), and methanol (MeOH)	50 mg 0.5 wt%RuO_2@TiO_2@1 wt% Pt	Glass quartz reactor UV light 3 W LED lamp (λ = 365 nm) Temperature at 30 °C	(4200 μmol g^{-1} h^{-1}) MeOH > EtOH > *n*-, PrOH > *n*-BuOH > *t*-BuOH	[120]
2015	10 vol% alcohol–water Water, Methanol and ethanol (1° alcohols), 2-propanol (2° alcohols), tertiary butanol (3° alcohol), 1,2-ethanediol and 1,2-propanediol (diols) and glycerol (a triol)	0.0065 g 1 wt% Pd/TiO_2	Tubular Pyrex reactor UV (365 nm, 5 mW cm^{-2}) Spectraline model SB-1000P/F lamp (200 W, 365 nm) Photon flux = 5.1 mW cm^{-2}	(47.5 mmol g^{-1} h^{-1}) Pd > Pt ≈ Au. Glycerol > 1,2-ethanediol > 1,2-propanediol > methanol > ethanol > 2-propanol > *tert*-butanol » water	[69]
2015	10 vol% alcohol–water Methanol, anhydrous ethanol, ethylene glycol and glycerol	450 mL aqueous solution, 2.5-Cu_2O/TiO_2	Quartz reactor system 500 W Xe arc lamp λ = 365 nm, photon flux = 3.6 mW cm^{-2} 40 °C under atmospheric pressure	(2048.25 μmol g^{-1} h^{-1}) Methanol > ethylene glycol ≈ glycerol > anhydrous ethanol	[98]
2015	10 vol% alcohol–water Water, methanol, ethanol, ethylene glycol and glycerol	6.5 mg 1.5 wt% Au/P25 TiO_2	Tubular pyrex reactor UV light Spectroline model SB-100P/F lamp (100 W, 365 nm) UV flux of 6.5 mW cm^{-2}	(27.9 mmol g^{-1} h^{-1}) Au/P25 > Au/anatase SG ≈ Au/brookite > Au/anatase HT ≈ Au/rutile HT Glycerol > ethylene glycol > methanol > ethanol	[72]
2015	Methanol, ethanol, ethylene glycol and glycerol	75 ml TiO_2 2.1 wt%Pt/TiO_2	Borosilicate photo reactor light source is 3 Philips Solarium lamps (4 × 15 W) λ = 300, 400 and <365 nm Temperature is 25 °C, pH = 5	(1134 μmol h^{-1}) Methanol (17.13 M) > ethanol (7.34 M) > ethylene glycol > glycerol.	[73]

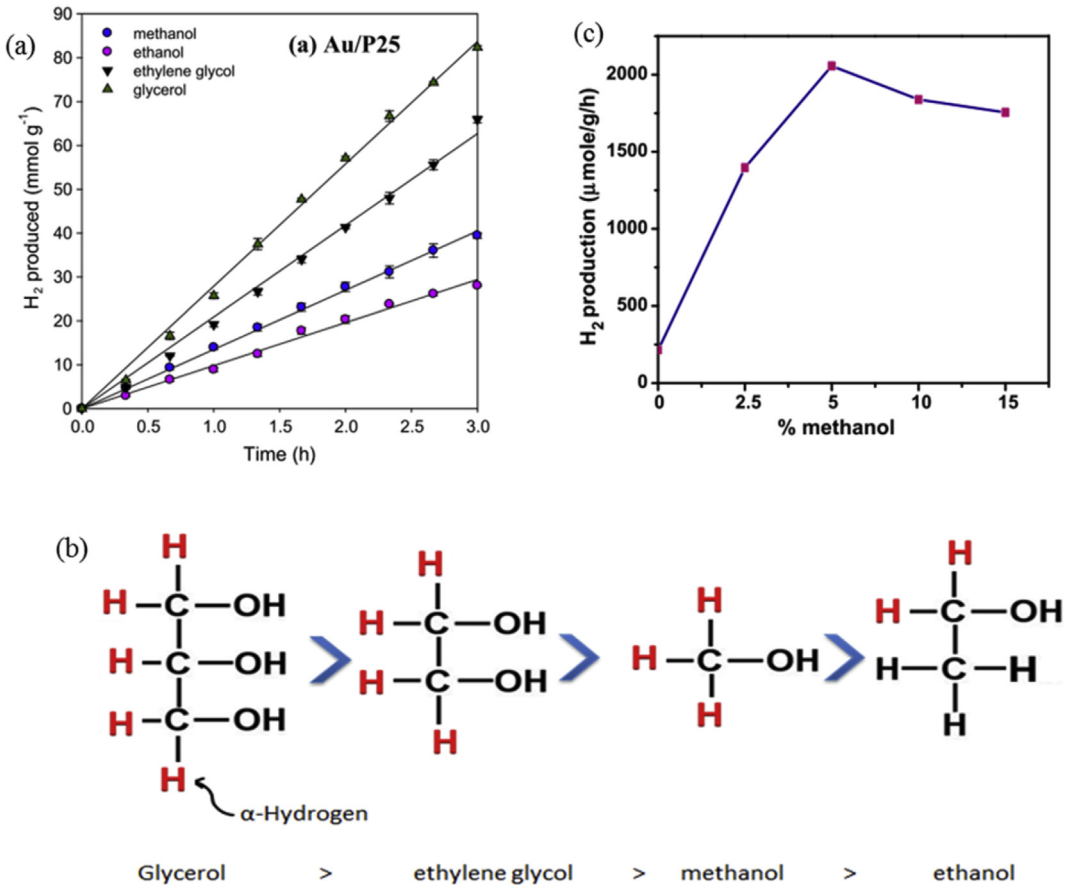

Fig. 16 – (a) Plot of H_2 production in different sacrificial reagent; (b) The structure of sacrificial agents according to the hydrogen production; and (c) Effect of methanol concentration [72,279].

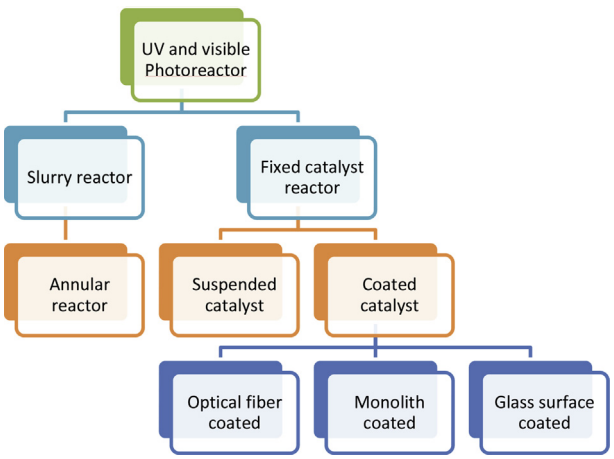

Fig. 17 – Type of photoreactors for UV and visible light photocatalytic H_2 production.

When powders or pellets are dispersed in liquid, the quantum efficiency of the catalyst, absorption properties of catalyst and reactants and light intensity determine the rate of reaction. The advantage of slurry system is the use of entire external surface illumination during the reaction. This is because the small particle size of the catalyst and phase segregation is not occurring as the solution is homogeneously mixed. Although, slurry system design offers high catalyst loading and simple structure design, separation of catalyst particles from mixture is quite difficult. The size of the catalyst crystals will determine the separation process required which could be costly and time consuming. However, the light utilization into the reaction medium can also be limited by the strong light absorption of organic species and catalyst particles. A large proportion of the catalyst surface might be inactive due to low photon energy received, as most of the light irradiation would be lost due to absorption by liquid when light approaches the catalyst through the bulk liquid phase. The amounts of photo catalyst used should be in a minimum quantity to avoid poor light penetration in the suspension [306].

Optical fiber and honeycomb reactors

Optical fibers are made by silica to transmit light between two ends of the fibers. The difference of refraction index between the semiconductor (e.g., TiO_2) coating and the quartz core causes the light to split into two beams when hitting the internal surface fiber. The light is reflected and transmitted along the fiber, while the rest penetrates and excites the

Table 12 – The advantages and limitations of different types of photoreactor.

Reactor design	Advantages	Limitation	Ref.
Slurry reactor	• Can be operated in fixed bed mode or continuous flow patterns • Combination of gas-liquid-solid phase	• Continuous stirring causes the additional cost • Active contact surface for reaction is low	[302,303]
Fluidized reactor	• High photocatalytic activity • Efficient heat and mass transfer rate by vigorous agitation of solid	• Abrasion of particles and attrition of the catalyst causes erosion at reactor • Catalyst is difficult to be separated from mixture	[302,303]
Optical fiber reactor	• Surface area is larger • Efficiency of light utilization is higher • Efficient processing capacities of the catalyst	• Deactivation catalyst at high temperature • Maximum reactor volume cannot be applying • Uniform coating of fibers is complex	[302–304]
Monolith reactor	• Ratio of surface to volume is higher • Pressure drop is low • Flow rate is higher	• Light efficiency is low • Catalyst adhesion on wall is lower	[302–304]
Fixed bed reactor	• Surface area is large • Reaction time is faster • Conversion rate per unit mass of catalyst is high • Operating cost is lower	• Temperature gradient between gas and solid surface is common • Exposure of catalyst to light is low • Conversion and yield rate is low	[302,303]

titania layer at the interface. Thus, the electron–hole pairs are generated and the photo-reactions would occur. Therefore, optical fibers can be used to radiate the light uniformly inside a photoreactor [307]. Light is transmitted along the fibers core by the cladding with lower refractive index that traps light in the core through total internal reflection [303]. Previously, photocatalytic water splitting have been conducted using optical fiber coated TiO_2 and SiO_2 with enhanced H_2 production rate [308].

Some of the advantages of optical fibers are high efficiency of uniform light distribution throughout the reactor and cause high interaction between irradiations and catalyst surface. Hence, it can give higher conversion and yield rates and it is economic with low cost operation. However, they have various disadvantages such as lower adhesion strength, relatively low surface area for chemical reaction and only 20–30% of the reactor volume is available for photocatalysis. The catalyst coating needs special method and uniform coating of fiber is complex with low adhesion strength.

Typically, in an optical fiber reactor, the photocatalyst is coated on the fibers, where light is propagated along the fiber length by reflection on the fiber wall as shown in Fig. 19(a). However, light intensity can decay exponentially along the axial direction of the coated fiber and the amount of refraction in the fiber depends on the thickness of the photo catalyst coating. In addition, the electrons and holes are generated from the interface between the photo catalyst and the reagents due to the back-irradiation and consequent susceptibility to recombination loss. Hence, an improvement has been done by designing optical fiber honeycomb reactors, where the photocatalyst is immobilized on the monolith wall [309]. As shown the Fig. 19(b), Taboada et al. [306] reported that the optical fiber honeycomb photoreactor is much better with fivefold increases than the slurry photo reactor system and Fig. 19(c) shows the H_2 production in the optical fiber honeycomb reactor. With this new design of reactor, the light efficiency and availability combined with optimum mass transfer and scale-up potential can be achieved.

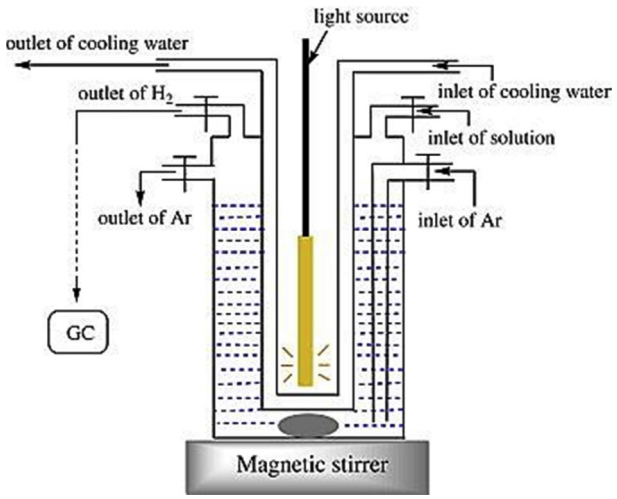

Fig. 18 – Annular reactor for photocatalytic water splitting to produce H_2 [305].

Monolith reactor

Usage of monolith having micro channels with higher light interaction surface area can increase the conversion and yield rates [310]. The monolith designs are uniform blocks with parallel channels that can be extruded into different shapes and sizes. Ceramic monolithic structures show an attractive option to conventionally prepared catalyst pellets or powders because of its excellent properties. Monoliths can provide better mass transfer, better porosity, good coating adherence, low pressure drop, good mechanical strength and thermal stability over typical catalyst powders or pellets [311].

Recent advancements in photo technology showed that monolith reactors have various benefits when compared with commercial reactors. In 2017, Gaudillere et al. [312] have tested water splitting for hydrogen production with ethanol as sacrificial agent in a monolith photoreactor. The quantum efficiency in microchannel monolith reactor was proven much higher (0.10%) than using cell type reactor (0.0005%) [313]. The photo catalyst employed was $NiO–In_2O_3/TiO_2$ and showed better performance efficiency in the batch monolith photoreactor than using cell type reactor under same reaction conditions with efficiency 14.13 folds higher [314]. Xiong et al.

Please cite this article as: Fajrina N, Tahir M, A critical review in strategies to improve photocatalytic water splitting towards hydrogen production, International Journal of Hydrogen Energy, https://doi.org/10.1016/j.ijhydene.2018.10.200

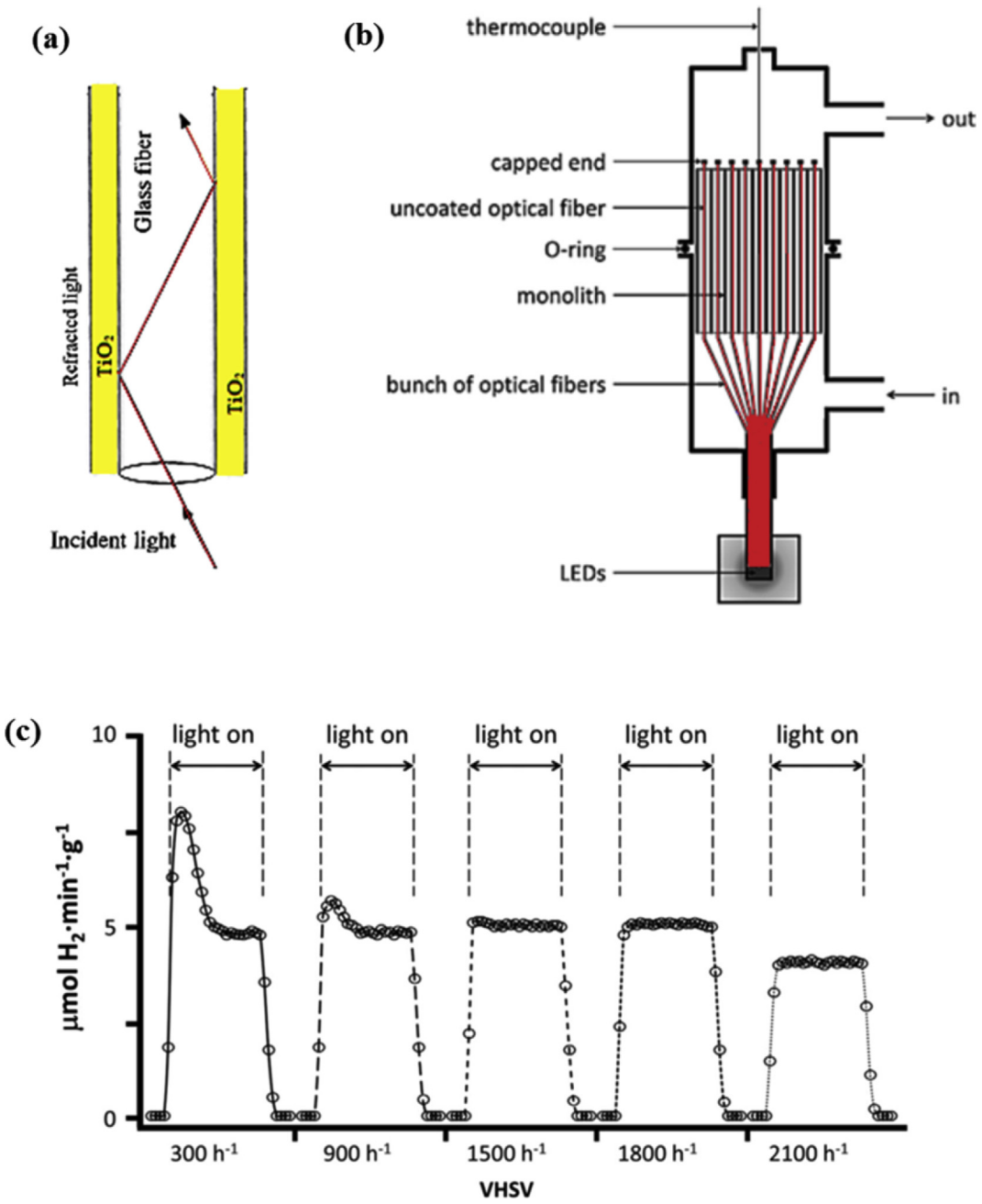

Fig. 19 – (a) Schematic diagram of light propagating in a TiO_2-coated optical fiber [306]; (b) Scheme of optical fiber honeycomb reactor; and (c) Hydrogen photo-production rate at different VHSV over 1 wt% Au/TiO_2 in the optical fiber honeycomb reactor.

[315] reported that V-W/TiO_2 produces H_2 of 0.27 mol g^{-1} h^{-1} using honeycomb reactor was much higher than using conventional reactor due to high surface area per unit volume.

For preparing a new monolith catalyst, the active species is required to be deposited onto a monolith and acts as secondary support. This secondary support layer usually provides high surface area for photocatalytic water splitting. The cross-sectional single monolith channel for monolithic catalyst is illustrated in Fig. 20(a) [316]. The typical methods used for depositing the catalysts at monolith are sol–gel, slurry coating and colloidal coating [317]. Coating active catalyst layer onto monolith depends upon what nature of the active species. The commonly used techniques are precipitation and wet impregnation. The illustration of monolith photoreactor is shown in Fig. 20(b) [314]. There are several key factors to be considered when coating the secondary support to the monolith. These key factors consist of pH scale, concentration of slurry, appropriate calcination and drying procedure. The rheology and coating homogeneity can be improved by altering the pH scale of the coating solution in acidic medium. For concentration of slurry, it can be described in term of viscosity and solid content. The higher secondary loading can

Please cite this article as: Fajrina N, Tahir M, A critical review in strategies to improve photocatalytic water splitting towards hydrogen production, International Journal of Hydrogen Energy, https://doi.org/10.1016/j.ijhydene.2018.10.200

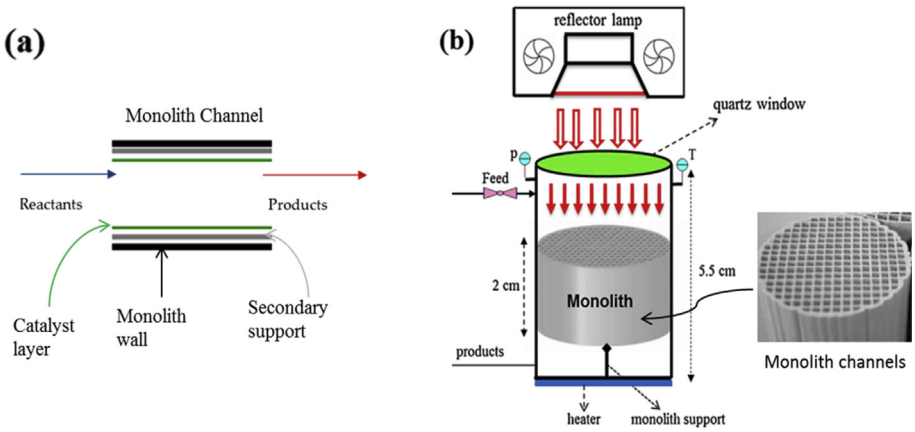

Fig. 20 – (a) The cross-sectional of single monolith channel; and (b) Monolith photo reactor [310].

be achieved at optimum slurry concentration of viscosity between 50 and 150 mPa and 25–45% of solid content. In addition, drying and calcining procedures must not be rushed, since this may affect coating on the monolith surface and to achieve good coat adherence [314].

Conclusion and future perspectives

With this review, recent progress in TiO_2 and g-C_3N_4 modification and development of photoreactors for photocatalytic H_2 production has been systematically discussed. The future efforts for more effective photocatalytic water splitting can be focused on the next aspects:

1. There are advantages and limitations for both TiO_2 and g-C_3N_4 modification strategies. However, these limitations can be overcome by ingenious ideas and engineering based on TiO_2 and g-C_3N_4. Combining TiO_2 and g-C_3N_4 with other semiconductors with Z-scheme construction can be predicted to generate more efficient photo-catalysts in water splitting. Although, the performance of Z-scheme is still low, it is expected to give impact to the innovation of catalyst in near future. While, the metal co-catalyst with SPR effect shown to have better potential and research into modification with suitable semiconductors can lead to great effect on the advancement of photocatalysts.
2. Recently, there is very little knowledge about the monolith photoreactor for photocatalytic water splitting. The monolith photoreactor, in which reaction is conducted in a gas phase, can lead to a new development in the reactor design due to higher photon flux utilization with larger illuminated surface area. It can inhibit the side product during the production of H_2 due to efficient absorption process, surface reactions and minimum mass transfer limitations. Hence, the monolith photo reactor can be expected to produce more yield of H_2 with higher selectivity.
3. It is well known that operating parameters such as temperature and pH also can enhance the efficiency of the photocatalysts. In addition, narrowing the band gap and controlling catalyst morphology enables efficient H_2 production. Therefore, future researches in catalyst synthesis and surface modification is necessary for the purpose of tuning the band gap to enhance visible light absorption with minimum charges recombination.
4. Previous researches of water splitting in the present of sacrificial agent only focus on the performance of H_2 production. Detailed study on role and mechanism of water splitting towards H_2 production in the presence of sacrificial agent should be given more attention. Specifically, gas phase water splitting reaction for H_2 production in the presence of sacrificial reagents has great importance.
5. Equipped with this comprehensive knowledge, the more effective system and performance of photo catalyst can be achieved.

In conclusion, regardless of the previous reports, the probability of TiO_2 and g-C_3N_4 modification for more efficient photocatalytic water splitting apparently has not been fully discovered. While the challenges in heterojunction have not been studied in detail, Z-scheme photocatalytic system is similar to the natural photosynthesis. It is recommended that full exploration of this can results in discovery in the efficiency of photocatalytic activity while using monolith photoreactor system. As a concluding remark, both opportunities and challenges are present in future development of this encouraging technology. Ideally, this review will enhance further advancement of TiO_2 and g-C_3N_4 modification for attaining its application for effective photocatalytic water splitting in the presence of sacrificial reagents with different types of photo-reactors.

Acknowledgments

The authors gratefully acknowledge to MOE (Ministroy of Education) Malaysia for the financial support of this research under FRGS (Fundamental Research Grant Scheme, Vote 4F876).

REFERENCES

[1] Ahmad H, Kamarudin SK, Minggu LJ, Kassim M. Hydrogen from photo-catalytic water splitting process: a review. Renew Sust Energy Rev 2015;43:599–610.

[2] Gupta NM. Factors affecting the efficiency of a water splitting photocatalyst: a perspective. Renew Sust Energy Rev 2016;71:585–601.
[3] Dubey PK, Tripathi P, Tiwari RS, Sinha ASK, Srivastava ON. Synthesis of reduced graphene oxide–TiO_2 nanoparticle composite systems and its application in hydrogen production. Int J Hydrogen Energy 2014;39:16282–92.
[4] Tee SY, Win KY, Teo WS, Koh LD, Liu S, Teng CP, et al. Recent progress in energy-driven water splitting. Adv Sci 2017;4:1600337.
[5] Acar C, Dincer I. Impact assessment and efficiency evaluation of hydrogen production methods. Int J Energy Res 2015;39:1757–68.
[6] Zhu J, Zäch M. Nanostructured materials for photocatalytic hydrogen production. Curr Opin Colloid Interface Sci 2009;14:260–9.
[7] Muradov N, Veziroglu T. "Green" path from fossil-based to hydrogen economy: an overview of carbon-neutral technologies. Int J Hydrogen Energy 2008;33:6804–39.
[8] Fujishima A. Electrochemical photolysis of water at a semiconductor electrode. Nature 1972;238:37–8.
[9] Pulido Melián E, González Díaz O, Ortega Méndez A, López CR, Nereida Suárez M, Doña Rodríguez JM, et al. Efficient and affordable hydrogen production by water photo-splitting using TiO_2-based photocatalysts. Int J Hydrogen Energy 2013;38:2144–55.
[10] Lin Y, Jiang Z, Zhu C, Hu X, Zhu H, Zhang X, et al. The optical absorption and hydrogen production by water splitting of (Si,Fe)-codoped anatase TiO_2 photocatalyst. Int J Hydrogen Energy 2013;38:5209–14.
[11] Ye S, Wang R, Wu M-Z, Yuan Y-P. A review on g-C_3N_4 for photocatalytic water splitting and CO_2 reduction. Appl Surf Sci 2015;358:15–27.
[12] Li H, Tu W, Zhou Y, Zou Z. Z-scheme photocatalytic systems for promoting photocatalytic performance: recent progress and future challenges. Adv Sci 2016;3:1500389.
[13] Boudjemaa A, Rebahi A, Terfassa B, Chebout R, Mokrani T, Bachari K, et al. Fe_2O_3/carbon spheres for efficient photo-catalytic hydrogen production from water and under visible light irradiation. Sol Energy Mater Sol Cells 2015;140:405–11.
[14] Ling C, Xue Q, Han Z, Zhang Z, Du Y, Liu Y, et al. High hydrogen response of Pd/TiO_2/SiO_2/Si multilayers at room temperature. Sens Actuators B 2014;205:255–60.
[15] Bahruji H, Bowker M, Davies PR, Pedrono F. New insights into the mechanism of photocatalytic reforming on Pd/TiO_2. Appl Catal B 2011;107:205–9.
[16] Umer M, Tahir M, Azam MU, Jaffar MM. Metals free MWCNTs@TiO_2@MMT heterojunction composite with MMT as a mediator for fast charges separation towards visible light driven photocatalytic hydrogen evolution. Appl Surf Sci 2019;463:747–57.
[17] Tahir B, Tahir M, Amin NS. Gold–indium modified TiO_2 nanocatalysts for photocatalytic CO_2 reduction with H_2 as reductant in a monolith photoreactor. Appl Surf Sci 2015;338:1–14.
[18] Abe R. Recent progress on photocatalytic and photoelectrochemical water splitting under visible light irradiation. J Photochem Photobiol C 2010;11:179–209.
[19] Shi N, Li X, Fan T, Zhou H, Zhang D, Zhu H. Artificial chloroplast: Au/chloroplast-morph-TiO_2 with fast electron transfer and enhanced photocatalytic activity. Int J Hydrogen Energy 2014;39:5617–24.
[20] Clarizia L, Spasiano D, Di Somma I, Marotta R, Andreozzi R, Dionysiou DD. Copper modified-TiO_2 catalysts for hydrogen generation through photoreforming of organics. A short review. Int J Hydrogen Energy 2014;39:16812–31.
[21] Dincer I, Acar C. Review and evaluation of hydrogen production methods for better sustainability. Int J Hydrogen Energy 2015;40:11094–111.
[22] Kondarides DI, Daskalaki VM, Patsoura A, Verykios XE. Hydrogen production by photo-induced reforming of biomass components and derivatives at ambient conditions. Catal Lett 2007;122:26–32.
[23] Tahir M, Amin NS. Advances in visible light responsive titanium oxide-based photocatalysts for CO_2 conversion to hydrocarbon fuels. Energy Convers Manage 2013;76:194–214.
[24] Chouhan N, Ameta R, Meena RK, Mandawat N, Ghildiyal R. Visible light harvesting Pt/CdS/Co-doped ZnO nanorods molecular device for hydrogen generation. Int J Hydrogen Energy 2016;41:2298–306.
[25] Grewe T, Meggouh M, Tuysuz H. Nanocatalysts for solar water splitting and a perspective on hydrogen economy. Chem Asian J 2016;11:22–42.
[26] Acar C, Dincer I, Zamfirescu C. A review on selected heterogeneous photocatalysts for hydrogen production. Int J Energy Res 2014;38:1903–20.
[27] Xu Y, Xu R. Nickel-based cocatalysts for photocatalytic hydrogen production. Appl Surf Sci 2015;351:779–93.
[28] Wen J, Xie J, Chen X, Li X. A review on g-C_3N_4-based photocatalysts. Appl Surf Sci 2017;391:72–123.
[29] Chiarello GL, Aguirre MH, Selli E. Hydrogen production by photocatalytic steam reforming of methanol on noble metal-modified TiO_2. J Catal 2010;273:182–90.
[30] Etacheri V, Di Valentin C, Schneider J, Bahnemann D, Pillai SC. Visible-light activation of TiO_2 photocatalysts: advances in theory and experiments. J Photochem Photobiol C 2015;25:1–29.
[31] Colon G. Towards the hydrogen production by photocatalysis. Appl Catal A 2016;518:48–59.
[32] Maeda K. Photocatalytic water splitting using semiconductor particles: history and recent developments. J Photochem Photobiol C 2011;12:237–68.
[33] Zamfirescu C, Naterer G, Dincer I. Photo-electro-chemical chlorination of cuprous chloride with hydrochloric acid for hydrogen production. Int J Hydrogen Energy 2012;37:9529–36.
[34] Zamfirescu C, Dincer I, Naterer G. Analysis of a photochemical water splitting reactor with supramolecular catalysts and a proton exchange membrane. Int J Hydrogen Energy 2011;36:11273–81.
[35] Liu B, Zhao X, Terashima C, Fujishima A, Nakata K. Thermodynamic and kinetic analysis of heterogeneous photocatalysis for semiconductor systems. Phys Chem Chem Phys 2014;16:8751–60.
[36] Shehzad N, Tahir M, Johari K, Murugesan T, Hussain M. A critical review on TiO_2 based photocatalytic CO_2 reduction system: strategies to improve efficiency. J CO2 Util 2018;26:98–122.
[37] Yan SC, Lv SB, Li ZS, Zou ZG. Organic-inorganic composite photocatalyst of g-C_3N_4 and TaON with improved visible light photocatalytic activities. Dalton Trans 2010;39:1488–91.
[38] Chun W-J, Ishikawa A, Fujisawa H, Takata T, Kondo JN, Hara M, et al. Conduction and valence band positions of Ta_2O_5, TaON, and Ta_3N_5 by UPS and electrochemical methods. J Phys Chem B 2003;107:1798–803.
[39] Long M, Cai W, Kisch H. Visible light induced photoelectrochemical properties of n-$BiVO_4$ and n-$BiVO_4$/p-Co_3O_4. J Phys Chem C 2008;112:548–54.
[40] Yi Z, Ye J, Kikugawa N, Kako T, Ouyang S, Stuart-Williams H, et al. An orthophosphate semiconductor with photooxidation properties under visible-light irradiation. Nat Mater 2010;9:559–64.

Please cite this article as: Fajrina N, Tahir M, A critical review in strategies to improve photocatalytic water splitting towards hydrogen production, International Journal of Hydrogen Energy, https://doi.org/10.1016/j.ijhydene.2018.10.200

[41] Li X, Yu J, Jaroniec M. Hierarchical photocatalysts. Chem Soc Rev 2016;45:2603–36.
[42] Chiarello GL, Dozzi MV, Scavini M, Grunwaldt J-D, Selli E. One step flame-made fluorinated Pt/TiO_2 photocatalysts for hydrogen production. Appl Catal B 2014;160–161:144–51.
[43] Mu R, Zhao ZJ, Dohnalek Z, Gong J. Structural motifs of water on metal oxide surfaces. Chem Soc Rev 2017;46:1785–806.
[44] Chiu I, Lin S-X, Kao C-T, Wu R-J. Promoting hydrogen production by loading PdO and Pt on N–TiO_2 under visible light. Int J Hydrogen Energy 2014;39:14574–80.
[45] Velázquez JJ, Fernández-González R, Díaz L, Pulido Melián E, Rodríguez VD, Núñez P. Effect of reaction temperature and sacrificial agent on the photocatalytic H_2-production of Pt-TiO_2. J Alloys Compd 2017;721:405–10.
[46] Chang X, Wang T, Zhang P, Wei Y, Zhao J, Gong J. Stable aqueous photoelectrochemical CO_2 reduction by a Cu_2O dark cathode with improved selectivity for carbonaceous products. Angew Chem Int Ed Engl 2016;55:8840–5.
[47] Zhang P, Wang T, Gong J. Current mechanistic understanding of surface reactions over water-splitting photocatalysts. Chem 2018;4:223–45.
[48] Low J, Cheng B, Yu J. Surface modification and enhanced photocatalytic CO_2 reduction performance of TiO_2: a review. Appl Surf Sci 2017;392:658–86.
[49] Rather RA, Singh S, Pal B. Visible and direct sunlight induced H_2 production from water by plasmonic Ag-TiO_2 nanorods hybrid interface. Sol Energy Mater Sol Cells 2017;160:463–9.
[50] Zhu Z, Kao C-T, Tang B-H, Chang W-C, Wu R-J. Efficient hydrogen production by photocatalytic water-splitting using Pt-doped TiO_2 hollow spheres under visible light. Ceram Int 2016;42:6749–54.
[51] Naik GK, Majhi SM, Jeong K-U, Lee I-H, Yu YT. Nitrogen doping on the core-shell structured Au@TiO_2 nanoparticles and its enhanced photocatalytic hydrogen evolution under visible light irradiation. J Alloys Compd 2019;771:505–12.
[52] Chen W-T, Chan A, Sun-Waterhouse D, Llorca J, Idriss H, Waterhouse GIN. Performance comparison of Ni/TiO_2 and Au/TiO_2 photocatalysts for H_2 production in different alcohol-water mixtures. J Catal 2018;367:27–42.
[53] Wang F, Shen T, Fu Z, Lu Y, Chen C. Enhanced photocatalytic water-splitting performance using Fe-doped hierarchical TiO_2 ball-flowers. Nanotechnology 2018;29:035702.
[54] Saravanan R, Manoj D, Qin J, Naushad M, Gracia F, Lee AF, et al. Mechanothermal synthesis of Ag/TiO_2 for photocatalytic methyl orange degradation and hydrogen production. Process Saf Environ Prot 2018;120:339–47.
[55] Liu Q-F, Zhang Q, Liu B-R, Li S, Ma J-J. Building surface defects by doping with transition metal on ultrafine TiO_2 to enhance the photocatalytic H_2 production activity. Chin J Catal 2018;39:542–8.
[56] Chen J, Ding T, Cai J, Wang Y, Wu M, Zhang H, et al. Synergistic effects of K addition and hydrogenation of TiO_2 on photocatalytic hydrogen production under simulated solar light. Appl Surf Sci 2018;453:101–9.
[57] He Q, Sun H, Shang Y, Tang Y, She P, Zeng S, et al. Au@TiO_2 yolk-shell nanostructures for enhanced performance in both photoelectric and photocatalytic solar conversion. Appl Surf Sci 2018;441:458–65.
[58] Si Y, Cao S, Wu Z, Ji Y, Mi Y, Wu X, et al. What is the predominant electron transfer process for Au NRs/TiO_2 nanodumbbell heterostructure under sunlight irradiation? Appl Catal B 2018;220:471–6.
[59] Kennedy J, Bahruji H, Bowker M, Davies PR, Bouleghlimat E, Issarapanacheewin S. Hydrogen generation by photocatalytic reforming of potential biofuels: polyols, cyclic alcohols, and saccharides. J Photochem Photobiol A 2018;356:451–6.
[60] Elbanna O, Kim S, Fujitsuka M, Majima T. TiO_2 mesocrystals composited with gold nanorods for highly efficient visible-NIR-photocatalytic hydrogen production. Nano Energy 2017;35:1–8.
[61] Sadanandam G, Valluri DK, Scurrell MS. Highly stabilized Ag_2O-loaded nano TiO_2 for hydrogen production from glycerol: water mixtures under solar light irradiation. Int J Hydrogen Energy 2017;42:807–20.
[62] Marchal C, Piquet A, Behr M, Cottineau T, Papaefthimiou V, Keller V, et al. Activation of solid grinding-derived Au/TiO_2 photocatalysts for solar H_2 production from water-methanol mixtures with low alcohol content. J Catal 2017;352:22–34.
[63] Nguyen NT, Hwang I, Kondo T, Yanagishita T, Masuda H, Schmuki P. Optimizing TiO_2 nanotube morphology for enhanced photocatalytic H_2 evolution using single-walled and highly ordered TiO_2 nanotubes decorated with dewetted Au nanoparticles. Electrochem Commun 2017;79:46–50.
[64] Lopez-Tenllado FJ, Hidalgo-Carrillo J, Montes V, Marinas A, Urbano FJ, Marinas JM, et al. A comparative study of hydrogen photocatalytic production from glycerol and propan-2-ol on M/TiO_2 systems (M=Au, Pt, Pd). Catal Today 2017;280:58–64.
[65] Li F, Gu Q, Niu Y, Wang R, Tong Y, Zhu S, et al. Hydrogen evolution from aqueous-phase photocatalytic reforming of ethylene glycol over Pt/TiO_2 catalysts: role of Pt and product distribution. Appl Surf Sci 2017;391:251–8.
[66] Wang Z, Yin Y, Williams T, Wang H, Sun C, Zhang X. Metal link: a strategy to combine graphene and titanium dioxide for enhanced hydrogen production. Int J Hydrogen Energy 2016;41:22034–42.
[67] Khalid NR, Ahmed E, Ahmad M, Niaz NA, Ramzan M, Shakil M, et al. Microwave-assisted synthesis of Ag–TiO_2/graphene composite for hydrogen production under visible light irradiation. Ceram Int 2016;42:18257–63.
[68] Melvin AA, Illath K, Das T, Raja T, Bhattacharyya S, Gopinath CS. M-Au/TiO_2 (M = Ag, Pd, and Pt) nanophotocatalyst for overall solar water splitting: role of interfaces. Nanoscale 2015;7:13477–88.
[69] Al-Azri ZHN, Chen W-T, Chan A, Jovic V, Ina T, Idriss H, et al. The roles of metal co-catalysts and reaction media in photocatalytic hydrogen production: performance evaluation of M/TiO_2 photocatalysts (M=Pd, Pt, Au) in different alcohol–water mixtures. J Catal 2015;329:355–67.
[70] Chen W-T, Chan A, Sun-Waterhouse D, Moriga T, Idriss H, Waterhouse GIN. Ni/TiO_2: a promising low-cost photocatalytic system for solar H_2 production from ethanol–water mixtures. J Catal 2015;326:43–53.
[71] Lopez Ortiz A, Melendez Zaragoza M, Salinas Gutierrez J, Marques da Silva Paula M, Collins-Martinez V. Silver oxidation state effect on the photocatalytic properties of Ag doped TiO_2 for hydrogen production under visible light. Int J Hydrogen Energy 2015;40:17308–15.
[72] Chen W-T, Chan A, Al-Azri ZHN, Dosado AG, Nadeem MA, Sun-Waterhouse D, et al. Effect of TiO_2 polymorph and alcohol sacrificial agent on the activity of Au/TiO_2 photocatalysts for H_2 production in alcohol–water mixtures. J Catal 2015;329:499–513.
[73] Lopez CR, Melian EP, Ortega Mendez JA, Santiago DE, Dona Rodriguez JM, Gonzalez Diaz O. Comparative study of alcohols as sacrificial agents in H_2 production by heterogeneous photocatalysis using Pt/TiO_2 catalysts. J Photochem Photobiol A 2015;312:45–54.
[74] Ortega Méndez JA, López CR, Pulido Melián E, González Díaz O, Doña Rodríguez JM, Fernández Hevia D, et al.

Please cite this article as: Fajrina N, Tahir M, A critical review in strategies to improve photocatalytic water splitting towards hydrogen production, International Journal of Hydrogen Energy, https://doi.org/10.1016/j.ijhydene.2018.10.200

Production of hydrogen by water photo-splitting over commercial and synthesised Au/TiO_2 catalysts. Appl Catal B 2014;147:439–52.
[75] Puskelova J, Baia L, Vulpoi A, Baia M, Antoniadou M, Dracopoulos V, et al. Photocatalytic hydrogen production using TiO_2–Pt aerogels. Chem Eng J 2014;242:96–101.
[76] Wang C, Hu Q, Huang J, Zhu C, Deng Z, Shi H, et al. Enhanced hydrogen production by water splitting using Cu-doped TiO_2 film with preferred (001) orientation. Appl Surf Sci 2014;292:161–4.
[77] Zhang D, Ma X, Zhang H, Liao Y, Xiang Q. Enhanced photocatalytic hydrogen evolution activity of carbon and nitrogen self-doped TiO_2 hollow sphere with the creation of oxygen vacancy and Ti^{3+}. Mater Today Energy 2018;10:132–40.
[78] Luo Z, Li C, Liu S, Wang T, Gong J. Gradient doping of phosphorus in Fe_2O_3 nanoarray photoanodes for enhanced charge separation. Chem Sci 2017;8:91–100.
[79] Wang C, Hu Q, Huang J, Wu L, Deng Z, Liu Z, et al. Efficient hydrogen production by photocatalytic water splitting using N-doped TiO_2 film. Appl Surf Sci 2013;283:188–92.
[80] Wang C, Hu Q-Q, Huang J-Q, Deng Z-H, Shi H-L, Wu L, et al. Effective water splitting using N-doped TiO_2 films: role of preferred orientation on hydrogen production. Int J Hydrogen Energy 2014;39:1967–71.
[81] Li H, Hao Y, Lu H, Liang L, Wang Y, Qiu J, et al. A systematic study on visible-light N-doped TiO_2 photocatalyst obtained from ethylenediamine by sol–gel method. Appl Surf Sci 2015;344:112–8.
[82] Xing Z, Li Z, Wu X, Wang G, Zhou W. In-situ S-doped porous anatase TiO_2 nanopillars for high-efficient visible-light photocatalytic hydrogen evolution. Int J Hydrogen Energy 2016;41:1535–41.
[83] Sudha D, Sivakumar P. Review on the photocatalytic activity of various composite catalysts. Chem Eng Process 2015;97:112–33.
[84] Lakshmana Reddy N, Emin S, Valant M, Shankar MV. Nanostructured Bi_2O_3@TiO_2 photocatalyst for enhanced hydrogen production. Int J Hydrogen Energy 2017. https://doi.org/10.1016/j.ijhydene.2016.12.154.
[85] Fujita S-i, Kawamori H, Honda D, Yoshida H, Arai M. Photocatalytic hydrogen production from aqueous glycerol solution using NiO/TiO_2 catalysts: effects of preparation and reaction conditions. Appl Catal B 2016;181:818–24.
[86] Hu X, Lu S, Tian J, Wei N, Song X, Wang X, et al. The selective deposition of MoS_2 nanosheets onto (101) facets of TiO_2 nanosheets with exposed (001) facets and their enhanced photocatalytic H_2 production. Appl Catal B 2019;241:329–37.
[87] Liu Y, Li Y, Peng F, Lin Y, Yang S, Zhang S, et al. 2H- and 1T-mixed phase few-layer MoS_2 as a superior to Pt co-catalyst coated on TiO_2 nanorod arrays for photocatalytic hydrogen evolution. Appl Catal B 2019;241:236–45.
[88] Pan J, Dong Z, Wang B, Jiang Z, Zhao C, Wang J, et al. The enhancement of photocatalytic hydrogen production via Ti^{3+} self-doping black TiO_2/g-C_3N_4 hollow core-shell nano-heterojunction. Appl Catal B 2019;242:92–9.
[89] El-Maghrabi HH, Barhoum A, Nada AA, Moustafa YM, Seliman SM, Youssef AM, et al. Synthesis of mesoporous core-shell CdS@TiO_2 (0D and 1D) photocatalysts for solar-driven hydrogen fuel production. J Photochem Photobiol A 2018;351:261–70.
[90] Wang J, Wang Z, Qu P, Xu Q, Zheng J, Jia S, et al. A 2D/1D TiO_2 nanosheet/CdS nanorods heterostructure with enhanced photocatalytic water splitting performance for H_2 evolution. Int J Hydrogen Energy 2018;43:7388–96.
[91] Liu J, Ke J, Li Y, Liu B, Wang L, Xiao H, et al. Co_3O_4 quantum dots/TiO_2 nanobelt hybrids for highly efficient photocatalytic overall water splitting. Appl Catal B 2018;236:396–403.
[92] Le L, Wu Y, Zhou Z, Wang H, Xiong R, Shi J. Cu_2O clusters decorated on flower-like TiO_2 nanorod array film for enhanced hydrogen production under solar light irradiation. J Photochem Photobiol A 2018;351:78–86.
[93] Tan Y, Shu Z, Zhou J, Li T, Wang W, Zhao Z. One-step synthesis of nanostructured g-C_3N_4/TiO_2 composite for highly enhanced visible-light photocatalytic H_2 evolution. Appl Catal B 2018;230:260–8.
[94] Pan C, Jia J, Hu X, Fan J, Liu E. In situ construction of g-C_3N_4/TiO_2 heterojunction films with enhanced photocatalytic activity over magnetic-driven rotating frame. Appl Surf Sci 2018;430:283–92.
[95] El-Bery HM, Matsushita Y, Abdel-moneim A. Fabrication of efficient TiO_2-RGO heterojunction composites for hydrogen generation via water-splitting: comparison between RGO, Au and Pt reduction sites. Appl Surf Sci 2017;423:185–96.
[96] Tian F, Hou D, Hu F, Xie K, Qiao X, Li D. Pouous TiO_2 nanofibers decorated CdS nanoparticles by SILAR method for enhanced visible-light-driven photocatalytic activity. Appl Surf Sci 2017;391:295–302.
[97] Al-Mayman SI, Al-Johani MS, Mohamed MM, Al-Zeghayer YS, Ramay SM, Al-Awadi AS, et al. TiO_2-ZnO photocatalysts synthesized by sol–gel auto-ignition technique for hydrogen production. Int J Hydrogen Energy 2016;42:5016–25.
[98] Li Y, Wang B, Liu S, Duan X, Hu Z. Synthesis and characterization of Cu_2O/TiO_2 photocatalysts for H_2 evolution from aqueous solution with different scavengers. Appl Surf Sci 2015;324:736–44.
[99] Li L, Cheng B, Wang Y, Yu J. Enhanced photocatalytic H_2-production activity of bicomponent NiO/TiO_2 composite nanofibers. J Colloid Interface Sci 2015;449:115–21.
[100] Kim HS, Kim D, Kwak BS, Han GB, Um M-H, Kang M. Synthesis of magnetically separable core@shell structured $NiFe_2O_4$@TiO_2 nanomaterial and its use for photocatalytic hydrogen production by methanol/water splitting. Chem Eng J 2014;243:272–9.
[101] Haldorai Y, Rengaraj A, Kwak CH, Huh YS, Han Y-K. Fabrication of nano TiO_2@graphene composite: reusable photocatalyst for hydrogen production, degradation of organic and inorganic pollutants. Synth Met 2014;198:10–8.
[102] Kum JM, Yoo SH, Ali G, Cho SO. Photocatalytic hydrogen production over CuO and TiO_2 nanoparticles mixture. Int J Hydrogen Energy 2013;38:13541–6.
[103] Pérez-Larios A, Lopez R, Hernandez-Gordillo A, Tzompantzi F, Gómez R, Torres-Guerra L. Improved hydrogen production from water splitting using TiO_2–ZnO mixed oxides photocatalysts. Fuel 2012;100:139–43.
[104] Serpone N, Emeline AV. Semiconductor photocatalysis — past, present, and future outlook. J Phys Chem Lett 2012;3:673–7.
[105] Xie M-Y, Su K-Y, Peng X-Y, Wu R-J, Chavali M, Chang W-C. Hydrogen production by photocatalytic water-splitting on Pt-doped TiO_2–ZnO under visible light. J Taiwan Inst Chem E 2017;70:161–7.
[106] Zhao H, Wu M, Liu J, Deng Z, Li Y, Su B-L. Synergistic promotion of solar-driven H_2 generation by three-dimensionally ordered macroporous structured TiO_2-Au-CdS ternary photocatalyst. Appl Catal B 2016;184:182–90.
[107] Ai Z, Shao Y, Chang B, Huang B, Wu Y, Hao X. Effective orientation control of photogenerated carrier separation via rational design of a $Ti_3C_2(TiO_2)$@CdS/MoS_2 photocatalytic system. Appl Catal B 2019;242:202–8.
[108] Guo X, Li X, Qin L, Kang S-Z, Li G. A highly active nano-micro hybrid derived from Cu-bridged TiO_2/porphyrin for

Please cite this article as: Fajrina N, Tahir M, A critical review in strategies to improve photocatalytic water splitting towards hydrogen production, International Journal of Hydrogen Energy, https://doi.org/10.1016/j.ijhydene.2018.10.200

enhanced photocatalytic hydrogen production. Appl Catal B 2019;243:1–9.
[109] Wang M, Zhen W, Tian B, Ma J, Lu G. The inhibition of hydrogen and oxygen recombination reaction by halogen atoms on over-all water splitting over Pt-TiO_2 photocatalyst. Appl Catal B 2018;236:240–52.
[110] Spanu D, Recchia S, Mohajernia S, Schmuki P, Altomare M. Site-selective Pt dewetting on WO_3-coated TiO_2 nanotube arrays: an electron transfer cascade-based H_2 evolution photocatalyst. Appl Catal B 2018;237:198–205.
[111] Peng C, Wei P, Li X, Liu Y, Cao Y, Wang H, et al. High efficiency photocatalytic hydrogen production over ternary Cu/TiO_2@$Ti_3C_2T_x$ enabled by low-work-function 2D titanium carbide. Nano Energy 2018;53:97–107.
[112] Du J, Wang H, Yang M, Zhang F, Wu H, Cheng X, et al. Highly efficient hydrogen evolution catalysis based on MoS_2/CdS/TiO_2 porous composites. Int J Hydrogen Energy 2018;43:9307–15.
[113] Zhao J, Zhang P, Fan J, Hu J, Shao G. Constructing 2D layered MoS_2 nanosheets-modified Z-scheme TiO_2/WO_3 nanofibers ternary nanojunction with enhanced photocatalytic activity. Appl Surf Sci 2018;430:466–74.
[114] Hafeez HY, Lakhera SK, Bellamkonda S, Rao GR, Shankar MV, Bahnemann DW, et al. Construction of ternary hybrid layered reduced graphene oxide supported g-C_3N_4-TiO_2 nanocomposite and its photocatalytic hydrogen production activity. Int J Hydrogen Energy 2018;43:3892–904.
[115] Rivero MJ, Iglesias O, Ribao P, Ortiz I. Kinetic performance of TiO_2/Pt/reduced graphene oxide composites in the photocatalytic hydrogen production. Int J Hydrogen Energy 2018. https://doi.org/10.1016/j.ijhydene.2018.02.115.
[116] Xu D, Hai Y, Zhang X, Zhang S, He R. Bi_2O_3 cocatalyst improving photocatalytic hydrogen evolution performance of TiO_2. Appl Surf Sci 2017;400:530–6.
[117] Yang C, Zhang X, Qin J, Shen X, Yu R, Ma M, et al. Porous carbon-doped TiO_2 on TiC nanostructures for enhanced photocatalytic hydrogen production under visible light. J Catal 2017;347:36–44.
[118] Yang Q, Peng P, Xiang Z. Covalent organic polymer modified TiO_2 nanosheets as highly efficient photocatalysts for hydrogen generation. Chem Eng Sci 2017;162:33–40.
[119] Zhao XG, Huang LQ. Iridium, carbon and nitrogen multiple-doped TiO_2 nanoparticles with enhanced photocatalytic activity. Ceram Int 2017;43:3975–80.
[120] Cao B, Li G, Li H. Hollow spherical RuO_2@TiO_2@Pt bifunctional photocatalyst for coupled H_2 production and pollutant degradation. Appl Catal B 2016;194:42–9.
[121] Lin H-y, Shih C-y. Efficient one-pot microwave-assisted hydrothermal synthesis of M (M=Cr, Ni, Cu, Nb) and nitrogen co-doped TiO_2 for hydrogen production by photocatalytic water splitting. J Mol Catal A Chem 2016;411:128–37.
[122] Oros-Ruiz S, Zanella R, Collins SE, Hernández-Gordillo A, Gómez R. Photocatalytic hydrogen production by Au–MxOy (MAg, Cu, Ni) catalysts supported on TiO_2. Catal Commun 2014;47:1–6.
[123] Cui E, Lu G. New evidence for the regulation of photogenerated electron transfer on surface potential energy controlled co-catalyst on TiO_2 – the investigation of hydrogen production over selectively exposed Au facet on Au/TiO_2. Int J Hydrogen Energy 2014;39:7672–85.
[124] Cao S, Low J, Yu J, Jaroniec M. Polymeric photocatalysts based on graphitic carbon nitride. Adv Mater 2015;27:2150–76.
[125] Liu J, Zhang T, Wang Z, Dawson G, Chen W. Simple pyrolysis of urea into graphitic carbon nitride with recyclable adsorption and photocatalytic activity. J Mater Chem 2011;21:14398–401.
[126] Pang X, Bian H, Wang W, Liu C, Khan MS, Wang Q, et al. A bio-chemical application of N-GQDs and g-C_3N_4 QDs sensitized TiO_2 nanopillars for the quantitative detection of pcDNA3-HBV. Biosens Bioelectron 2017;91:456–64.
[127] Patnaik S, Martha S, Parida KM. An overview of the structural, textural and morphological modulations of g-C_3N_4 towards photocatalytic hydrogen production. RSC Adv 2016;6:46929–51.
[128] Zhu B, Xia P, Li Y, Ho W, Yu J. Fabrication and photocatalytic activity enhanced mechanism of direct Z-scheme g-C_3N_4/Ag_2WO_4 photocatalyst. Appl Surf Sci 2017;391:175–83.
[129] Zhang J, Wang Y, Jin J, Zhang J, Lin Z, Huang F, et al. Efficient visible-light photocatalytic hydrogen evolution and enhanced photostability of core/shell CdS/g-C_3N_4 nanowires. ACS Appl Mater Interfaces 2013;5:10317–24.
[130] Sun J, Zhang J, Zhang M, Antonietti M, Fu X, Wang X. Bioinspired hollow semiconductor nanospheres as photosynthetic nanoparticles. Nat Commun 2012;3:1139.
[131] Niu P, Zhang L, Liu G, Cheng HM. Graphene-like carbon nitride nanosheets for improved photocatalytic activities. Adv Funct Mater 2012;22:4763–70.
[132] Yang S, Gong Y, Zhang J, Zhan L, Ma L, Fang Z, et al. Exfoliated graphitic carbon nitride nanosheets as efficient catalysts for hydrogen evolution under visible light. Adv Mater 2013;25:2452–6.
[133] Wu M, Yan J-M, Zhang X-w, Zhao M. Synthesis of g-C_3N_4 with heating acetic acid treated melamine and its photocatalytic activity for hydrogen evolution. Appl Surf Sci 2015;354:196–200.
[134] Zhang L, Liu D, Guan J, Chen X, Guo X, Zhao F, et al. Metal-free g-C_3N_4 photocatalyst by sulfuric acid activation for selective aerobic oxidation of benzyl alcohol under visible light. Mater Res Bull 2014;59:84–92.
[135] Li C, Luo Z, Wang T, Gong J. Surface, bulk, and interface: rational design of hematite architecture toward efficient photo-electrochemical water splitting. Adv Mater 2018;30:1707502.
[136] Chen M, Liu Y, Li C, Li A, Chang X, Liu W, et al. Spatial control of cocatalysts and elimination of interfacial defects towards efficient and robust CIGS photocathodes for solar water splitting. Energy Environ Sci 2018;11:2025–34.
[137] Ong W-J, Tan L-L, Ng YH, Yong S-T, Chai S-P. Graphitic carbon nitride (g-C_3N_4)-based photocatalysts for artificial photosynthesis and environmental remediation: are we a step closer to achieving sustainability? Chem Rev 2016;116:7159–329.
[138] Chen P-W, Li K, Yu Y-X, Zhang W-D. Cobalt-doped graphitic carbon nitride photocatalysts with high activity for hydrogen evolution. Appl Surf Sci 2017;392:608–15.
[139] Bi L, Xu D, Zhang L, Lin Y, Wang D, Xie T. Metal Ni-loaded g-C_3N_4 for enhanced photocatalytic H_2 evolution activity: the change in surface band bending. Phys Chem Chem Phys 2015;17:29899–905.
[140] Chen D, Liu J, Jia Z, Fang J, Yang F, Tang Y, et al. Efficient visible-light-driven hydrogen evolution and Cr(VI) reduction over porous P and Mo co-doped g-C_3N_4 with feeble N vacancies photocatalyst. J Hazard Mater 2019;361:294–304.
[141] Humayun M, Fu Q, Zheng Z, Li H, Luo W. Improved visible-light catalytic activities of novel Au/P-doped g-C_3N_4 photocatalyst for solar fuel production and mechanism. Appl Catal A 2018;568:139–47.
[142] Yan X, Jia Z, Che H, Chen S, Hu P, Wang J, et al. A selective ion replacement strategy for the synthesis of copper doped carbon nitride nanotubes with improved photocatalytic hydrogen evolution. Appl Catal B 2018;234:19–25.

Please cite this article as: Fajrina N, Tahir M, A critical review in strategies to improve photocatalytic water splitting towards hydrogen production, International Journal of Hydrogen Energy, https://doi.org/10.1016/j.ijhydene.2018.10.200

[143] Sun C, Zhang H, Liu H, Zheng X, Zou W, Dong L, et al. Enhanced activity of visible-light photocatalytic H_2 evolution of sulfur-doped g-C_3N_4 photocatalyst via nanoparticle metal Ni as cocatalyst. Appl Catal B 2018;235:66–74.
[144] Qi K, Xie Y, Wang R, Liu S-y, Zhao Z. Electroless plating Ni-P cocatalyst decorated g-C_3N_4 with enhanced photocatalytic water splitting for H_2 generation. Appl Surf Sci 2019;466:847–53.
[145] Liu M, Xia P, Zhang L, Cheng B, Yu J. Enhanced photocatalytic H_2-production activity of g-C_3N_4 nanosheets via optimal photodeposition of Pt as cocatalyst. ACS Sustain Chem Eng 2018;6:10472–80.
[146] Wang Y, Zhao S, Zhang Y, Fang J, Zhou Y, Yuan S, et al. One-pot synthesis of K-doped g-C_3N_4 nanosheets with enhanced photocatalytic hydrogen production under visible-light irradiation. Appl Surf Sci 2018;440:258–65.
[147] Qian X-B, Peng W, Huang J-H. Fluorescein-sensitized Au/g-C_3N_4 nanocomposite for enhanced photocatalytic hydrogen evolution under visible light. Mater Res Bull 2018;102:362–8.
[148] Zhao N, Kong L, Dong Y, Wang G, Wu X, Jiang P. Insight into the crucial factors for photochemical deposition of cobalt cocatalysts on g-C_3N_4 photocatalysts. ACS Appl Mater Interfaces 2018;10:9522–31.
[149] Caux M, Fina F, Irvine JTS, Idriss H, Howe R. Impact of the annealing temperature on Pt/g-C_3N_4 structure, activity and selectivity between photodegradation and water splitting. Catal Today 2017;287:182–8.
[150] Zhang P, Song T, Wang T, Zeng H. Effectively extending visible light absorption with a broad spectrum sensitizer for improving the H_2 evolution of in-situ Cu/g-C_3N_4 nanocomponents. Int J Hydrogen Energy 2017;42:14511–21.
[151] Ou M, Wan S, Zhong Q, Zhang S, Wang Y. Single Pt atoms deposition on g-C_3N_4 nanosheets for photocatalytic H_2 evolution or NO oxidation under visible light. Int J Hydrogen Energy 2017;42:27043–54.
[152] Rahman MZ, Ran J, Tang Y, Jaroniec M, Qiao SZ. Surface activated carbon nitride nanosheets with optimized electro-optical properties for highly efficient photocatalytic hydrogen production. J Mater Chem A 2016;4:2445–52.
[153] Fan M, Song C, Chen T, Yan X, Xu D, Gu W, et al. Visible-light-drived high photocatalytic activities of Cu/gC_3N_4 photocatalysts for hydrogen production. RSC Adv 2016;6:34633–40.
[154] Han C, Wu L, Ge L, Li Y, Zhao Z. AuPd bimetallic nanoparticles decorated graphitic carbon nitride for highly efficient reduction of water to H_2 under visible light irradiation. Carbon 2015;92:31–40.
[155] Huang Z, Li F, Chen B, Yuan G. Porous and low-defected graphitic carbon nitride nanotubes for efficient hydrogen evolution under visible light irradiation. RSC Adv 2015;5:102700–6.
[156] Ma L, Fan H, Li M, Tian H, Fang J, Dong G. A simple melamine-assisted exfoliation of polymeric graphitic carbon nitrides for highly efficient hydrogen production from water under visible light. J Mater Chem A 2015;3:22404–12.
[157] Samanta S, Martha S, Parida K. Facile synthesis of Au/g-C_3N_4 nanocomposites: an inorganic/organic hybrid plasmonic photocatalyst with enhanced hydrogen gas evolution under visible-light irradiation. ChemCatChem 2014;6:1453–62.
[158] Zhong Y, Wang Z, Feng J, Yan S, Zhang H, Li Z, et al. Improvement in photocatalytic H_2 evolution over g-C_3N_4 prepared from protonated melamine. Appl Surf Sci 2014;295:253–9.
[159] Chang X, Wang T, Zhang P, Zhang J, Li A, Gong J. Enhanced surface reaction kinetics and charge separation of p-n heterojunction Co_3O_4/$BiVO_4$ photoanodes. J Am Chem Soc 2015;137:8356–9.
[160] Zhang P, Wang T, Chang X, Zhang L, Gong J. Synergistic cocatalytic effect of carbon nanodots and Co_3O_4 nanoclusters for the photoelectrochemical water oxidation on hematite. Angew Chem Int Ed 2016;55:5851–5.
[161] Yin L, Yuan Y-P, Cao S-W, Zhang Z, Xue C. Enhanced visible-light-driven photocatalytic hydrogen generation over g-C_3N_4 through loading the noble metal-free NiS_2 cocatalyst. RSC Adv 2014;4:6127.
[162] Wu M, Yan J-M, Zhang X-W, Zhao M, Jiang Q. Ag_2O modified g-C_3N_4 for highly efficient photocatalytic hydrogen generation under visible light irradiation. J Mater Chem A 2015;3:15710–4.
[163] Chen P, Xing P, Chen Z, Hu X, Lin H, Zhao L, et al. In-situ synthesis of $AgNbO_3$/g-C_3N_4 photocatalyst via microwave heating method for efficiently photocatalytic H_2 generation. J Colloid Interface Sci 2018;534:163–71.
[164] Zeng D, Xu W, Ong W-J, Xu J, Ren H, Chen Y, et al. Toward noble-metal-free visible-light-driven photocatalytic hydrogen evolution: monodisperse sub–15 nm Ni_2P nanoparticles anchored on porous g-C_3N_4 nanosheets to engineer 0D-2D heterojunction interfaces. Appl Catal B 2018;221:47–55.
[165] Wulan B-R, Yi S-S, Li S-J, Duan Y-X, Yan J-M, Jiang Q. Amorphous nickel pyrophosphate modified graphitic carbon nitride: an efficient photocatalyst for hydrogen generation from water splitting. Appl Catal B 2018;231:43–50.
[166] Liu J, Jia Q, Long J, Wang X, Gao Z, Gu Q. Amorphous NiO as co-catalyst for enhanced visible-light-driven hydrogen generation over g-C_3N_4 photocatalyst. Appl Catal B 2018;222:35–43.
[167] Lu Z, Li C, Han J, Wang L, Wang S, Ni L, et al. Construction 0D/2D heterojunction by highly dispersed Ni_2P QDs loaded on the ultrathin g-C_3N_4 surface towards superhigh photocatalytic and photoelectric performance. Appl Catal B 2018;237:919–26.
[168] Liu Y, Xu X, Zhang J, Zhang H, Tian W, Li X, et al. Flower-like MoS_2 on graphitic carbon nitride for enhanced photocatalytic and electrochemical hydrogen evolutions. Appl Catal B 2018;239:334–44.
[169] Ji C, Yin S-N, Sun S, Yang S. An in situ mediator-free route to fabricate Cu_2O/g-C_3N_4 type-II heterojunctions for enhanced visible-light photocatalytic H_2 generation. Appl Surf Sci 2018;434:1224–31.
[170] Guo F, Shi W, Zhu C, Li H, Kang Z. CoO and g-C_3N_4 complement each other for highly efficient overall water splitting under visible light. Appl Catal B 2018;226:412–20.
[171] Dong Z, Wu Y, Thirugnanam N, Li G. Double Z-scheme ZnO/ZnS/g-C_3N_4 ternary structure for efficient photocatalytic H_2 production. Appl Surf Sci 2018;430:293–300.
[172] Hao X, Zhou J, Cui Z, Wang Y, Wang Y, Zou Z. Zn-vacancy mediated electron-hole separation in ZnS/g-C_3N_4 heterojunction for efficient visible-light photocatalytic hydrogen production. Appl Catal B 2018;229:41–51.
[173] Li N, Zhou J, Sheng Z, Xiao W. Molten salt-mediated formation of g-C_3N_4-MoS_2 for visible-light-driven photocatalytic hydrogen evolution. Appl Surf Sci 2018;430:218–24.
[174] Yi S-S, Yan J-M, Wulan B-R, Li S-J, Liu K-H, Jiang Q. Noble-metal-free cobalt phosphide modified carbon nitride: an efficient photocatalyst for hydrogen generation. Appl Catal B 2017;200:477–83.
[175] Zhao H, Sun S, Jiang P, Xu ZJ. Graphitic C_3N_4 modified by Ni_2P cocatalyst: an efficient, robust and low cost photocatalyst for visible-light-driven H_2 evolution from water. Chem Eng J 2017;315:296–303.

Please cite this article as: Fajrina N, Tahir M, A critical review in strategies to improve photocatalytic water splitting towards hydrogen production, International Journal of Hydrogen Energy, https://doi.org/10.1016/j.ijhydene.2018.10.200

[176] Wang W, An T, Li G, Xia D, Zhao H, Yu JC, et al. Earth-abundant $Ni_2P/g\text{-}C_3N_4$ lamellar nanohydrids for enhanced photocatalytic hydrogen evolution and bacterial inactivation under visible light irradiation. Appl Catal B 2017;217:570–80.
[177] Qin Z, Xue F, Chen Y, Shen S, Guo L. Spatial charge separation of one-dimensional $Ni_2P\text{-}Cd_{0.9}Zn_{0.1}S/g\text{-}C_3N_4$ heterostructure for high-quantum-yield photocatalytic hydrogen production. Appl Catal B 2017;217:551–9.
[178] Jiang Z, Zhu C, Wan W, Qian K, Xie J. Constructing graphite-like carbon nitride modified hierarchical yolk–shell TiO_2 spheres for water pollution treatment and hydrogen production. J Mater Chem A 2016;4:1806–18.
[179] Yang X, Huang H, Kubota M, He Z, Kobayashi N, Zhou X, et al. Synergetic effect of MoS_2 and $g\text{-}C_3N_4$ as cocatalysts for enhanced photocatalytic H_2 production activity of TiO_2. Mater Res Bull 2016;76:79–84.
[180] Lu Y, Chu D, Zhu M, Du Y, Yang P. Exfoliated carbon nitride nanosheets decorated with NiS as an efficient noble-metal-free visible-light-driven photocatalyst for hydrogen evolution. Phys Chem Chem Phys 2015;17:17355–61.
[181] Yuan J, Wen J, Zhong Y, Li X, Fang Y, Zhang S, et al. Enhanced photocatalytic H_2 evolution over noble-metal-free NiS cocatalyst modified CdS nanorods/$g\text{-}C_3N_4$ heterojunctions. J Mater Chem A 2015;3:18244–55.
[182] Chen Z, Sun P, Fan B, Zhang Z, Fang X. In situ template-free ion-exchange process to prepare visible-light-active $g\text{-}C_3N_4$/NiS hybrid photocatalysts with enhanced hydrogen evolution activity. J Phys Chem C 2014;118:7801–7.
[183] Jiang D, Chen L, Xie J, Chen M. $Ag_2S/g\text{-}C_3N_4$ composite photocatalysts for efficient Pt-free hydrogen production. The co-catalyst function of Ag/Ag_2S formed by simultaneous photodeposition. Dalton Trans 2014;43:4878–85.
[184] Shi F, Chen L, Xing C, Jiang D, Li D, Chen M. ZnS microsphere/$g\text{-}C_3N_4$ nanocomposite photo-catalyst with greatly enhanced visible light performance for hydrogen evolution: synthesis and synergistic mechanism study. RSC Adv 2014;4:62223–9.
[185] Hong J, Wang Y, Wang Y, Zhang W, Xu R. Noble-metal-free NiS/C_3N_4 for efficient photocatalytic hydrogen evolution from water. ChemSusChem 2013;6:2263–8.
[186] Zhou Y, Zhang L, Huang W, Kong Q, Fan X, Wang M, et al. N-doped graphitic carbon-incorporated $g\text{-}C_3N_4$ for remarkably enhanced photocatalytic H_2 evolution under visible light. Carbon 2016;99:111–7.
[187] Chen J, Hong Z, Chen Y, Lin B, Gao B. One-step synthesis of sulfur-doped and nitrogen-deficient gC_3N_4 photocatalyst for enhanced hydrogen evolution under visible light. Mater Lett 2015;145:129–32.
[188] Lan Z-A, Zhang G, Wang X. A facile synthesis of Br-modified $g\text{-}C_3N_4$ semiconductors for photoredox water splitting. Appl Catal B 2016;192:116–25.
[189] Wang H, Bian Y, Hu J, Dai L. Highly crystalline sulfur-doped carbon nitride as photocatalyst for efficient visible-light hydrogen generation. Appl Catal B 2018;238:592–8.
[190] Wu M, Zhang J, He B-b, Wang H-w, Wang R, Gong Y-s. In-situ construction of coral-like porous P-doped $g\text{-}C_3N_4$ tubes with hybrid 1D/2D architecture and high efficient photocatalytic hydrogen evolution. Appl Catal B 2019;241:159–66.
[191] Zeng Y, Liu X, Liu C, Wang L, Xia Y, Zhang S, et al. Scalable one-step production of porous oxygen-doped $g\text{-}C_3N_4$ nanorods with effective electron separation for excellent visible-light photocatalytic activity. Appl Catal B 2018;224:1–9.
[192] Zhang J-W, Gong S, Mahmood N, Pan L, Zhang X, Zou J-J. Oxygen-doped nanoporous carbon nitride via water-based homogeneous supramolecular assembly for photocatalytic hydrogen evolution. Appl Catal B 2018;221:9–16.
[193] Wang H, Yang C, Li M, Chen F, Cui Y. Enhanced photocatalytic hydrogen production of restructured B/F codoped $g\text{-}C_3N_4$ via post-thermal treatment. Mater Lett 2018;212:319–22.
[194] Xiao P, Jiang D, Liu T, Li D, Chen M. Facile synthesis of carbon-doped $g\text{-}C_3N_4$ for enhanced photocatalytic hydrogen evolution under visible light. Mater Lett 2018;212:111–3.
[195] Guo S, Tang Y, Xie Y, Tian C, Feng Q, Zhou W, et al. P-doped tubular $g\text{-}C_3N_4$ with surface carbon defects: universal synthesis and enhanced visible-light photocatalytic hydrogen production. Appl Catal B 2017;218:664–71.
[196] Xu Q, Cheng B, Yu J, Liu G. Making co-condensed amorphous carbon/$g\text{-}C_3N_4$ composites with improved visible-light photocatalytic H_2-production performance using Pt as cocatalyst. Carbon 2017;118:241–9.
[197] She X, Liu L, Ji H, Mo Z, Li Y, Huang L, et al. Template-free synthesis of 2D porous ultrathin nonmetal-doped $g\text{-}C_3N_4$ nanosheets with highly efficient photocatalytic H_2 evolution from water under visible light. Appl Catal B 2016;187:144–53.
[198] Guo S, Zhu Y, Yan Y, Min Y, Fan J, Xu Q. Holey structured graphitic carbon nitride thin sheets with edge oxygen doping via photo-Fenton reaction with enhanced photocatalytic activity. Appl Catal B 2016;185:315–21.
[199] Zhu Y-P, Ren T-Z, Yuan Z-Y. Mesoporous phosphorus-doped $g\text{-}C_3N_4$ nanostructured flowers with superior photocatalytic hydrogen evolution performance. ACS Appl Mater Interfaces 2015;7:16850–6.
[200] Zhou Y, Zhang L, Liu J, Fan X, Wang B, Wang M, et al. Brand new P-doped $g\text{-}C_3N_4$: enhanced photocatalytic activity for H_2 evolution and Rhodamine B degradation under visible light. J Mater Chem A 2015;3:3862–7.
[201] Zhang J, Huang F. Enhanced visible light photocatalytic H_2 production activity of $g\text{-}C_3N_4$ via carbon fiber. Appl Surf Sci 2015;358:287–95.
[202] Wu Z, Gao H, Yan S, Zou Z. Synthesis of carbon black/carbon nitride intercalation compound composite for efficient hydrogen production. Dalton Trans 2014;43:12013–7.
[203] Ge L, Han C, Xiao X, Guo L, Li Y. Enhanced visible light photocatalytic hydrogen evolution of sulfur-doped polymeric $g\text{-}C_3N_4$ photocatalysts. Mater Res Bull 2013;48:3919–25.
[204] Chen X, Shen S, Guo L, Mao SS. Semiconductor-based photocatalytic hydrogen generation. Chem Rev 2010;110:6503–70.
[205] Chen X, Li C, Gratzel M, Kostecki R, Mao SS. Nanomaterials for renewable energy production and storage. Chem Soc Rev 2012;41:7909–37.
[206] Fu J, Cao S, Yu J. Dual Z-scheme charge transfer in TiO_2–Ag–Cu_2O composite for enhanced photocatalytic hydrogen generation. J Materiomics 2015;1:124–33.
[207] Xing X, Zhang M, Hou L, Xiao L, Li Q, Yang J. Z-scheme BCN-TiO_2 nanocomposites with oxygen vacancy for high efficiency visible light driven hydrogen production. Int J Hydrogen Energy 2017;42:28434–44.
[208] Rosseler O, Shankar MV, Du MK-L, Schmidlin L, Keller N, Keller V. Solar light photocatalytic hydrogen production from water over Pt and Au/TiO_2(anatase/rutile) photocatalysts: influence of noble metal and porogen promotion. J Catal 2010;269:179–90.
[209] Bard AJ. Photoelectrochemistry and heterogeneous photo-catalysis at semiconductors. J Photochem 1979;10:59–75.
[210] Abe R, Higashi M, Domen K. Overall water splitting under visible light through a two-step photoexcitation between

Please cite this article as: Fajrina N, Tahir M, A critical review in strategies to improve photocatalytic water splitting towards hydrogen production, International Journal of Hydrogen Energy, https://doi.org/10.1016/j.ijhydene.2018.10.200

TaON and WO_3 in the presence of an iodate-iodide shuttle redox mediator. ChemSusChem 2011;4:228–37.
[211] Chen S, Qi Y, Hisatomi T, Ding Q, Asai T, Li Z, et al. Efficient visible-light-driven Z-scheme overall water splitting using a $MgTa_2O_{6-x}N_y$/TaON heterostructure photocatalyst for H_2 evolution. Angew Chem Int Ed Engl 2015;54:8498–501.
[212] Mo Z, Xu H, Chen Z, She X, Song Y, Lian J, et al. Construction of MnO_2/Monolayer g-C_3N_4 with Mn vacancies for Z-scheme overall water splitting. Appl Catal B 2019;241:452–60.
[213] Jia Y, Zhao D, Li M, Han H, Li C. La and Cr Co-doped $SrTiO_3$ as an H_2 evolution photocatalyst for construction of a Z-scheme overall water splitting system. Chin J Catal 2018;39:421–30.
[214] Qi Y, Chen S, Cui J, Wang Z, Zhang F, Li C. Inhibiting competing reactions of iodate/iodide redox mediators by surface modification of photocatalysts to enable Z-scheme overall water splitting. Appl Catal B 2018;224:579–85.
[215] Iwase Y, Tomita O, Naito H, Higashi M, Abe R. Molybdenum-substituted polyoxometalate as stable shuttle redox mediator for visible light driven Z-scheme water splitting system. J Photochem Photobiol A 2018;356:347–54.
[216] Qin Z, Fang W, Liu J, Wei Z, Jiang Z, Shangguan W. Zinc-doped g-C_3N_4/$BiVO_4$ as a Z-scheme photocatalyst system for water splitting under visible light. Chin J Catal 2018;39:472–8.
[217] Qi Y, Zhao Y, Gao Y, Li D, Li Z, Zhang F, et al. Redox-based visible-light-driven Z-scheme overall water splitting with apparent quantum efficiency exceeding 10%. Joule 2018. https://doi.org/10.1016/j.joule.2018.07.029.
[218] Miseki Y, Fujiyoshi S, Gunji T, Sayama K. Photocatalytic Z-scheme water splitting for independent H_2/O_2 production via a stepwise operation employing a vanadate redox mediator under visible light. J Phys Chem C 2017;121:9691–7.
[219] Yang PJ, Zhao JH, Wang J, Cao BY, Li L, Zhu ZP. Construction of Z-scheme carbon nanodots/WO_3 with highly enhanced photocatalytic hydrogen production. J Mater Chem A 2015;3:8256–9.
[220] Maeda K, Abe R, Domen K. Role and function of ruthenium species as promoters with TaON-based photocatalysts for oxygen evolution in two-step water splitting under visible light. J Phys Chem C 2011;115:3057–64.
[221] Tabata M, Maeda K, Higashi M, Lu D, Takata T, Abe R, et al. Modified Ta_3N_5 powder as a photocatalyst for O_2 evolution in a two-step water splitting system with an iodate/iodide shuttle redox mediator under visible light. Langmuir 2010;26:9161–5.
[222] Sasaki Y, Iwase A, Kato H, Kudo A. The effect of co-catalyst for Z-scheme photocatalysis systems with an Fe^{3+}/Fe^{2+} electron mediator on overall water splitting under visible light irradiation. J Catal 2008;259:133–7.
[223] Maeda K, Domen K. Photocatalytic water splitting: recent progress and future challenges. J Phys Chem Lett 2010;1:2655–61.
[224] Kochuveedu ST, Jang YH, Kim DH. A study on the mechanism for the interaction of light with noble metal-metal oxide semiconductor nanostructures for various photophysical applications. Chem Soc Rev 2013;42:8467–93.
[225] Shehzad N, Tahir M, Johari K, Murugesan T, Hussain M. Fabrication of highly efficient and stable indirect Z-scheme assembly of AgBr/TiO_2 via graphene as a solid-state electron mediator for visible light induced enhanced photocatalytic H_2 production. Appl Surf Sci 2019;463:445–55.
[226] Tada H, Mitsui T, Kiyonaga T, Akita T, Tanaka K. All-solid-state Z-scheme in CdS-Au-TiO_2 three-component nanojunction system. Nat Mater 2006;5:782–6.
[227] Iwashina K, Iwase A, Ng YH, Amal R, Kudo A. Z-schematic water splitting into H_2 and O_2 using metal sulfide as a hydrogen-evolving photocatalyst and reduced graphene oxide as a solid-state electron mediator. J Am Chem Soc 2015;137:604–7.
[228] Liu Ca, Fu Y, Zhao J, Wang H, Huang H, Liu Y, et al. All-solid-state Z-scheme system of NiO/CDs/$BiVO_4$ for visible light-driven efficient overall water splitting. Chem Eng J 2019;358:134–42.
[229] Dong J, Shi Y, Huang C, Wu Q, Zeng T, Yao W. A New and stable Mo-Mo_2C modified g-C_3N_4 photocatalyst for efficient visible light photocatalytic H_2 production. Appl Catal B 2019;243:27–35.
[230] Zhang Y, Wang L, Yu S, Jiang H, Yun Y, Sun Y, et al. Ag-induced synthesis of three dimensionally ordered macroporous anatase/rutile homojunction for solar light-driven Z-scheme photocatalysis. Solar Energy 2018;174:770–9.
[231] Liang S, Han B, Liu X, Chen W, Peng M, Guan G, et al. 3D spatially branched hierarchical Z-scheme CdS-Au nanoclusters-ZnO hybrids with boosted photocatalytic hydrogen evolution. J Alloys Compd 2018;754:105–13.
[232] Yang G, Ding H, Chen D, Feng J, Hao Q, Zhu Y. Construction of urchin-like $ZnIn_2S_4$-Au-TiO_2 heterostructure with enhanced activity for photocatalytic hydrogen evolution. Appl Catal B 2018;234:260–7.
[233] Jiang Z, Pan J, Wang B, Li C. Two dimensional Z-scheme AgCl/Ag/$CaTiO_3$ nano-heterojunctions for photocatalytic hydrogen production enhancement. Appl Surf Sci 2018;436:519–26.
[234] Jo W-K, Kumar S, Eslava S, Tonda S. Construction of Bi_2WO_6/RGO/g-C_3N_4 2D/2D/2D hybrid Z-scheme heterojunctions with large interfacial contact area for efficient charge separation and high-performance photoreduction of CO_2 and H_2O into solar fuels. Appl Catal B 2018;239:586–98.
[235] Zhao W, Liu J, Deng Z, Zhang J, Ding Z, Fang Y. Facile preparation of Z-scheme CdS-Ag-TiO_2 composite for the improved photocatalytic hydrogen generation activity. Int J Hydrogen Energy 2018;43:18232–41.
[236] Wu X, Zhao J, Wang L, Han M, Zhang M, Wang H, et al. Carbon dots as solid-state electron mediator for $BiVO_4$/CDs/CdS Z-scheme photocatalyst working under visible light. Appl Catal B 2017;206:501–9.
[237] Zhao H, Ding X, Zhang B, Li Y, Wang C. Enhanced photocatalytic hydrogen evolution along with byproducts suppressing over Z-scheme $Cd_xZn_{1-x}S$/Au/g-C_3N_4 photocatalysts under visible light. Sci Bull 2017;62:602–9.
[238] Wan S, Ou M, Zhong Q, Zhang S, Song F. Construction of Z-scheme photocatalytic systems using $ZnIn_2S_4$, CoO_X-loaded Bi_2MoO_6 and reduced graphene oxide electron mediator and its efficient nonsacrificial water splitting under visible light. Chem Eng J 2017;325:690–9.
[239] Jo W-K, Selvam NCS. Z-scheme CdS/g-C_3N_4 composites with RGO as an electron mediator for efficient photocatalytic H_2 production and pollutant degradation. Chem Eng J 2017;317:913–24.
[240] Shen H, Liu G, Yan X, Jiang J, Hong Y, Yan M, et al. All-solid-state Z-scheme system of RGO-Cu_2O/Fe_2O_3 for simultaneous hydrogen production and tetracycline degradation. Mater Today Energy 2017;5:312–9.
[241] Zhu R, Tian F, Cao G, Ouyang F. Construction of Z scheme system of $ZnIn_2S_4$/RGO/$BiVO_4$ and its performance for hydrogen generation under visible light. Int J Hydrogen Energy 2017;42:17350–61.
[242] Kobayashi R, Kurihara K, Takashima T, Ohtani B, Irie H. A silver-inserted zinc rhodium oxide and bismuth vanadium

Please cite this article as: Fajrina N, Tahir M, A critical review in strategies to improve photocatalytic water splitting towards hydrogen production, International Journal of Hydrogen Energy, https://doi.org/10.1016/j.ijhydene.2018.10.200

oxide heterojunction photocatalyst for overall pure-water splitting under red light. J Mater Chem A 2016;4:3061–7.
[243] Wang Q, Hisatomi T, Ma SSK, Li Y, Domen K. Core/shell structured La- and Rh-codoped $SrTiO_3$ as a hydrogen evolution photocatalyst in Z-scheme overall water splitting under visible light irradiation. Chem Mater 2014;26:4144–50.
[244] Ding L, Zhou H, Lou S, Ding J, Zhang D, Zhu H, et al. Butterfly wing architecture assisted CdS/Au/TiO_2 Z-scheme type photocatalytic water splitting. Int J Hydrogen Energy 2013;38:8244–53.
[245] Wang X, Liu G, Wang L, Chen Z-G, Lu GQM, Cheng H-M. ZnO-CdS@Cd heterostructure for effective photocatalytic hydrogen generation. Adv Energy Mater 2012;2:42–6.
[246] Guo H-L, Du H, Jiang Y-F, Jiang N, Shen C-C, Zhou X, et al. Artificial photosynthetic Z-scheme photocatalyst for hydrogen evolution with high quantum efficiency. J Phys Chem C 2017;121:107–14.
[247] Wang X, Liu G, Chen ZG, Li F, Wang L, Lu GQ, et al. Enhanced photocatalytic hydrogen evolution by prolonging the lifetime of carriers in ZnO/CdS heterostructures. Chem Commun 2009;0:3452–4.
[248] Bin Yousaf A, Imran M, Zaidi SJ, Kasak P. Highly efficient photocatalytic Z-scheme hydrogen production over oxygen-deficient WO_{3-x} nanorods supported $Zn_{0.3}Cd_{0.7}S$ heterostructure. Sci Rep 2017;7.
[249] Liu Y, Liu H, Zhou H, Li T, Zhang L. A Z-scheme mechanism of N-ZnO/g-C_3N_4 for enhanced H_2 evolution and photocatalytic degradation. Appl Surf Sci 2019;466:133–40.
[250] Wang S, Zhu B, Liu M, Zhang L, Yu J, Zhou M. Direct Z-scheme ZnO/CdS hierarchical photocatalyst for enhanced photocatalytic H_2-production activity. Appl Catal B 2019;243:19–26.
[251] Hua S, Qu D, An L, Jiang W, Wen Y, Wang X, et al. Highly efficient p-type Cu_3P/n-type g-C_3N_4 photocatalyst through Z-scheme charge transfer route. Appl Catal B 2019;240:253–61.
[252] Cui H, Li B, Zhang Y, Zheng X, Li X, Li Z, et al. Constructing Z-scheme based $CoWO_4$/CdS photocatalysts with enhanced dye degradation and H_2 generation performance. Int J Hydrogen Energy 2018;43:18242–52.
[253] Kong L, Zhang X, Wang C, Xu J, Du X, Li L. Ti^{3+} defect mediated g-C_3N_4/TiO_2 Z-scheme system for enhanced photocatalytic redox performance. Appl Surf Sci 2018;448:288–96.
[254] Arif M, Min Z, Yuting L, Yin H, Liu X. A Bi_2WO_6-based hybrid heterostructures photocatalyst with enhanced photodecomposition and photocatalytic hydrogen evolution through Z-scheme process. J Ind Eng Chem 2018. https://doi.org/10.1016/j.jiec.2018.09.026.
[255] Imran M, Bin Yousaf A, Farooq M, Kasak P. Enhanced Z-scheme visible light photocatalytic hydrogen production over α-Bi_2O_3/CZS heterostructure. Int J Hydrogen Energy 2018;43:4256–64.
[256] Hu T, Li P, Zhang J, Liang C, Dai K. Highly efficient direct Z-scheme WO_3/CdS-diethylenetriamine photocatalyst and its enhanced photocatalytic H_2 evolution under visible light irradiation. Appl Surf Sci 2018;442:20–9.
[257] Liu Y, Zhang H, Ke J, Zhang J, Tian W, Xu X, et al. 0D (MoS_2)/2D (g-C_3N_4) heterojunctions in Z-scheme for enhanced photocatalytic and electrochemical hydrogen evolution. Appl Catal B 2018;228:64–74.
[258] Zhang X, Xiao J, Hou M, Xiang Y, Chen H. Robust visible/near-infrared light driven hydrogen generation over Z-scheme conjugated polymer/CdS hybrid. Appl Catal B 2018;224:871–6.
[259] Liang Y-H, Liao M-W, Mishra M, Perng T-P. Fabrication of Ta_3N_5-ZnO direct Z-scheme photocatalyst for hydrogen generation. Int J Hydrogen Energy 2018. https://doi.org/10.1016/j.ijhydene.2018.07.117.
[260] Li Y-p, Li F-t, Wang X-j, Zhao J, Wei J-n, Hao Y-j, et al. Z-scheme electronic transfer of quantum-sized α-Fe_2O_3 modified g-C_3N_4 hybrids for enhanced photocatalytic hydrogen production. Int J Hydrogen Energy 2017;42:28327–36.
[261] Imran M, Yousaf AB, Kasak P, Zeb A, Zaidi SJ. Highly efficient sustainable photocatalytic Z-scheme hydrogen production from an α-Fe_2O_3 engineered ZnCdS heterostructure. J Catal 2017;353:81–8.
[262] Gao H, Zhang P, Zhao J, Zhang Y, Hu J, Shao G. Plasmon enhancement on photocatalytic hydrogen production over the Z-scheme photosynthetic heterojunction system. Appl Catal B 2017;210:297–305.
[263] Zhou FQ, Fan JC, Xu QJ, Min YL. $BiVO_4$ nanowires decorated with CdS nanoparticles as Z-scheme photocatalyst with enhanced H_2 generation. Appl Catal B 2017;201:77–83.
[264] Jia X, Tahir M, Pan L, Huang Z-F, Zhang X, Wang L, et al. Direct Z-scheme composite of CdS and oxygen-defected $CdWO_4$: an efficient visible-light-driven photocatalyst for hydrogen evolution. Appl Catal B 2016;198:154–61.
[265] Katsumata H, Tachi Y, Suzuki T, Kaneco S. Z-scheme photocatalytic hydrogen production over WO_3/g-C_3N_4 composite photocatalysts. RSC Adv 2014;4:21405–9.
[266] Xu F, Xiao W, Cheng B, Yu J. Direct Z-scheme anatase/rutile bi-phase nanocomposite TiO_2 nanofiber photocatalyst with enhanced photocatalytic H_2 production activity. Int J Hydrogen Energy 2014;39:15394–402.
[267] Liu C, Tang J, Chen HM, Liu B, Yang P. A fully integrated nanosystem of semiconductor nanowires for direct solar water splitting. Nano Lett 2013;13:2989–92.
[268] Ma SS, Maeda K, Hisatomi T, Tabata M, Kudo A, Domen K. A redox-mediator-free solar-driven Z-scheme water-splitting system consisting of modified Ta_3N_5 as an oxygen-evolution photocatalyst. Chemistry 2013;19:7480–6.
[269] Yang P, Zhao ZJ, Chang X, Mu R, Zha S, Zhang G, et al. The functionality of surface hydroxy groups on the selectivity and activity of carbon dioxide reduction over cuprous oxide in aqueous solutions. Angew Chem Int Ed 2018;57:7724–8.
[270] Zheng Y, Lin L, Wang B, Wang X. Graphitic carbon nitride polymers toward sustainable photoredox catalysis. Angew Chem Int Ed 2015;54:12868–84.
[271] Zhang Y, Antonietti M. Photocurrent generation by polymeric carbon nitride solids: an initial step towards a novel photovoltaic system. Chem Asian J 2010;5:1307–11.
[272] Guo S, Deng Z, Li M, Jiang B, Tian C, Pan Q, et al. Phosphorus-doped carbon nitride tubes with a layered micro-nanostructure for enhanced visible-light photocatalytic hydrogen evolution. Angew Chem Int Ed 2016;55:1830–4.
[273] Li J, Shen B, Hong Z, Lin B, Gao B, Chen Y. A facile approach to synthesize novel oxygen-doped g-C_3N_4 with superior visible-light photoreactivity. Chem Commun 2012;48:12017–9.
[274] Dong G, Zhao K, Zhang L. Carbon self-doping induced high electronic conductivity and photoreactivity of g-C_3N_4. Chem Commun 2012;48:6178–80.
[275] Han Q, Hu C, Zhao F, Zhang Z, Chen N, Qu L. One-step preparation of iodine-doped graphitic carbon nitride nanosheets as efficient photocatalysts for visible light water splitting. J Mater Chem A 2015;3:4612–9.
[276] Wang T, Gong J. Single-crystal semiconductors with narrow band gaps for solar water splitting. Angew Chem Int Ed 2015;54:10718–32.
[277] Zuo F, Wang L, Feng P. Self-doped Ti^{3+}@TiO_2 visible light photocatalyst: influence of synthetic parameters on the H_2 production activity. Int J Hydrogen Energy 2014;39:711–7.

Please cite this article as: Fajrina N, Tahir M, A critical review in strategies to improve photocatalytic water splitting towards hydrogen production, International Journal of Hydrogen Energy, https://doi.org/10.1016/j.ijhydene.2018.10.200

[278] Bafaqeer A, Tahir M, Amin NAS. Well-designed ZnV_2O_6/g-C_3N_4 2D/2D nanosheets heterojunction with faster charges separation via pCN as mediator towards enhanced photocatalytic reduction of CO_2 to fuels. Appl Catal B 2019;242:312–26.
[279] Police AKR, Basavaraju S, Valluri DK, Muthukonda VS, Machiraju S, Lee JS. $CaFe_2O_4$ sensitized hierarchical TiO_2 photo composite for hydrogen production under solar light irradiation. Chem Eng J 2014;247:152–60.
[280] Miranda C, Mansilla H, Yáñez J, Obregón S, Colón G. Improved photocatalytic activity of g-C_3N_4/TiO_2 composites prepared by a simple impregnation method. J Photochem Photobiol A 2013;253:16–21.
[281] Paunovic P, Cesnovar A, Grozdanov A, Makreski P, Fidancevska E. Preparation of nano-crystalline TiO_2 by sol-gel method using titanium tetraisopropoxide (TTIP) as a precursor. Adv Nat Sci Theory Appl 2012;1:133–42.
[282] Wang X, Song J, Huang J, Zhang J, Wang X, Ma R, et al. Activated carbon-based magnetic TiO_2 photocatalyst codoped with iodine and nitrogen for organic pollution degradation. Appl Surf Sci 2016;390:190–201.
[283] Sampaio MJ, Oliveira JWL, Sombrio CIL, Baptista DL, Teixeira SR, Carabineiro SAC, et al. Photocatalytic performance of Au/ZnO nanocatalysts for hydrogen production from ethanol. Appl Catal A 2016;518:198–205.
[284] Kumar DP, Kumari VD, Karthik M, Sathish M, Shankar MV. Shape dependence structural, optical and photocatalytic properties of TiO_2 nanocrystals for enhanced hydrogen production via glycerol reforming. Sol Energy Mater Sol Cells 2017;163:113–9.
[285] Luo Z, Wang T, Zhang J, Li C, Li H, Gong J. Dendritic hematite nanoarray photoanode modified with a conformal titanium dioxide interlayer for effective charge collection. Angew Chem Int Ed Engl 2017;56:12878–82.
[286] Li C, Li A, Luo Z, Zhang J, Chang X, Huang Z, et al. Surviving high-temperature calcination: ZrO_2-induced hematite nanotubes for photoelectrochemical water oxidation. Angew Chem Int Ed 2017;56:4150–5.
[287] Cai J, Wu M, Wang Y, Zhang H, Meng M, Tian Y, et al. Synergetic enhancement of light harvesting and charge separation over surface-disorder-engineered TiO_2 photonic crystals. Chem 2017;2:877–92.
[288] Al-Hamdi AM, Rinner U, Sillanpaa M. Tin dioxide as a photocatalyst for water treatment: a review. Process Saf Environ Prot 2017;107:190–205.
[289] Puga AV. Photocatalytic production of hydrogen from biomass-derived feedstocks. Coord Chem Rev 2016;315:1–66.
[290] Baniasadi E, Dincer I, Naterer GF. Measured effects of light intensity and catalyst concentration on photocatalytic hydrogen and oxygen production with zinc sulfide suspensions. Int J Hydrogen Energy 2013;38:9158–68.
[291] Tambago HMG, Leon RLd. Intrinsic kinetic modeling of hydrogen production by photocatalytic water splitting using cadmium zinc sulfide catalyst. Int J Chem Eng Appl 2015;6:220–7.
[292] Huaxu L, Fuqiang W, Ziming C, Shengpeng H, Bing X, Xiangtao G, et al. Analyzing the effects of reaction temperature on photo-thermo chemical synergetic catalytic water splitting under full-spectrum solar irradiation: an experimental and thermodynamic investigation. Int J Hydrogen Energy 2017;42:12133–42.
[293] Zhang Z, Maggard PA. Investigation of photocatalytically-active hydrated forms of amorphous titania, $TiO_2 \cdot nH_2O$. J Photochem Photobiol A 2007;186:8–13.
[294] Wu Y, Lu G, Li S. The role of Cu(I) species for photocatalytic hydrogen generation over CuO_x/TiO_2. Catal Lett 2009;133:97–105.
[295] Liu S, Luo Z, Li L, Li H, Chen M, Wang T, et al. Multifunctional TiO_2 overlayer for p-Si/n-CdS heterojunction photocathode with improved efficiency and stability. Nano Energy 2018;53:125–9.
[296] Brahimi R, Bessekhouad Y, Bouguelia A, Trari M. $CuAlO_2$/TiO_2 heterojunction applied to visible light H_2 production. J Photochem Photobiol A 2007;186:242–7.
[297] Maeda K. Photocatalytic properties of rutile TiO_2 powder for overall water splitting. Catal Sci Technol 2014;4:1949–53.
[298] Nada A, Hamed H, Barakat M, Mohamed N, Veziroglu T. Enhancement of photocatalytic hydrogen production rate using photosensitized TiO_2/RuO_2-MV^{2+}. Int J Hydrogen Energy 2008;33:3264–9.
[299] Baniasadi E, Dincer I, Naterer G. Performance analysis of a water splitting reactor with hybrid photochemical conversion of solar energy. Int J Hydrogen Energy 2012;37:7464–72.
[300] Lu J, Wang Y, Huang J, Fei J, Cao L, Li C. In situ synthesis of mesoporous C-doped TiO_2 single crystal with oxygen vacancy and its enhanced sunlight photocatalytic properties. Dyes Pigm 2017;144:203–11.
[301] Bouchy M, Zahraa O. Photocatalytic reactors. Int J Photoenergy 2003;5:191–7.
[302] Tahir M, Amin NS. Recycling of carbon dioxide to renewable fuels by photocatalysis: prospects and challenges. Renew Sust Energy Rev 2013;25:560–79.
[303] Ola O, Maroto-Valer MM. Review of material design and reactor engineering on TiO_2 photocatalysis for CO_2 reduction. J Photochem Photobiol C 2015;24:16–42.
[304] Lin H, Valsaraj KT. An optical fiber monolith reactor for photocatalytic wastewater treatment. AlChE J 2006;52:2271–80.
[305] Hu S, Li F, Fan Z, Gui J. Improved photocatalytic hydrogen production property over Ni/NiO/N–TiO_{2-x} heterojunction nanocomposite prepared by NH_3 plasma treatment. J Power Sources 2014;250:30–9.
[306] Taboada E, Angurell I, Llorca J. Dynamic photocatalytic hydrogen production from ethanol–water mixtures in an optical fiber honeycomb reactor loaded with Au/TiO_2. J Catal 2014;309:460–7.
[307] Nguyen T-V, Wu JCS. Photoreduction of CO_2 to fuels under sunlight using optical-fiber reactor. Sol Energy Mater Sol Cells 2008;92:864–72.
[308] Hu Y. A single TiO_2-coated side-glowing optical fiber for photocatalytic wastewater treatment. Chin Sci Bull 2005;50:1979.
[309] Du P, Carneiro JT, Moulijn JA, Mul G. A novel photocatalytic monolith reactor for multiphase heterogeneous photocatalysis. Appl Catal A 2008;334:119–28.
[310] Tahir M, Tahir B, Amin NS. Photocatalytic CO_2 reduction by CH_4 over montmorillonite modified TiO_2 nanocomposites in a continuous monolith photoreactor. Mater Res Bull 2015;63:13–23.
[311] Boyjoo Y, Sun H, Liu J, Pareek VK, Wang S. A review on photocatalysis for air treatment: from catalyst development to reactor design. Chem Eng J 2017;310:537–59.
[312] Gaudillere C, González JJ, Chica A, Serra JM. YSZ monoliths promoted with Co as catalysts for the production of H_2 by steam reforming of ethanol. Appl Catal A 2017;538:165–73.
[313] Tahir M, Amin NS. Photocatalytic CO_2 reduction and kinetic study over In/TiO_2 nanoparticles supported microchannel monolith photoreactor. Appl Catal A 2013;467:483–96.
[314] Tahir M, Amin NS. Performance analysis of nanostructured NiO–In_2O_3/TiO_2 catalyst for CO_2 photoreduction with H_2 in a monolith photoreactor. Chem Eng J 2016;285:635–49.
[315] Xiong Z, Lei Z, Ma S, Chen X, Gong B, Zhao Y, et al. Photocatalytic CO_2 reduction over V and W codoped TiO_2 catalyst in an internal-illuminated honeycomb

Please cite this article as: Fajrina N, Tahir M, A critical review in strategies to improve photocatalytic water splitting towards hydrogen production, International Journal of Hydrogen Energy, https://doi.org/10.1016/j.ijhydene.2018.10.200

photoreactor under simulated sunlight irradiation. Appl Catal B 2017;219:412–24.
[316] Liu H, Zhao J, Li C, Ji S. Conceptual design and CFD simulation of a novel metal-based monolith reactor with enhanced mass transfer. Catal Today 2005;105:401–6.
[317] Tahir M, Tahir B. Dynamic photocatalytic reduction of CO_2 to CO in a honeycomb monolith reactor loaded with Cu and N doped TiO_2 nanocatalysts. Appl Surf Sci 2016;377:244–52.
[318] Tian J, Zhao Z, Kumar A, Boughton RI, Liu H. Recent progress in design, synthesis, and applications of one-dimensional TiO_2 nanostructured surface heterostructures: a review. Chem Soc Rev 2014;43:6920–37.

Please cite this article as: Fajrina N, Tahir M, A critical review in strategies to improve photocatalytic water splitting towards hydrogen production, International Journal of Hydrogen Energy, https://doi.org/10.1016/j.ijhydene.2018.10.200